A COMPARISON OF NMHC OXIDATION MECHANISMS USING SPECIFIED GAS MIXTURES AND TRACE-P FIELD DATA

A Dissertation
Presented to
The Academic Faculty

By

Xingyi Gong

In Partial Fulfillment
Of the Requirement for the Degree
Doctor of Philosophy in the
School of Earth and Atmospheric Sciences

Georgia Institute of Technology

December, 2005

A Comparison of NMHC Oxidation Mechanisms Using Specified Gas Mixtures and TRACE-P Field Data

Approved by:

Dr. Douglas D. Davis, Advisor
School of Earth and Atmospheric Sciences
Georgia Institute of Technology

Dr. Derek M. Cunnold
School of Earth and Atmospheric Sciences
Georgia Institute of Technology

Dr. James A. Mulholland
School of Civil and Environmental Engineering
Georgia Institute of Technology

Dr. Yuhang Wang
School of Earth and Atmospheric Sciences
Georgia Institute of Technology

Dr. Paul H. Wine
School of Chemistry and Biochemistry
Georgia Institute of Technology

Date Approved: November 8th, 2005

Dedicated

To my parents!

ACKNOWLEDGEMENTS

I would like to express my gratitude to all those who gave me the possibility to complete this thesis.

First I must thank my thesis advisor, Dr. Douglas D. Davis. Without his patient and insightful guidance, I would not be even close to where I am. His generous encouragement and support through the past seven years have helped me tremendously. His unchanging enthusiasm and integral view on research has also made deep impression on me.

I owe Dr. Gao Chen lots of gratitude for the countless help he has given me on my research. To me, he is actually a second advisor as well as a good friend. In addition, I would like to thank the rest of my thesis committee, Drs. Derek M. Cunnold, James A. Mulholland, Yuhang Wang, and Paul H. Wine, for providing me with valuable comments.

I am grateful to my officemates Qing Yang and Oleksandr Karabanov as well as other EAS fellows, Dr. Tao Zeng, Dr. Ping Jing, Steve Sjostedt, and Amy Sullivan for their help on the completion of my thesis. Thank all my friends in Atlanta for all great time we have enjoyed together here.

Thank my relatives and friends in China, thank my girlfriend Jade, thank my sister Effie, and finally, thank my parents for all of their love and support throughout my life.

TABLE OF CONTENTS

LIST OF TABLES

LIST OF FIGURES

LIST OF SYMBOLS AND ABBREVIATIONS

BL	Boundary Layer
CBIV	Carbon Bond IV Mechanism
CCF	Cloud Correction Factor
FT	Free Troposphere
GTE	Global Tropospheric Experiment
NASA	National Aeronautics and Space Administration
NCAR	National Center for Atmospheric Research
NMHCs	Non-Methane HydroCarbons
RACM	Regional Atmospheric Chemistry Mechanism
RADM	Regional Acid Deposition Model
SAPRC	Statewide Air Pollution Research Center mechanism
TRACE-P	TRAnsport and Chemical Evolution over the Pacific
VOCs	Volatile Organic Compounds

All species are listed in the Appendix.

SUMMARY

This work has focused on showing the differences among four different NMHC oxidation mechanisms: GT (Georgia Tech) version of the Lurmann mechanism, CBIV (Carbon Bond IV) mechanism, RACM mechanism (Regional Atmospheric Chemistry Mechanism), and SAPRC (Statewide Air Pollution Research Center) mechanism. This study was carried out to characterize these mechanisms using both specified NO_x/NMHC gas mixtures and observational data from NASA's TRACE-P campaign.

The differences among these mechanisms were found to be mainly driven by the use of different kinetic data and the specifics of each oxidation scheme. In the test runs, the differences between mechanisms were shown to be dependent on the levels of NO_x and NMHC, as well as the reactivity of NMHC species used. Typically, the mechanism differences seen in the product species from a given NMHC were larger at higher levels of NO_x. Propane had the smallest impact on all product species, whereas propene had the largest. Differences in the predicted levels of OH and HO_2 were much smaller compared to those for CH_3O_2 and CH_2O due to the fact that HO_x species were generally less sensitive to the presence of NMHCs.

During TRACE-P, which involved flights over only marine areas that were slightly polluted by the inflow of pollutants, the alkanes were the dominant NMHC family. Thus, most of the model runs involved relatively low levels of NMHCs and NO_x. As a result, the levels of OH, HO_2, CH_3O_2, and CH_2O predicted by the four mechanisms were not dramatically different. A net O_3 increase was found only in areas where the NMHC reactivity was high. Because of the similar O_3 destruction rates given by all four

mechanisms, the difference in O_3 tendency among these mechanisms was mainly determined by the O_3 formation rate. A significantly higher (e.g., ~30%) O_3 formation was found in the Lurmann mechanism than in CBIV due to the stronger contribution from the NO/RO_2 channel in this mechanism. This resulted in a difference in the O_3 tendency of a factor of 1.5. For the other two mechanisms the difference was somewhat smaller, closer to a factor of 1.3. A major need in terms of future studies will be that of examining these same four mechanisms with a data set that enfolds observations in regions having very significant levels of anthropogenic pollution.

CHAPTER 1

INTRODUCTION

1.1 Overview of Tropospheric Chemistry

Free radicals have been considered as critical species in the troposphere since the early 1970s (Levy, 1971, 1972), and the most important among them is the OH free radical. OH can react with most atmospheric trace gases, some of which are important to climate change, e.g., O_3, CH_4. HO_x ($OH+HO_2$) radicals together with nitrogen oxides are also critical to the formation and destruction of O_3. Non-methane hydrocarbons (NMHC) can also be oxidized by the OH radical and some other oxidants such as O_3 and the NO_3 radical. The products include CO and CO_2 as well as intermediate species, e.g., organic perxoy radicals (RO_2). RO_2 may react with NO to form NO_2 whose photolysis produces oxygen atom which leads to O_3 formation or with HO_2 and other RO_2 species to generate peroxides, carbonyls, organic acids, or other oxygen-contained species. The reactions of RO_2 radicals with NO may also lead to the formation of organic nitrates such as peroxyacetyl nitrate (PAN) which has a longer lifetime than NO_x in the troposphere and thus can serve as a temporary reservoir for nitrogen. For example, through long-range transport, PAN can be decomposed to release NO back into the atmosphere which can then affect the concentrations of OH and O_3. Thus, since in many cases NMHC chemistry can be a very important component of the overall chemistry for a region, we need to have a comprehensive understanding of this chemistry if we are to have an overall understanding of tropospheric photochemistry.

The impact of NMHC on ozone formation in the troposphere has been recognized for a long time (Chameides and Walker, 1973; Crutzen, 1973, 1974). Further studies have showed that NMHC could play significant roles in tropospheric chemistry on a regional scale under polluted conditions (Kasting and Singh, 1986; Liu et al., 1987; Trainer et al, 1987; and Lin et al., 1988). Since then, great effort has been made to modeling this chemistry to quantify the effects of NMHC in the troposphere. Hough (1991) estimated that the contribution from organic peroxy radicals other than methyl peroxy radical to photochemical ozone production was less than 10%, but the contribution from HO_2 generated by NMHC oxidation was not counted. Strand and Hov (1994) calculated that a 50% reduction in VOC emission over the northern hemisphere would lead to a 1.6×10^{10} molecules/cm^2/s decrease in the ozone production rate from the original rate of 16.6×10^{10} molecules/cm^2/s, which was close to a 10% drop. Wang et al. (1998) made a sensitivity test in which the NMHC emissions were ignored, and the results showed that ozone concentrations decreased by 10-20% in the lower troposphere and the global mean OH concentration increased by 20% because of the elimination of NMHC. Houweling et al. (1998) concluded that the photochemical ozone production increased by 40% due to NMHC, which was equivalent to a 17% increase of the tropospheric ozone column density, but OH was depleted by NMHC over the continents. Poisson et al. (2000) also stated that the NMHC oxidation accounted for a 20-30% increase in ozone concentration for the remote marine atmosphere, but decreased the OH levels by 10-20 in the marine boundary layer. Obviously, a more accurate understanding of the mechanistic details within each model would help clarify the magnitude of the impact from NMHC chemistry on tropospheric O_3 and OH.

1.2 Previous Studies Involving Intercomparisons of NMHC Mechanisms

The chemical mechanism is a critical part of any air quality model, and NMHC chemistry is a major component in the overall chemical mechanism, especially when the research involves the presence of photochemical pollutants. Since the early 1980s, several chemical mechanisms have been used to simulate the atmospheric oxidation of NMHCs and to predict ozone formation as well as other oxidants for purpose of designing control strategies for O_3. However, it was found impossible to treat all photochemical processes explicitly in an oxidation mechanism because the resulting chemical system would contain nearly 20000 or more reactions involving several hundred organic reactants and products (Dodge, 2000). Therefore, a balance must be found between the accuracy of the simulation and computing efficiency, resulting in some simplifications in the NMHC oxidation mechanisms. Generally, lumped or surrogate species are introduced to represent a chemical family containing chemically similar species, and this method has been widely used in almost every chemical mechanism but in different ways.

For example, the oxidation of propane by the OH radical starts with the H-abstraction to generate propyl radical $C_3H_7\cdot$, and the propyl radical reacts with O_2 to form a propyl peroxy radical, $C_3H_7O_2\cdot$, as shown in reactions R1.1 and R1.2 below:

(R1.1) $C_3H_8 + OH \rightarrow C_3H_7\cdot + H_2O$

(R1.2) $C_3H_7\cdot + O_2 + M \rightarrow C_3H_7O_2\cdot$

In the troposphere, propyl peroxy radicals may react with NO to produce propoxy radicals $C_3H_7O\cdot$ or propyl nitrates $C_3H_7ONO_2$, or react with NO_2 to form propyl peroxynitrates RO_2NO_2, which can decompose back to its reactants. $C_3H_7O\cdot$ may also react with O_2 to form HO_2 and CH_2O. In addition, it may react with HO_2, or undergo self-reaction, or react with other peroxy radicals to produce a variety of oxygenated hydrocarbon species. The whole process is so complicated that it has to be simplified, and the methods of simplification are different in different mechanisms.

In the Georgia Tech (GT) version of the Lurmann mechanism, two isomeric propyl peroxy radicals are produced initially, and then they react with NO and HO_2, respectively, or undergo self-destruction. The products include aldehydes, ketone, peroxides, and propanols.

(R1.3a) $C_3H_8 + OH \rightarrow n\text{-}C_3H_7O_2\cdot + H_2O$

(R1.3b) $C_3H_8 + OH \rightarrow i\text{-}C_3H_7O_2\cdot + H_2O$

In the structure-lumped CBIV mechanism, propane is considered equivalent to 1.5 single C-C bond units, PAR, at first, and PAR can react with OH to generate two peroxy radicals, RO_2 and RO_2R, which represent primary and secondary peroxy radicals, respectively. These two peroxy radicals further react with NO to produce aldehydes, nitrate, and secondary organic oxy radicals.

(R1.4a) $PAR + OH \rightarrow RO_2\cdot$

(R1.4b) $PAR + OH \rightarrow RO_2R\cdot$

In the RACM mechanism, propane is labeled as HC3 which reacts with OH to produce peroxy radical, aldehydes, formic acid, glyoxal, OH, HO_2, and formaldehyde. But the whole process is generalized in one stoichiometric reaction:

(R1.5) $HC3 + OH \rightarrow 0.583\ HC3P + 0.381\ HO_2 + 0.335\ ALD_2 + 0.036\ ORA1 + 0.036\ CO + 0.036\ GLY + 0.036\ OH + 0.01\ CH_2O + H_2O$

Similarly, propane is labeled as ALK2 in the SAPRC mechanism, and its oxidation by OH is also expressed in the following stoichiometric reaction:

(R1.6) $ALK2 + OH \rightarrow 0.246\ OH + 0.121\ HO_2 + 0.612\ RO_2R + 0.021\ RO_2N + 0.16\ CO + 0.039\ CH_2O + 0.155\ RCHO + 0.417\ ACET + 0.248\ GLY + 0.121\ HCOOH$

As shown above, the simplification for NMHC reactions could be quite different in different chemical mechanisms. In addition, the performance of a given chemical mechanism also depends on the kinetic data available such as reaction rate constants as well as the numerical algorithms used in the calculation. It is not surprising that differences in mechanisms lead to different results. Thus, an evaluation of these different mechanisms becomes very necessary. One way of doing this is comparing the results from smog chambers for the different mechanisms. Of particular interest here are sensitivity studies in which certain critical parameters are varied.

The focus of this study will involve the comparison of four NMHC oxidation mechanisms popularly used in recent years: the Lurmann, CBIV, RACM, and SAPRC mechanisms. In the text that follows some intercomparison studies involving different NMHC mechanisms are given based on the past ten years of effort.

Derwent (1990, 1993) compared a series of chemical mechanisms by implementing them in a two-layer photochemical trajectory model in a base case and then exploring their respective responses to the decreasing emissions of both NMHC and NO_x. Among the mechanisms discussed, of interest in this study are the Lurmann mechanism (Lurmann et al., 1986), RADM-II mechanism (the early version of RACM mechanism)

(Stockwell et al., 1990), Carbon Bond Mechanism - Version IV (CBM-IV) (Gery et al., 1988, 1989). The same precursor emissions, photolysis rate coefficients, and the life cycles of the secondary pollutants such as ozone, PAN, H_2O_2, and HNO_3 were applied. Additionally, identical inorganic chemistry, i.e., H-O-N-CO chemistry, and methane chemistry were assigned to each mechanism. As a result, the target of the study was to show the pure impact of the parameterization of NMHC oxidation and the subsequent reactions of photochemical peroxy radicals on the formation of several key secondary pollutants. The results showed that all three mechanisms successfully responded to the emission control scenarios in which either NMHC or NO_x concentrations were reduced by 50%, and the percentage changes for peak O_3 levels were within the range of 12-18%. The predicted peak O_3 concentration from the Lurmann and CBM-IV mechanisms were very close, but differed from that of the RADM mechanism by nearly 10%. Among the three mechanisms, concurrent peak concentrations of O_3, PAN, and H_2O_2 were found only when using the Lurmann mechanism.

Jefferies and Tonnesen (1994) compared the Carbon Bond IV (CB4) with the early version of SAPRC mechanism (SAPRC90, Carter, 1990) in a simulation using a Lagrangian box model. A process analysis method was applied to the smog chamber study which is based on a complete mass balance by which several particular characteristic reactivity parameters reflecting the differences between the two mechanisms were calculated. The simulation was made at a fixed initial VOC mixing ratio of 767 ppbv but with different initial NO mixing ratios ranging from 20 to 160 ppbv. The results showed that generally similar predictions were given by the two mechanisms in terms of total reactivity (measured as total O_x production) and maximal O_3

concentration although differences in NMHC lumping and aromatic chemistry resulted in different patterns for the temporal change in these two parameters. However, the SAPRC90 mechanism appeared to be more reactive and, as a result, produced a higher maximal O_3 level when NO_x level is low.

Olson et al. (1997) reported the results from the Intergovernmental Panel on Climate Change (IPCC) tropospheric photochemical model intercomparison (PhotoComp) which was a modeling study designed to test the consistency among mechanisms used to predict tropospheric ozone. Generally speaking, the differences between the mechanisms mainly resulted from the use of inconsistent photolysis rates for H_2O_2 and CH_2O (caused by their using different radiative transfer calculations) or from the use of different reaction rate constants for the HO_2 self-destruction reaction. The NMHC oxidation chemistry schemes for most mechanisms were derived from one of three sources, the Lurmann mechanism, RADM2, or Carbon-Bond IV. The relative errors for the predicted O_3 concentration doubled with the addition of NMHCs, but no obvious consistency of results was found as a function of these groups.

Kuhn et al. (1998) compared several chemical mechanisms of which eight were derived from the RADM2, Carbon-Bond IV, or Lurmann mechanisms. Actually it was a similar study with PhotoComp but with the emphasis on the more polluted environment for a region. A simple box model was used in the simulation for three different scenarios of which only one was with NMHC emission (polluted case). In this case, the mixing ratios of NMHC increased from 0 to 43 ppbC. Generally, the results from the Lurmann mechanism fell in the mid-range for most species (except for CH_2O). CBIV type mechanisms typically gave lower O_3 concentrations (20% less than the mean value on average). The lowest predicted concentrations for OH, CH_2O, and PAN were also found when using the CBIV type mechanisms. The highest H_2O_2 concentrations were always produced by RADM2 type mechanisms.

Luecken et al. (1999) compared RADM2 and CB4 mechanisms with an explicit mechanism mainly in order to describe the production and speciation of reactive oxidized nitrogen (NO_y). The simulation was made using a time-dependent one-dimensional model for three scenarios which represented low-emission rural, high-emission rural, and heavily polluted environments, respectively. In all three cases, the predicted O_3 concentrations from the CB4 mechanism were always higher than those based on the RADM2 mechanism, but the difference was small (typically less than 5%). The NO_y production in CB4 was also higher, especially under rural conditions, because less HNO_3 was produced, and thus less nitrogen was removed via dry deposition in the CB4 mechanism. The largest differences in NO_y species occurred for the rural cases in which the most important contributor to NO_y formation was isoprene. In each of the three scenarios, RADM2 gave higher PAN concentrations, and the difference between the two mechanisms was approximately 30%. The reasons for this difference appeared to be due to higher rates for PAN destruction and the competing C_2O_3/NO reaction used in the CB4 mechanism.

Dodge (2000) reviewed five chemical mechanisms often used in air quality simulation models (AQSMs). Among them were CB4, SAPRC, RADM2, and RACM, which is an update of RADM (Stockwell et al., 1997). The predictions from all mechanisms were compared against data of several smog chambers (UNC, UCR, TVA, CRISO, EPA, GM, and European smog chambers). For the CB4 mechanism, in 85% of the runs the model predicted maximum O_3 concentrations agreed within 30% of the observations for UNC and UCR chambers. The agreement was particularly good for model runs containing toluene, xylene, and isoprene in which the model over-predicted by only 5% on average. The disagreement between model calculations and observations for the alkene-containing runs were much bigger. For example, the butene-containing experiments were over predicted by over 50%. For the TVA and CRISO chambers, good agreement with experiments was obtained when VOC/NO_x ratios were high. However, when VOC/NO_x ratios were low (~4), the O_3 yields were underestimated by over 60%. The conclusion was that CB4 might under-predict O_3 concentrations when the levels of reactants were low. For the SAPRC mechanism, in 63% of the runs the model calculated maximum O_3 productions agreed within 30% of the experimental values from UNC and UCR chambers. On average, the SAPRC mechanism over-predicted maximum O_3 concentrations by 46% for those alkane-containing experiments, due to the low reactivity of alkanes. The agreement was also poor for isoprene-containing runs, with the average model under-prediction of 24%. Better agreement was found when using alkenes, aromatics, and formaldehyde. On average, the predicted O_3 concentrations were higher than the observations by 12%, reflecting a slight tendency of over-prediction for the SAPRC mechanism. For the RADM2 mechanism, the agreement for alkane-containing models runs was much better than that for the SAPRC mechanism, with the average difference being only 6%. The agreement for those alkene- and formaldehyde-containing runs was also excellent. However, the model did not well agree with experiments containing aromatics and isoprene, with the average differences of 21% and 42%, respectively. Overall, the RADM2 mechanism over-predicted O_3 concentration levels by only 4%. Compared to RADM2, the RACM mechanism over-predicted O_3 levels to a larger extent (on average by 13% for 20 experiments), but it predicted the timing of the O_3 peak in a better manner.

Jimenez et al. (2003) compared seven photochemical mechanisms using a zero-dimensional box model for a scenario representing a remote troposphere. Selected were all lumped mechanisms which included the Lurmann mechanism, CBM-IV, RADM2, RACM, and SAPRC99 (Carter, 2000). Results showed that most mechanisms produced similar concentrations of ozone, with the average deviation between 1% and 10%. RADM2 predicted the lowest O_3 concentration with a 25% deviation below average. Significant discrepancies among mechanisms existed in simulated concentrations of relatively long-lived species such as HNO_3, H_2O_2, and PAN. For PAN, the highest concentration was found when using the Lurmann mechanism, whereas the lowest was found in CB4, due to different rates for the reaction of aldehydes with NO_3 in the different mechanisms. As for H_2O_2 and HO_2, the highest prediction was also found in the Lurmann mechanism, whereas the lowest was given by RADM2. The differences in H_2O_2 and HO_2 were related as a result of inconsistent reaction rates for HO_2-to-H_2O_2 conversion and of different dependences of water-vapor concentration on the HO_2 self-destruction.

Based on these previous studies, a general trend for these mechanisms could be seen in terms of O_3 concentration. Typically, the CBIV mechanism tends to over-predict to the largest extent, and it becomes more obvious when the levels of reactants are low. Slight tendency of over-prediction is seen on the SAPRC and RACM (RADM) mechanisms. The results based on the Lurmann mechanism typically lie in between, but closer to those of the CBIV mechanism.

1.3 Objectives of This Study

This study is an intercomparison of four established photochemical mechanisms which have been widely used during the past several years. The focus of the study will be 1) how differences in the four NMHC chemistry mechanisms impact final photochemical results in terms of the concentration levels of product species, in all cases for the same set of NMHC conditions, i.e., concentration and species type; and 2) how these four mechanisms impact on the predicted results when actual field data are employed.

Chapter 2 will give a general description for all four mechanisms with the emphasis on the differences in the NMHC chemistry. Chapter 3 will take a brief look at the TRACE-P database which will be utilized in the model predictions of chapter 5. In chapter 4, the mechanisms will be examined by a group of specified NMHC/NO_x gas mixtures designed to be representative of different conditions in the troposphere. And Chapter 5 will compare the results from the same mechanisms using the NASA's TRACE-P (TRAnsport and Chemical Evolution over the Pacific) data set.

Major questions to be addressed in chapters 4 and 5 of this study are:

1) How do the differences in the lumping methods for the four mechanisms lead to the differences in model results?

2) How do variations in atmospheric conditions, e.g., different levels of photochemical precursors, affect the results from these mechanisms?

3) When using these four mechanisms, what is the impact of different families of NMHC on the concentrations of the critical photochemical species HO_x, CH_2O, and CH_3O_2?

4) How are the production and destruction of ozone influenced by different NMHC mechanisms?

5) As related to the NASA TRACE-P field program, how significant is the impact from using four different NMHC mechanisms?

CHAPTER 2

MODEL DESCRIPTIONS

2.1 Detailed Description of Original GT Lurmann Model

The model used in this study is a time-dependent (TD) photochemical box model which is similar to that used previously by Davis et al. (1993, 1996, 2001), Chen (1995), Crawford (1997), Crawford et al. (1997, 1999a), and Chen et al. (2001). Except for NO, basic input parameters like O_3, CO, CH_4, NMHCs (which will be discussed later), temperature, dew point, and pressure, are typically held constant over a diurnal cycle because they do not vary much at a given location during a given day. Model calculations can also be constrained by the following species: H_2O_2, CH_3OOH, HNO_3, PAN, CH_2O, CH_3OH, C_2H_5OH, HCOOH, and CH_3COOH. As for NO, it can not be treated as a constant because the partitioning of NO_x keeps changing diurnally. Instead, total short-lived nitrogen, which is defined as the sum of NO, NO_2, NO_3, N_2O_5, HONO, and HO_2NO_2, is held constant so that the predicted NO concentration matches the observed NO level at the appropriate time of day (Crawford, 1997; Crawford et al., 1999a). Consequently, the partitioning between these short-lived nitrogen species is determined by the photochemical mechanism.

Photolysis rate coefficients are calculated based on a DISORT 4-stream implementation of the NCAR Tropospheric Ultroviolet-Visible (TUV) radiative transfer code (Madronich and Flocke, 1998). A more detailed description of the photolysis rate calculation can be found in Crawford et al. (1999b). All model-calculated J-values were adjusted to reflect to actual cloud conditions. This was done by using cloud correction factor (CCF), which was defined by Davis et al. (1993, 1996).

Model-calculated species are assumed to be at quasi-steady state which means that the concentrations are integrated in time until their diurnal cycles no longer vary from day to day. Although the time-dependent model gives realistic predictions for short-lived species, it does not consider long-distance transport. As a result, there are still considerable uncertainties on the concentrations of certain species (e.g., HNO_3, PAN, etc.) which can be much affected by transport or physical removal processes. Final concentrations of all species presented in this text are diurnal averaged values, if not specified.

The overall chemical mechanism is divided into two components: HO_x-NO_x-CH_4 chemistry, and NMHC chemistry. The latter will be discussed in greater detail in the following text.

2.1.1 NO_x-HO_x-CH_4 Chemistry

The HO_x-NO_x-CH_4 chemistry is the core of the mechanism, containing 64 gas phase reactions, 12 photolytic reactions, and 14 heterogeneous removal processes for 7 species. It was designed to describe source and sink reactions for the species OH, HO_2, CH_3O_2, H_2O_2, CH_3OOH, etc., and some chemical intermediates such as $O(^1D)$ and H. All gas phase reaction rate constants and absorption cross section and quantum yield data for the photolytic processes are those taken from Demore et al. (1997) and Sander et al. (2002). Wet deposition rates are treated with an expression from Logan et al. (1981) that consists of a constant removal rate below 4 km and a rate that decreases exponentially with height above 4 km. Dry deposition rates are in the form of first-order removal rates that are applied only to data in marine boundary layer at altitudes lower than 1 km (Crawford, 1997).

In order to be reasonably and efficiently compared with the other three mechanisms for purposes of emphasizing the differences on NMHC chemistry in this study, we went through the HO_x-NO_x-CH_4 chemistry of other mechanisms and then made some modest changes to the Lurmann mechanism to make this modeling component identical for all four mechanisms. The major modifications consist of adding three new species, FROX (the adduct of HO_2+CH_2O), CH_3ONO (the adduct of CH_3O+NO), and CH_3ONO_2 (the adduct of CH_3O+NO_2), and their sink reactions, respectively. Other changes can be seen from some reactions between the NO_x species themselves.

2.1.2 NMHC Chemistry

NMHC chemistry is another important component of the mechanism and the major focus of this study. The NMHC chemistry used in the current mechanism is based on the condensed mechanism developed by Lurmann et al. (1986) with some modifications that were made later on by Crawford (1997). However, due to both the large number and the complexity of the NMHC reactions, some assumptions had to be made to simplify the NMHC mechanism to make it compatible with the model's computational ability. In Lurmann's condensed model approach, a specific organic molecule is used as a surrogate species to represent a chemical family containing chemically similar species. For example, in this mechanism all alkanes are lumped into three species: ethane, propane, and ≥ C4 alkanes (ALKA). Likewise, all alkenes are grouped into ethene and ≥ C3 alkenes (ALKE), and all aromatics are grouped into benzene and other aromatics (AROM). Isoprene, however, is treated explicitly as a stable biogenic organic species, as discussed later. Oxygenated hydrocarbons are treated in a similar way. For instance, aldehydes are represented by formaldehyde and ≥ C2 aldehydes, and ketones are represented by three different species, acetone, methyl ethyl ketone (MEK), and methyl vinyl ketone (MVK). Four species such as unsaturated dicarbonyl (DIAL), glyoxal (GLYX), methacrolein (MACR), and α-dicarbonyl (MGGY) are used to denote other carbonyl compounds. Except for methyl hydrogen peroxide, 15 other peroxides are produced and treated explicitly in this mechanism. Four of them originate from alkanes (ETP, n/i-R3P, and RAP), two from alkenes (EP and PP), one from isoprene (XAP1), two from aromatics (TP and ZP), and six from carbonyls (DAP, HEP, MCP, RP, TCP, and XAP2). Other oxygenated hydrocarbons include two organic acids (formic acid and acetic acid), one alcohol (methanol), and some nitrates. Peroxy radicals (RO_2) are also represented rather explicitly in that a total of 13 peroxy radicals are produced from methane, ethane, propane, ≥ C4 alkanes, ethene, ≥ C3 alkenes, isoprene, aromatics, MACR, MEK, and MVK, respectively.

Additional modifications in the mechanism were made because the original Lurmann mechanism was designed to reproduce smog chamber observations, and thus some assumptions in this mechanism were not appropriate in representing the remote environment being studied in this analysis. First of all, additional reactions for remote environments were included. For example, isoprene chemistry was added into the mechanism since isoprene is highly chemically reactive and can have a considerable impact on the chemistry of remote continental areas. (Note, however, since most of this work was focused on marine areas, no isoprene was detected in the field data and it therefore had no impact on the results of this paper.) In Lurmann's condensed mechanism, organic peroxides (ROOH) are also treated as final products. Thus, loss pathways such as reaction with OH, photodisassociation, or heterogeneous removal, were not included. These processes can have a significant impact on OH levels so that they are included in our modified mechanism. Likewise, the chemistry of organic acids and alcohols was taken into account in the new mechanism. In addition, some species previously lumped into families have been treated explicitly in the new mechanism. For instance, in Lurmann's condensed mechanism all ketones were represented by only one surrogate species. Acetone, however, is very important source of HO_x in the upper troposphere. Therefore, acetone was treated separately from other ketones in the modified Lurmann mechanism. The detailed lists of reactions and species can be found in appendix A.

2.2 Development of An Operational Lurmann Model

The execution of our version of the Lurmann model is done by running an executable program derived from its source code. This means that it is first necessary to build up a chemical mechanism, and then to collect the relevant data and information from the mechanism so as to convert the data into several subroutines of the driver code. These subroutines correspond to several key components such as the time derivatives for each species (differential equations), partial derivatives of the differential equations (Jacobian matrix), reaction rate constants, as well as photo-stationary-state equations for purposes of estimating steady-state concentration. However, this is very time-consuming and it is also relatively easy to make mistakes when done manually with a mechanism containing as many as 250 reactions. Therefore, several improvements were made in the model as detailed in the following subchapters.

2.2.1 Addition of Jacobian Matrix

The significance of using a Jacobian matrix for a set of partial derivatives in a differential equation is that it can solve the stiffness problem. For a system of differential equations f(x), the Jacobian matrix of partial derivatives can be expressed as:

$$J_{ij} = \frac{\partial f_i}{\partial x_j} \qquad (2.1)$$

where x_j is the time derivative of the jth variable of the differential equation.

In our previous version of the Lurmann model, we did not give an analytical expression for the Jacobian matrix but instead estimated it by numerical differencing in the code because it costs less time in coding. However, the solution is more reliable if one provides the partial derivatives via the Jacobian matrix (Davis, 1984), although the numerical differencing approach is in some cases cheaper, depending on what problem is being solved. Here we have given an accurate analytical formula for the Jacobian matrix and used it throughout this paper. The results have demonstrated that very little difference exists between the two methods, but the solution is more stable in the Jacobian case and it takes a bit less time to run the model.

2.2.2 Development of Modeling Tools

As mentioned earlier, the conversion of a chemical mechanism to a source code is challenging in that it takes a great deal of time and mistakes are likely. Generally it takes at least three days to write down the code of a mechanism whose size is approximately 250 reactions. Several more days are also required to check for any possible mistakes by doing test model runs. This makes it extremely troublesome when continual changes to the mechanisms are likely to occur by including or excluding certain species, e.g., halo-hydrocarbons. Thus, in order to have a more flexible (time efficient) model, we have found it useful to use an equation assembler and Jacobian matrix assembler to do these jobs semi-automatically.

In this case, two input spreadsheets are needed for any given chemical mechanism. The first one represents a list of all the species concerned in a numerical order. Then the whole mechanism is typed onto the second spreadsheet. Each species as well as its stoichiometric coefficient occupies a single cell, and every reaction is given a number to be identified. All reactions are labeled differently according to their types. Once the input is done, a set of FORTRAN programs is run to automatically generate the most important subroutines of the code for the time-dependent model. Those subroutines include differential equations, partial derivatives of the differential equations (Jacobian matrix), reaction rate constants, and photo-stationary-state equations. Although some other work on the driver code needs to be done manually for the new mechanism, using these new tools the major parts of the code can be completed in minutes. As a result, it typically takes less than a day to complete the entire coding. Equally important, the final product represents a much more reliable result.

2.3 General Description of CBIV, RACM, and SAPRC Mechanisms

Three other commonly employed NMHC mechanisms are presented in this study for purposes of showing the level of difference that can result in some model products when compared to those from the modified Lurmann mechanism. As mentioned earlier, the HO_x-NO_x-CH_4 chemistry for these three mechanisms is exactly the same as that of the Lurmann mechanism. As for the NMHC chemistry, all three mechanisms either apply lumped molecule methods (e.g., RACM and SAPRC mechanisms) or lumped structure methods as done in the carbon bond mechanism (CBIV). The main features as well as differences of the three mechanisms relative to the Lurmann mechanism are listed in Table 2.1.

Table 2.1. Characteristics of the four mechanisms.

Mechanisms	Lurmann	CBIV	RACM	SAPRC
Number of reactions	254	210	258	221
Number of species				
NO_x-HO_x-CH_4 chemistry	22	22	22	22
NMHC chemistry				
Alkanes	3	1	4	5
Anthropogenic alkenes	2	1	4	2
Biogenic alkenes	1	1	3	2
Aromatics	2	2	3	2
Carbonyls	9	9	9	16
Peroxides	16	1	3	2
Organic acids	2	5	2	5
Peroxy radicals	13	9	19	9

2.3.1 CBIV Mechanism

The Carbon Bond approach was first published by Whitten et al. (1980), and since then has been further developed into the most current version, i.e., Carbon Bond Mechanism - Version IV (CBM-IV) (Gery et al., 1988, 1989). As a lumped structure method, the lumping of NMHC species in CBM-IV is done according to their bond types. In another words, the organic species are decomposed into several basic functional groups determined only by chemical bonds. For example, all single C-C bonds in any given NMHC species are considered the same no matter what kind of molecule they are in and no matter where they are located. Consequently, much fewer lumped species are needed in CBM-IV to represent the large number of organic reactants and products as compared to the Lurmann mechanism. Thus, The CBM-IV has only 81 reactions in total.

In CBM-IV, all single C-C bonds are represented by PAR (paraffin) and all double C=C bonds except ethene are represented by OLE (olefin). Ethene is treated explicitly because it is much less reactive than other alkenes and has a high emission rate. By following this approach, all alkanes and alkenes can be interpreted in different ways. For instance, both n-butane and i-butane that contain four alkyl carbon atoms are represented as four PAR units, and propene is represented by one PAR and one OLE. As the most important biogenic alkene, isoprene is also treated explicitly in CBIV due both to its high reactivity, compared to most other alkenes, and to its widespread large source. Other biogenic alkenes such as terpenes are represented by structure-lumped species. For example, α-pinene is decomposed into 0.5 OLE, 6 PAR, and 1.5 ALD2. Aromatics are represented by two species, TOL, for mono-substituted aromatics, and XYL, for disubstituted aromatics. Therefore, ethylbenzene is a combination of one TOL and one PAR unit. Benzene is specially treated as one PAR in CBIV because of its low reactivity.

As for carbonyls, formaldehyde is handled explicitly since it is highly reactive and its oxidation scheme is quite different from that of other aldehydes. The carbonyl in all other alkyl aldehydes is represented by a two-carbon-atom surrogate ALD2 that has one C-C bond and one C=O bond (R-CHO, R>H). Internal alkenes are also considered to act like aldehydes. For example, both trans-2-butene and cis-2-butene are represented by two ALD2 units. Two other species are included to represent methylglyoxal and the production of aromatic oxidation, respectively. Ketones are generally represented by several PAR units because they are less reactive than aldehydes. For example, acetone is considered to have three PAR units, methyl ethyl ketone has four PAR units, and methyl vinyl ketone is decomposed into one OLE and two PAR units.

In order to simplify the process of organic oxidation by OH in the atmosphere, a universal peroxy radical species RO_2 is used in CBM-IV. RO_2 is supposed to represent all peroxy radicals which can react with NO to form NO_2. The introduction of RO_2 successfully avoids the problem that every organic lumped and surrogate species has its own individual peroxy radical, thus reducing the size of the mechanism. This is also one of those major characteristics that make the Carbon Bond Mechanism so different from the Lurmann mechanism. In order to identify the sinks of all peroxy radicals, two counter species are added. XO_2 represents NO-to-NO_2 conversion by RO_2, and XO_2N represents the nitrate formation from RO_2.

CBM-IV is such a highly generalized mechanism that it works well in several air quality models. However, in this paper we chose to use a more detailed Carbon Bond mechanism (CBM-EX) (Gery et al., 1989) which forms the basis of CBM-IV. (Note, CBM-EX is not as simplified as CBM-IV but it gave a more complete coverage of the organic species found in the NASA TRACE-P field-program observations of hydrocarbons that have been examined in chapter 5.) With some modifications we made on this mechanism, it is still a relatively compact mechanism.

Additional changes in the CBM-EX relative to CBM-IV involve the former having more lumped and surrogate species are used. For example, in CBM-EX, acetone is explicitly treated, KET is used to represent all ketone carbonyl groups, and another species is added to represent benzaldehyde. Other carbonyl species such as MACR and MVK are also represented as they are in the Lurmann mechanism. As for peroxy radicals, not only methyl hydrogen peroxy radical is explicitly treated in CBM-EX, but other peroxy adjustments are also made. For example, the universal peroxy species RO_2 in CBM-IV is replaced by two new lumped species in CBM-EX. RO_2 is used to represent primary peroxy radicals, whereas RO_2R is used to represent secondary peroxy radicals. Additionally, some other specific peroxy radicals originating from species such as dimethyl-alkanes, aldehyde, acetone, ethene, toluene, xylene, and cresol, are all separately represented in CBM-EX. Besides formic acid and acetic acid, three other acidic species are added to represent acids formed from the oxidation of ethene, olefin, and aromatics, respectively. Peroxides in CBM-EX are all lumped into one species, PROX. Finally, three other operator species are added to account for secondary organic oxy radical, paraffin loss, and paraffin-to-peroxy conversion, respectively.

For simplification, this modified CBM-EX mechanism will be referred to as the CBIV mechanism in this text.

2.3.2 RACM Mechanism

RACM (Regional Atmospheric Chemistry Mechanism) was developed by Stockwell et al. (1997), and it is actually an updated version of RADM (Regional Acid Deposition Model) (Stockwell, 1986; Stockwell et al., 1990) with some improvements and revisions on both the reaction rate constants and the chemical mechanism itself.

In RACM, four species are used to generalize alkanes. Except for ethane, which is treated explicitly, all other alkanes, alcohols, esters, epoxides, and alkynes are separated and then represented by three lumped alkane species HC3, HC5, and HC8. The classification is based on the reaction rate constants of the alkanes with OH (k_{OH}) at 298K, 1atm. For the alkanes with k_{OH} lower than 3.4×10^{-12} cm^3 $(molec.\cdot s)^{-1}$, e.g., ethyne, propane, and n-butane, they are represented by HC3; for those whose k_{OH} are higher than 6.8×10^{-12} cm^3 $(molec.\cdot s)^{-1}$, e.g., heptane and octane, they are represented by HC8; and for those falling between 3.4×10^{-12} and 6.8×10^{-12} cm^3 $(molec.\cdot s)^{-1}$, e.g., n-pentane and hexane, they are represented by HC5. The two threshold values were determined from an analysis of regional emissions of NMHCs (Middleton et al., 1990).

Four model species are used to represent all the anthropogenic alkenes. Ethene is treated separately because of its relatively low reactivity with OH and its relatively high concentration. Terminal alkenes (the double bond attached to a C atom at the end of the molecule) such as propene are represented by OLT, whereas internal alkenes (the double bond located within the molecule) are represented by OLI. 1, 3-butadiene and other anthropogenic dienes are lumped into another species DIEN since their reaction rate constants with OH are quite different from those of other internal alkenes. Three other alkene species are used to represent the biogenic sources. As in the Lurmann mechanism, isoprene is treated explicitly, while API and LIM are added to represent α-pinene and other cyclic terpenes with one double bond, and d-limonene and other cyclic diene-terpenes, respectively. Unlike the Lurmann mechanism, benzene is not treated explicitly but represented by TOL because of its low reactivity. Other aromatic species used in RACM are XYL that represents xylene and more reactive aromatics, and CSL that represents cresol and other hydroxy substituted aromatics.

There are also a total of nine carbonyls species in RACM. However, some of them do not represent exactly the same thing as in the Lurmann mechanism. Similarly, formaldehyde is considered explicitly, but ALD is used to represent acetaldehyde and higher saturated aldehydes. Acetone, on the other hand, is not treated explicitly but combined with higher saturated ketone to represent all ketones in the RACM mechanism. As in the Lurmann mechanism, unsaturated dicarbonyls (DCB), glyoxal (GLY), methacrolein (MACR), and methylglyoxal as well as other α-dicarbonyl (MGLY) are included in RACM to represent some other carbonyl compounds. Moreover, the isomerization of alkoxy radicals created by the oxidation of higher alkanes leads to the introduction of two surrogate species dealing with hydroxy ketone and unsaturated dihydroxy dicarbonyl, respectively. Unlike the Lurmann mechanism, peroxides are highly simplified in the RACM mechanism. Except for methyl peroxide, all other higher peroxides are represented by OP2. And another species PAA is used to represent perxoyacetic acid and higher analogs. The treatment of ordinary organic acids and alcohols in RACM resembles that of the Lurmann mechanism.

In RACM peroxy radicals are treated in more detail than in the Lurmann mechanism. Each stable lumped or surrogate organic species reacts with OH through a pseudo first-order reaction to produce a specific RO_2 of its own. Thirteen peroxy radicals are created this way. Additionally, three RO_2 species are used to represent saturated acyl peroxy radicals, unsaturated acyl peroxy radicals, and peroxy radicals formed from ketones, respectively. Two other peroxy radicals, OLNN and OLND both represent the products of NO_3-alkene reactions. Their difference is that OLNN primarily produces nitrate, whereas OLND tends to produce carbonyls and NO_2. Similar to CBIV, an artificial chemical operator XO_2 is used in RACM to account for the extra NO-to-NO_2 conversion when one peroxy radical reacts to form another peroxy radical that can also convert NO to NO_2.

2.3.3 SAPRC Mechanism

SAPRC (Statewide Air Pollution Research Center) mechanism was first introduced by Carter (1990), and was designed to reflect the reactivity scale of various volatile organic compounds (VOCs). It has been updated several times since then (Carter et al., 1995, 1997; Carter, 2000), and was developed with the idea of serving in urban and/or regional models.

As in the case of the Lurmann and RACM mechanisms, SAPRC also uses a lumped parameter approach. The reaction rate constants and the product yield parameters of some lumped species are determined by the composition of a given VOC mixture. Thus, they can be different from case to case. However, it is not realistic to use this approach in the time-dependant model calculations done in this study. Therefore, we have chosen a fixed-parameter version of the SAPRC mechanism to implement in this paper. This fixed-parameter SAPRC mechanism includes all the recent updates on input parameters such as cross-sections and rate constants, and is similar to RACM in that all the reaction rate constants and the product yield parameters listed in the mechanism are derived from an ambient mixture analysis from the reactivity simulations of Carter (1994, 2000).

In the SAPRC mechanism, alkanes and other non-aromatic compounds that only react with OH are lumped in a similar but more specific way than that in the RACM mechanism. Five lumped species, from ALK1 to ALK5, are used to represent all alkanes. ALK1, which is primarily ethane, represents the alkane whose rate constant of the reaction with OH (k_{OH}) under 298k and 1 atm between 2×10^2 and 5×10^2 ppm^{-1} min^{-1} (equivalent to 1.4×10^{-13} and 3.4×10^{-13} cm^3 $(molec.\cdot s)^{-1}$, respectively). ALK2, which is primarily propane and ethyne, represents alkanes with k_{OH} falling between 5×10^2 and 2.5×10^3 ppm^{-1} min^{-1} (equivalent to 1.7×10^{-12} cm^3 $(molec.\cdot s)^{-1}$). Likewise, the ranges for k_{OH} of ALK3 (e.g., butane) and ALK4 (e.g., n-pentane) are 2.5×10^3 to 5×10^3 ppm^{-1} min^{-1} (equivalent to 3.4×10^{-12} cm^3 $(molec.\cdot s)^{-1}$), and 5×10^3 to 1×10^4 ppm^{-1} min^{-1} (equivalent to 1.4×10^{-11} cm^3 $(molec.\cdot s)^{-1}$), respectively. For those that have k_{OH} higher than 1×10^4 ppm^{-1} min^{-1}, they are represented by ALK5.

Two lumped species are used to represent all anthropogenic alkenes other than ethene, which is also treated separately in the SAPRC mechanism. Alkenes with k_{OH} less than 7×10^4 ppm^{-1} min^{-1} (equivalent to 9.5×10^{-11} cm^3 $(molec.\cdot s)^{-1}$) are represented by OLE1, and more reactive alkenes whose k_{OH} are higher than 7×10^4 ppm^{-1} min^{-1} are represented by OLE2. Isoprene is again one of the surrogates for biogenic alkenes, and TERP represent the biogenic alkenes other than isoprene, primarily terpenes. The same approach is used to generalize aromatics. Aromatics with k_{OH} lower than 2×10^4 ppm^{-1} min^{-1} (equivalent to 2.7×10^{-11} cm^3 $(molec.\cdot s)^{-1}$) are represented by ARO1, primarily toluene, and more reactive aromatics with k_{OH} higher than 2×10^4 ppm^{-1} min^{-1} are represented by ARO2, primarily xylene. Benzene and other inactive aromatics are lumped using reactivity weighing based on the ratios of their k_{OH} to that of toluene.

More lumped and surrogate species are used for the carbonyls in SAPRC than in Lurmann and RACM mechanisms. First of all, besides the explicitly treated formaldehyde and acetaldehyde, higher saturated aldehydes are lumped into RCHO. In addition, BALD is added to represent aromatic aldehydes, e.g., benzaldehyde. Ketones and other saturated non-aldehyde oxygenated species are generalized by three species. Except for acetone, other ketones are again separated by their reactivity with OH radical. For ketones with k_{OH} higher than 5×10^{-12} cm^3 $(molec.\cdot s)^{-1}$, they are represented by methyl ethyl ketone (MEK), and the less reactive ketones (k_{OH} less than 5×10^{-12} cm^3 $(molec.\cdot s)^{-1}$) are represented by PROD2. Methyl vinyl ketone (MVK) is the surrogate species for all unsaturated ketones. The other four carbonyl species, glyoxal (GLY), methylglyoxal (MGLY), acrolein and methacrolein (MACR), and biacetyl (BACL), play similar roles as they do in both Lurmann and RACM. But another species ISOPROD is added in SAPRC to represent unsaturated aldehydes other than acrolein and methacrolein that produced by isoprene oxidation. Additionally, three carbonyl lumped species, DCB1, DCB2, and DCB3, are used to represent different aromatic fragmentation products that undergo various subsequent reactions. Organic acids are treated specifically in SAPRC. Except for formic acid and acetic acid, three other lumped acid species are used to represent higher organic acid, peroxy acetic acid, and higher organic peroxy acid, respectively.

Similar to CBIV mechanism, an approximation is applied in SAPRC involving the fact that several chemical operator species are used to represent the peroxy radicals in order to substantially reduce the number of RO_2 required. After updates were made on the earlier versions of the SAPRC mechanism, only nine RO_2 species now appear in the latest version of SAPRC. As a result, there are nearly 30 less reactions in this version than in both Lurmann and RACM, and its size is actually very close to that of CBIV. Among the remaining RO_2 species, three of them are pure chemical operators that account for NO-to-NO_2 conversion with HO_2 formation (RO_2R), NO-to-NO_2 conversion without HO_2 formation (R_2O_2), and NO consumption with alkyl nitrate formation (RO_2N), respectively. Four other peroxy radicals are used to represent different acyl RO_2 species such as acetyl peroxy radical, peroxy propionyl and higher peroxy acyl radicals, peroxy radical produced from aromatic aldehyde and from methacrolein or other acroleins. Two additional RO_2 species are introduced to take care of phenoxy radicals formed from the oxidation of aromatics.

CHAPTER 3

TRACE-P DATABASE

The field data used in this paper were collected during NASA's TRACE-P campaign. TRACE-P (TRAnsport and Chemical Evolution over the Pacific) was a two-aircraft (DC-8 and P-3B) mission over the western Pacific in March and April 2001 and represented yet another study in the series of GTE missions. The purpose of this mission was to better understand the pathways and chemical evolution of outflow from eastern Asia and how it was affecting the global atmosphere. The two aircraft operated out of two air bases, one in Hong Kong and the other in Japan. In this chapter some details are provided to illustrate the observational database and the distributions of several important species measured during TRACE-P.

3.1 Geographic Distribution of Measurements

The geographic distribution of the flight tracks for the DC-8 and the P-3B are shown in Figure 3.1. From these we can see that the latitude range from 5°N to 50°N was very well covered by the two aircraft, making this field study a good monitor of the outflow of pollution from eastern Asia.

During TRACE-P, all critical photochemical precursors, such as O_3, CO, NO, H_2O, and UV flux, were measured. The concentrations of a number of NMHC species

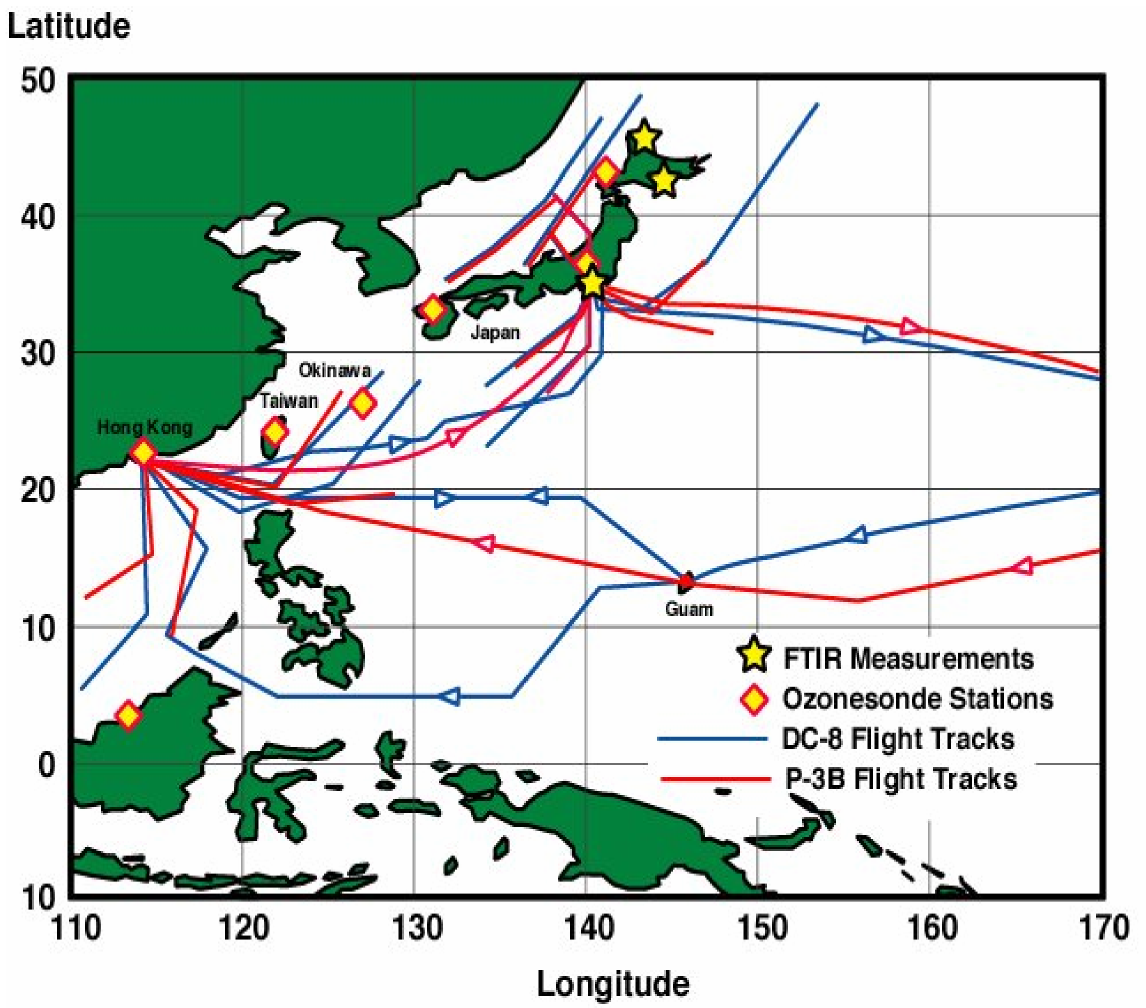

Figure 3.1. Nominal flight tracks for the NASA aircraft during TRACE-P mission.

were also recorded, the details of which will be given later. Moreover, some other important physical and meteorological parameters needed for the model calculations, including time, altitude, longitude, latitude, pressure, temperature, dew point, were recorded during most flights.

3.2 Criteria for Choosing Areas for Intense Study and Data-filtering

Since most variables were measured with different time resolutions during TRACE-P, in order to build up an input file for the model runs, we merged all the variables to a common time interval of 60 seconds. Excluding the transit flights, a total of 18,251 runs were thus produced, of which 8,746 were those generated by the DC-8, and 9,505 by the P-3B. After filtering out the runs missing one or more critical variables and those time periods associated with taking off or landing, 13,865 runs remained as shown in Table 3.1.

Table 3.1. The statistics of the TRACE-P database.

Number of Model Runs	DC-8	P-3B	TRACE-P
Total	8745	9506	18251
After Filtering (takeoff and landing)	7078	6787	13865
Within Working Areas	4043	4447	8490
With NMHC (at least one)	2388	2240	4628
After Interpolation and Extrapolation	3801	4423	8224

As stated earlier, among the major objectives of the TRACE-P study were identifying the major pathways for Asian outflow into the western Pacific and the chemical characterization of this outflow such that it could be used for a quantitative model analysis. Thus, areas needed to be defined that were representative of the Asian outflow. Consequently, we identified the latitude range of 5°N to 45°N as the target area. From 5°N to 25°N, the western border is seen as defined by the Pacific coast with the eastern border being longitude 145°E. From 25°N to 45°N, the western border is again the Pacific coast but the eastern border is now seen as longitude 155°E. The difference in concentrations of several measured species between the east-west boundaries of 5°N to 25°N and 25°N to 45°N reflects the latitudinal concentration gradients for these critical species (Davis et al., 2003). From Table 3.1, we can see that 8,490 runs fall within the above cited working areas.

During the TRACE-P study, NMHC measurements were only available for about 30% of the time, and in most cases the time resolution of the measurements was less than 60 seconds. As shown in Table 3.1, of the 8,490 model runs in our designated working areas, only approximately half of these (4,628 runs) encompassed at least one NMHC species measured. However, since for this analysis we would like to have as many NMHC measurements as possible, interpolation methods were considered. Thus, gaps of less than 5 minutes were typically filled with interpolated values; whereas, for time gaps longer than 5 minutes, only extrapolation by 60 seconds was applied to both ends. As a result, we were able to use most data (97%) we had in the coastal regions based on having NMHC input. Several other non-critical variables with lower time resolution than 60 seconds (e.g., acetone and DMS) were also treated the same way as described above.

All of the data analysis and discussion in Chapter 5 will be based on this near coast TRACE-P data.

3.3 Latitudinal and Altitudinal Distributions of Several Key Species

The latitudinal and altitudinal distribution of the airborne data recorded during TRACE-P are those shown in Figure 3.2. This database, with over 8,200 observations, can be divided into several smaller components according to several criteria, which will be discussed in greater detail in the subsequent text.

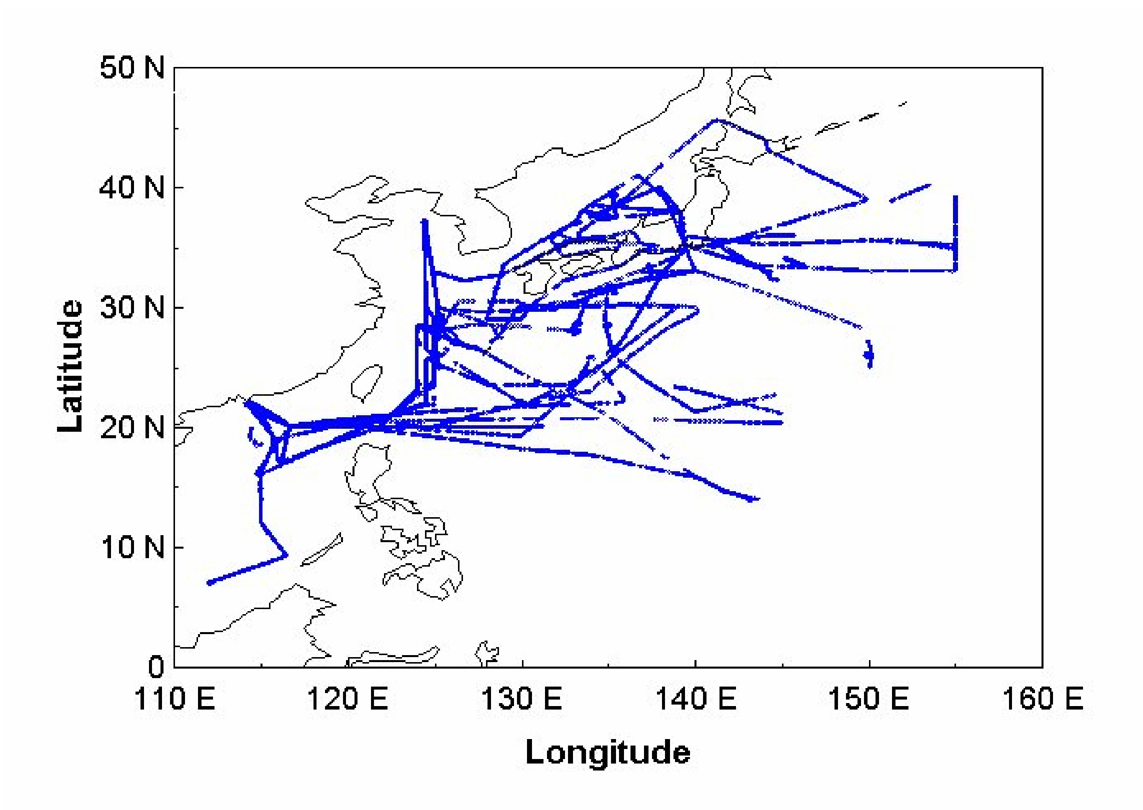

Figure 3.2. Geographic distribution of TRACE-P data.

3.3.1 Photochemical Precursors

As mentioned earlier, all critical photochemical O_3 precursor species were measured during TRACE-P. Figures 3.3 to 3.6 show the vertical geographic distributions of O_3, CO, NO, and dew point temperature, all of which play important roles in tropospheric photochemistry of O_3. In these figures, the data were vertically broken up into four sub-regions, 0-2 km, 2-5 km, 5-8 km, and 8-12 km. Among them the 0-2 km region represents the marine BL, and thus will be of the most interest in the discussion presented in chapter 5.

From Figure 3.3 to 3.6, some trends can be seen in the concentration levels of the four photochemical precursor species, both vertically and latitudinally. In general, both O_3 and NO increase with the height, whereas CO and water vapor decrease with increasing altitude. Although no apparent latitudinal concentration gradient was found for any species in the lower troposphere (0-5 km), the concentrations of O_3, CO, and NO are all obviously higher between 25°N to 45°N than in the 5°N to 25°N region. This demonstrates the rational of the selection of the working areas done earlier in this chapter. In the upper troposphere (>5 km), however, it appears that some significant changes on the concentration levels occur around the latitude of 25°N to 35°N. For example, in contrast to the extremely high O_3 level (>100 ppbv) at about 35°N in the 8-12 km region, O_3 concentrations decrease to a moderate level of about 50 ppbv in the neighborhood of 25°N.

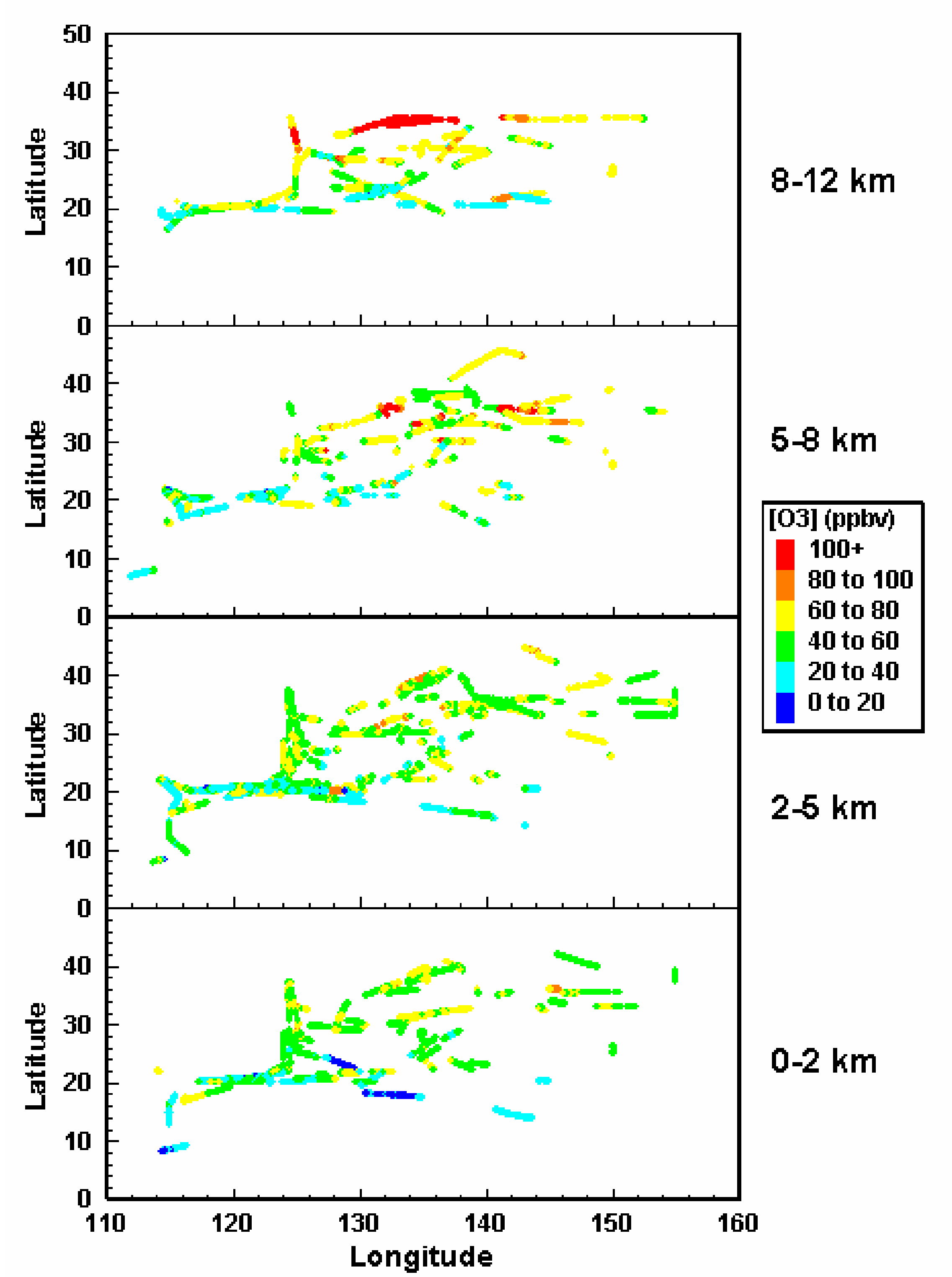

Figure 3.3. Vertical distribution of O_3 mixing ratios during TRACE-P mission.

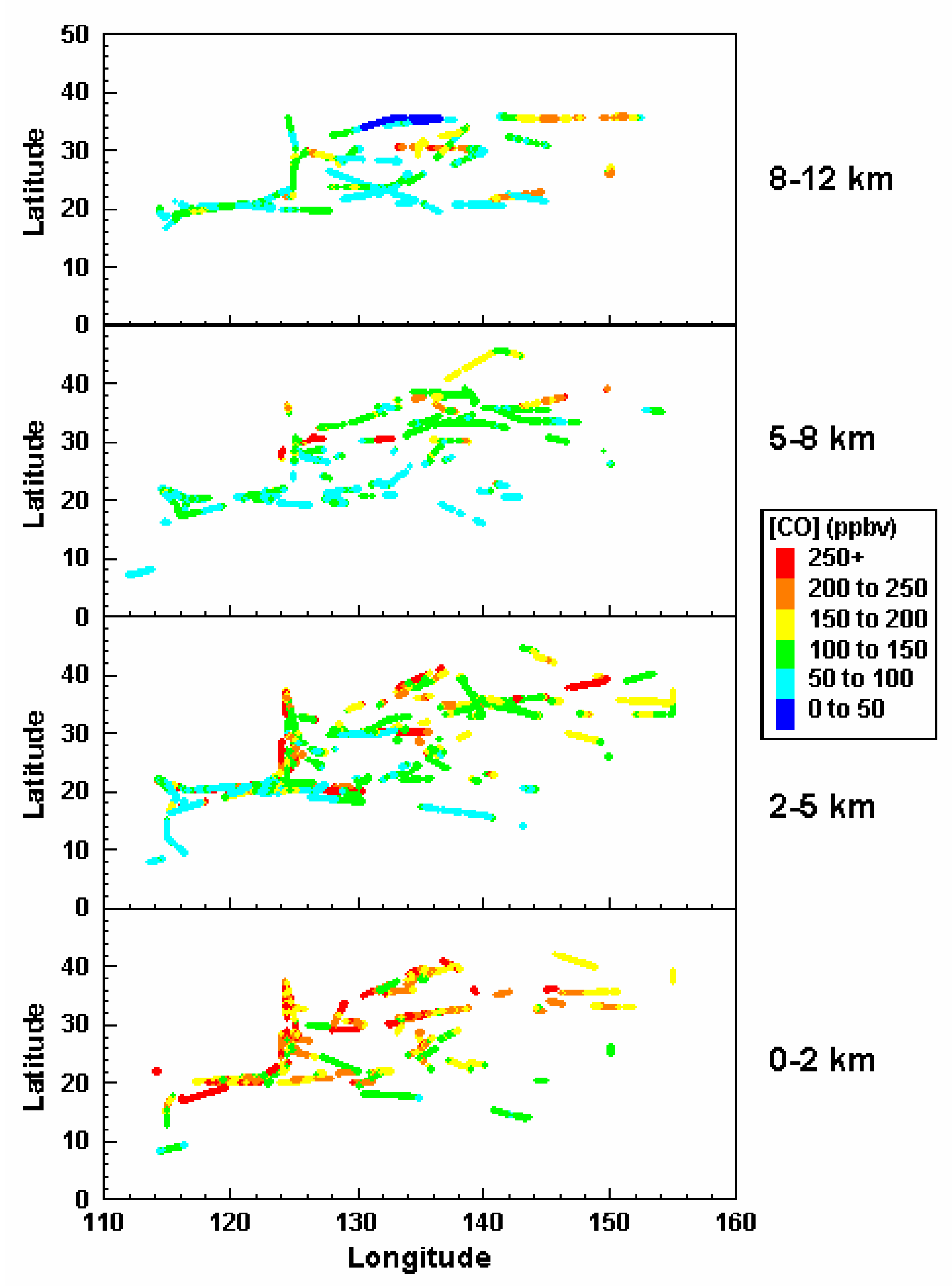

Figure 3.4. Vertical distribution of CO mixing ratios during TRACE-P mission.

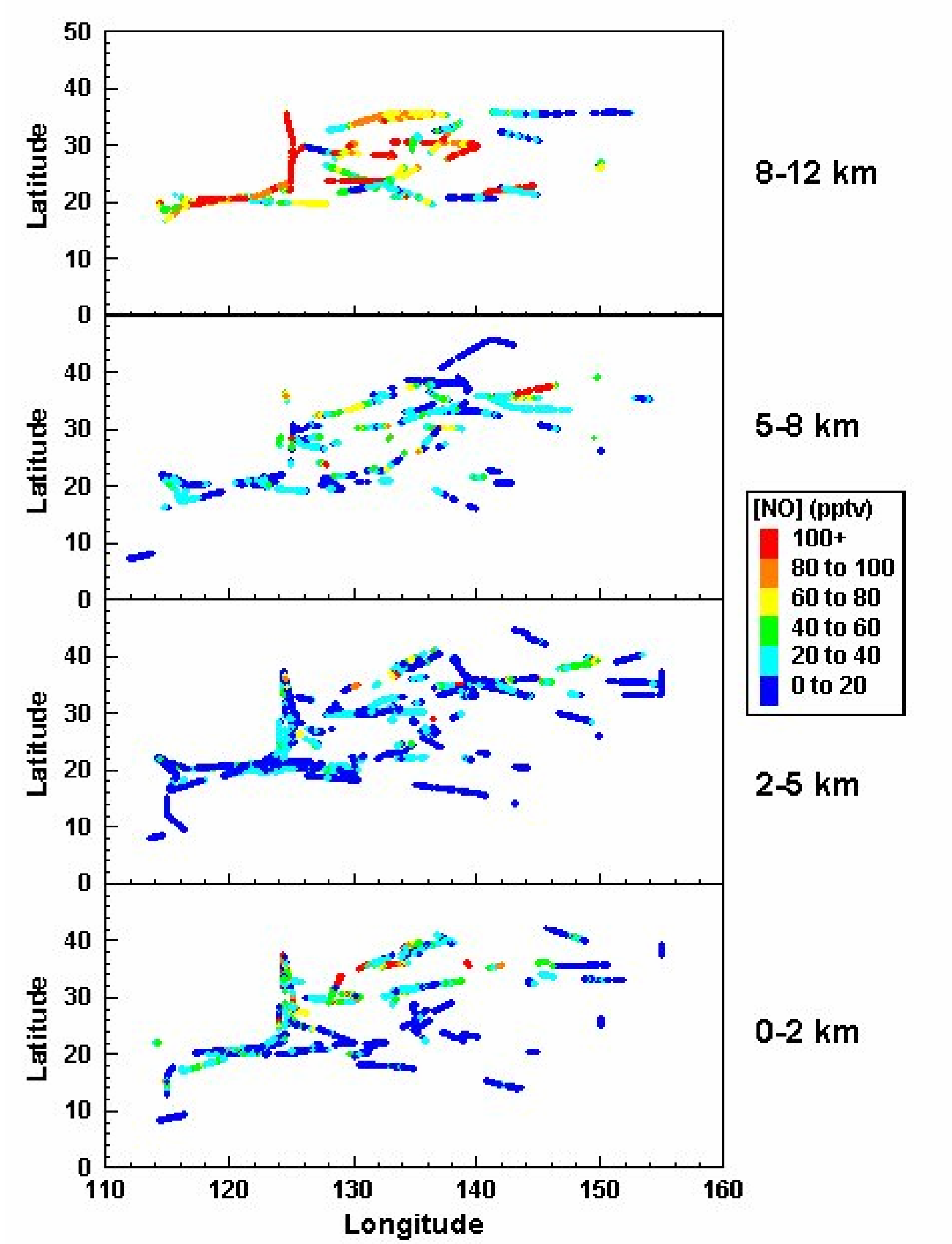

Figure 3.5. Vertical distribution of NO mixing ratios during TRACE-P mission.

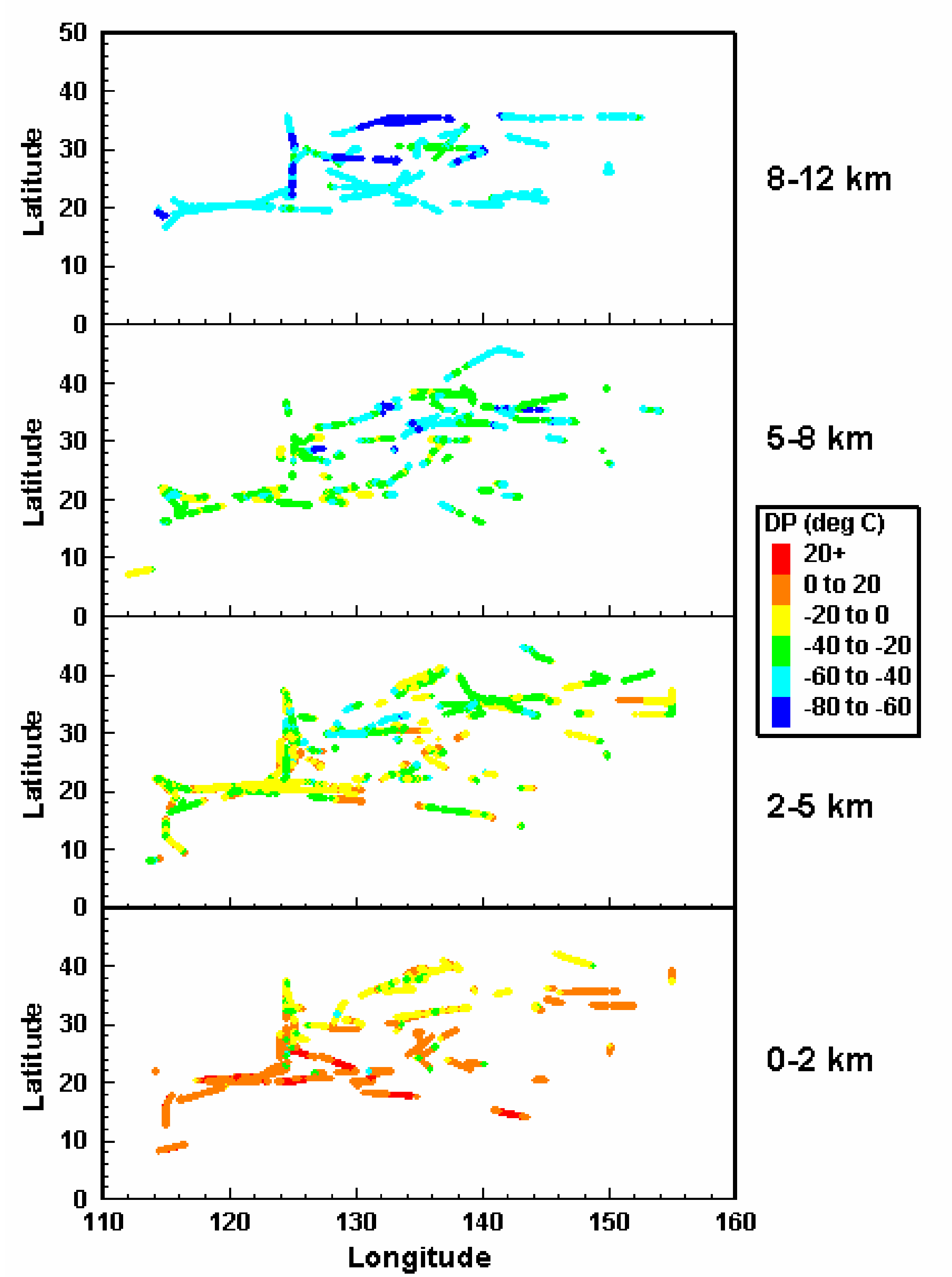

Figure 3.6. Vertical distribution of dew point temperature during TRACE-P mission.

3.3.2 NMHCs

The non-methane hydrocarbon species measured during TRACE-P include ethane (C_2H_6), ethene (C_2H_4), ethyne (C_2H_2), propane (C_3H_8), propene (C_3H_6), i-butane (i-C_4H_{10}), n-butane (n-C_4H_{10}), trans-2-butene (t-2-C_4H_8), n-pentane (n-C_5H_{12}), i-pentane (i-C_5H_{12}), benzene (C_6H_6), toluene (C_7H_8), ethylbenzene (C_8H_{10}), n-hexane (n-C_6H_{14}), and xylene (C_8H_{10}). The geographic distributions of total NMHCs and total reactive NMHCs (excluding ethane, ethyne, and benzene) are displayed in Figures 3.7 and 3.8, respectively.

The median level for total NMHCs during TRACE-P (about 8,200 runs) is about 2200 pptv, as compared to 365 pptv for the total reactive NMHCs. The corresponding two median mixing ratios for the BL (0-2 km, about 2,700 runs) are seen as 4000 and 1085 pptv, respectively. Here we can conclude that the NMHC levels decrease sharply with height. This trend is exhibited in Figure 3.9 which shows the vertical distribution of total reactive NMHCs during TRACE-P. For both total NMHCs and total reactive NMHCs, we can find a similar latitudinal distribution mode as found for the critical photochemical precursors O_3 and CO. Specifically, we can see that relatively high NMHC levels occur in the region of 25°N to 45°N (e.g., mostly along the coastal lines of Japan) and dramatically lower NMHC concentrations are evident in the 5°N to 25°N region.

3.3.3 NMHC Reactivity in the BL

Like for many species in the troposphere, the reaction with OH is the single most important sink for NMHCs. Consequently, we define the reactivity of any given NMHC as the product of its OH rate coefficient and the OH concentration level. As we discussed

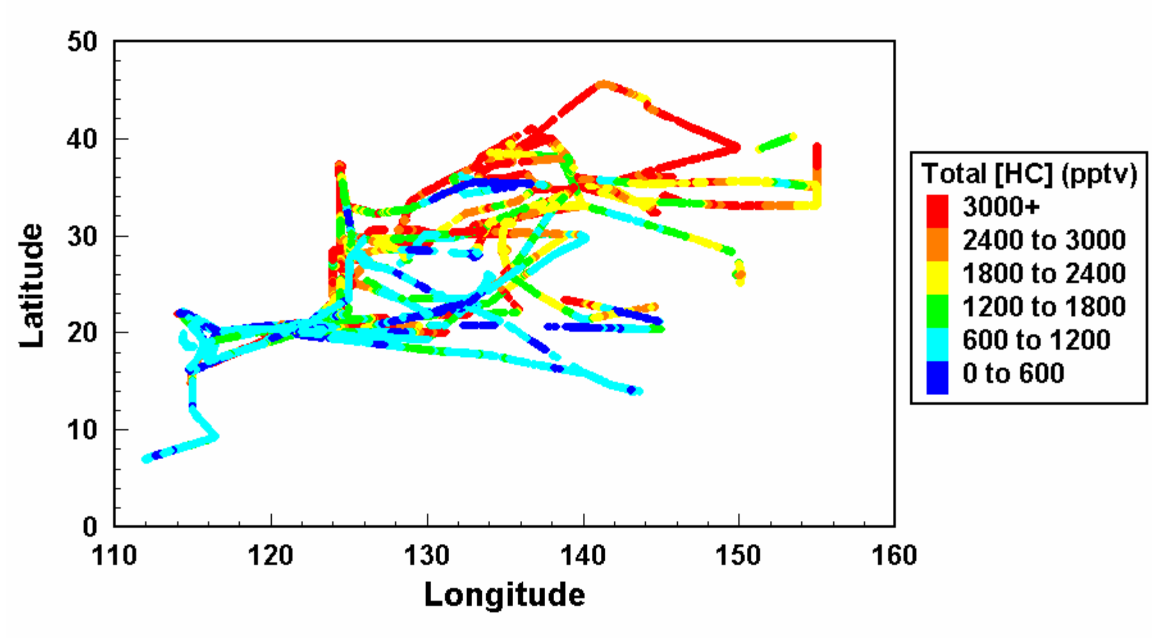

Figure 3.7. Geographic distribution of total NMHCs during TRACE-P mission.

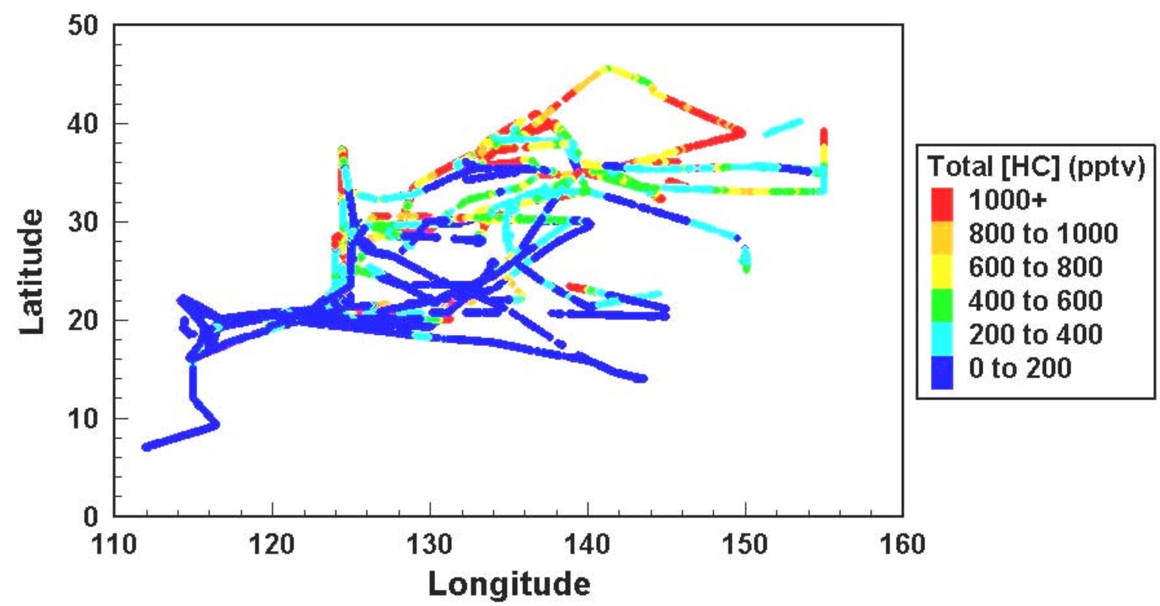

Figure 3.8. Geographic distribution of total reactive NMHCs during TRACE-P mission.

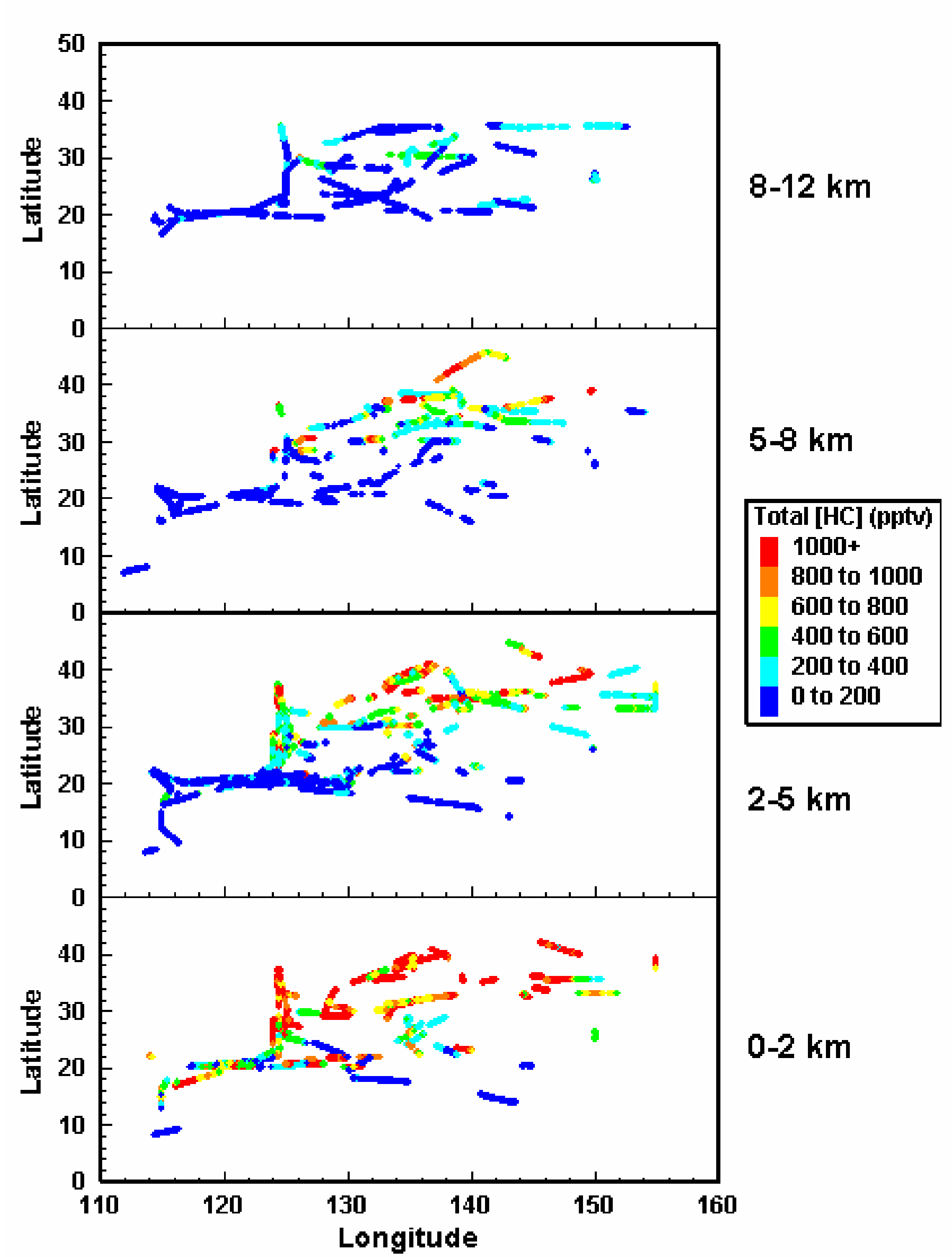

Figure 3.9. Vertical distribution of total reactive NMHCs during TRACE-P mission.

in chapter 2, the four mechanisms have different ways of treating the oxidation of hydrocarbon species. In a structure-lumped mechanism like CBIV, all the NMHC molecules are broken into several types of chemical bonds all of which will react with OH with an assigned averaged rate. In the other three mechanisms, NMHC species are also treated quite differently. For instance, fewer species are used to represent alkanes in Lurmann than in both RACM and SAPRC, and the Lurmann mechanism does not identify toluene and xylene whose reaction rate constants with OH are somewhat different. As Figure 3.10 shows, the four mechanisms give different outlooks of the total NMHC reactivity in the marine BL during TRACE-P, the area of primary concern in this study. CBIV produces the lowest total NMHC reactivity, while RACM tends to produce the highest. Actually, the reactivity distribution maps generated by the four mechanisms follow the same pattern, and they all correspond well to the concentration distribution of total reactive NMHC in the BL (Figure 3.8). In another words, we could erase the numerical divergence in NMHC reactivity by using different scales for different mechanisms. For simplicity, therefore, we will use the Lurmann mechanism, as seen in Figure 3.11, as the reference mechanism to determine the total NMHC reactivity. According to the distribution of the total NMHC reactivity at 0-2 km during TRACE-P, we can horizontally divide the BL into three regions of which region 1 is the least reactive, region 2 is moderately reactive, and region 3 is the most reactive. These three regions are characterized by different levels of NMHC reactivity and thus different levels of impact from NMHCs on the photochemistry of the region. Thus, different mechanisms may be applied in each region, which will be discussed more extensively in chapter 5.

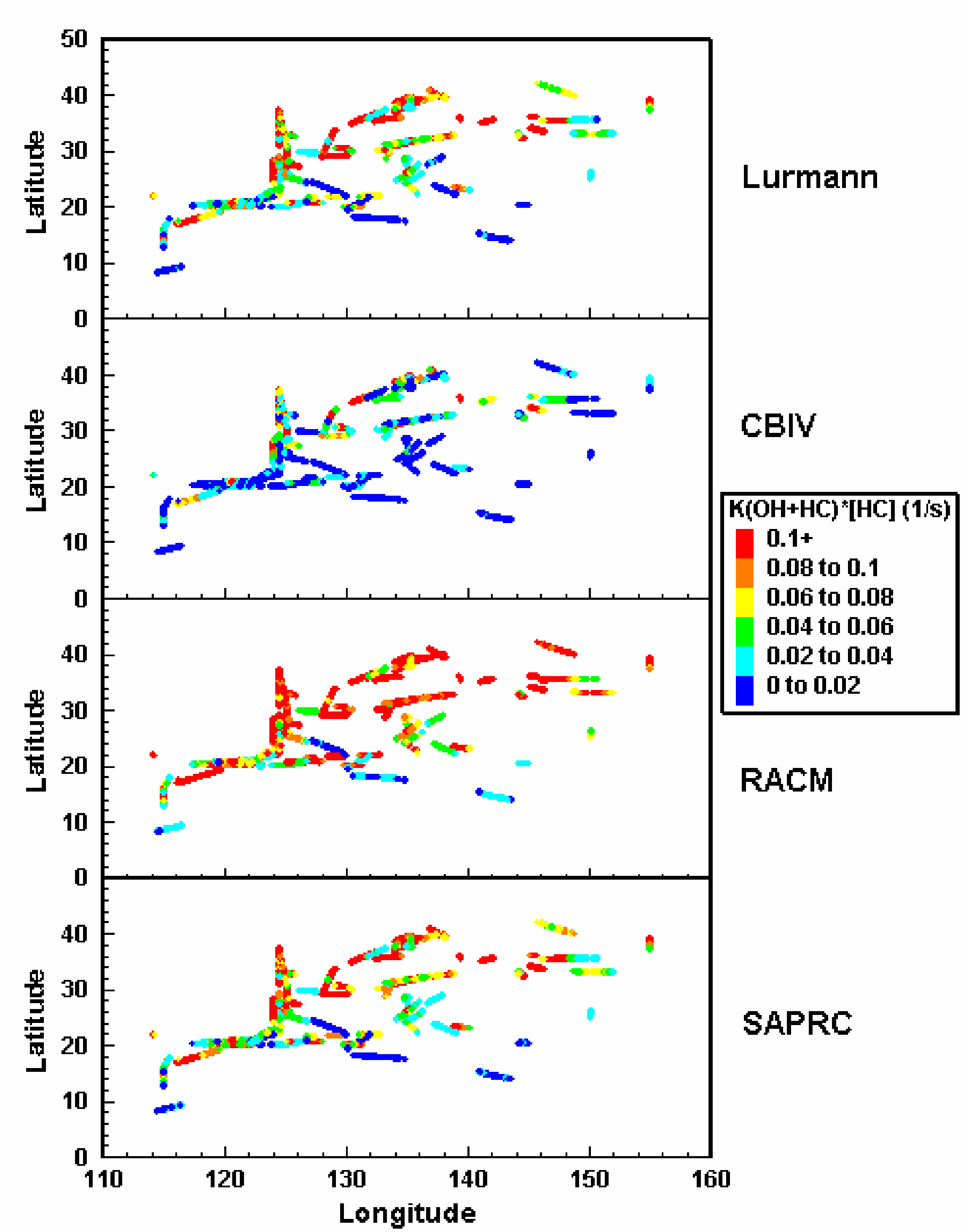

Figure 3.10. Calculated total NMHC reactivity in the BL (0-2 km) by four different mechanisms using TRACE-P data.

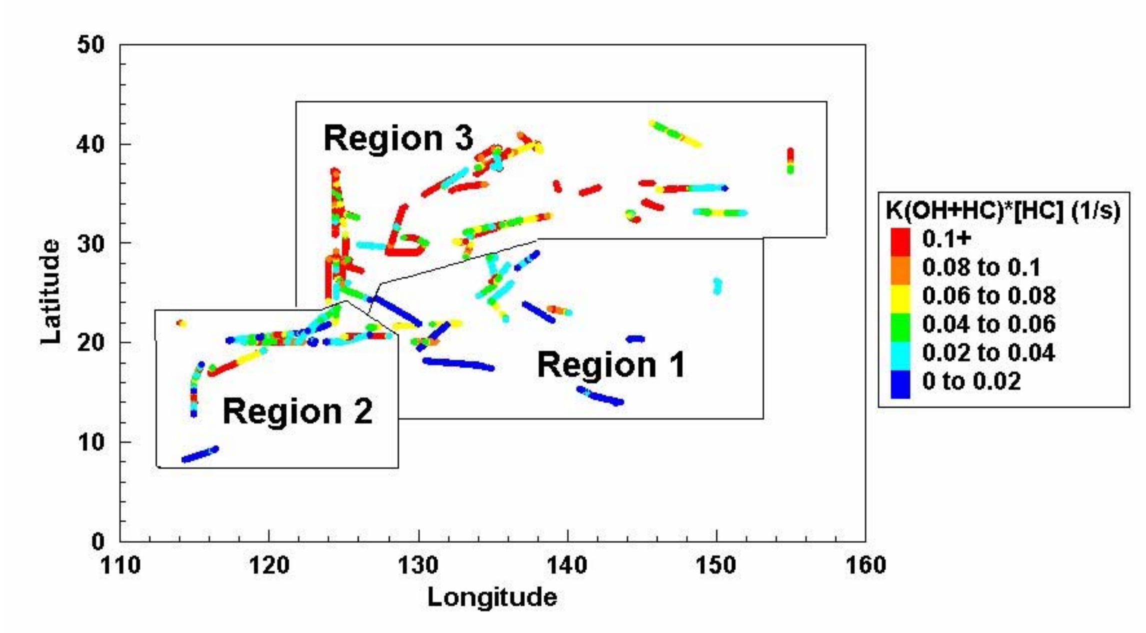

Figure 3.11. Regional separation of the BL (0-2 km) during TRACE-P based on calculated total NMHC reactivity from the Lurmann mechanism.

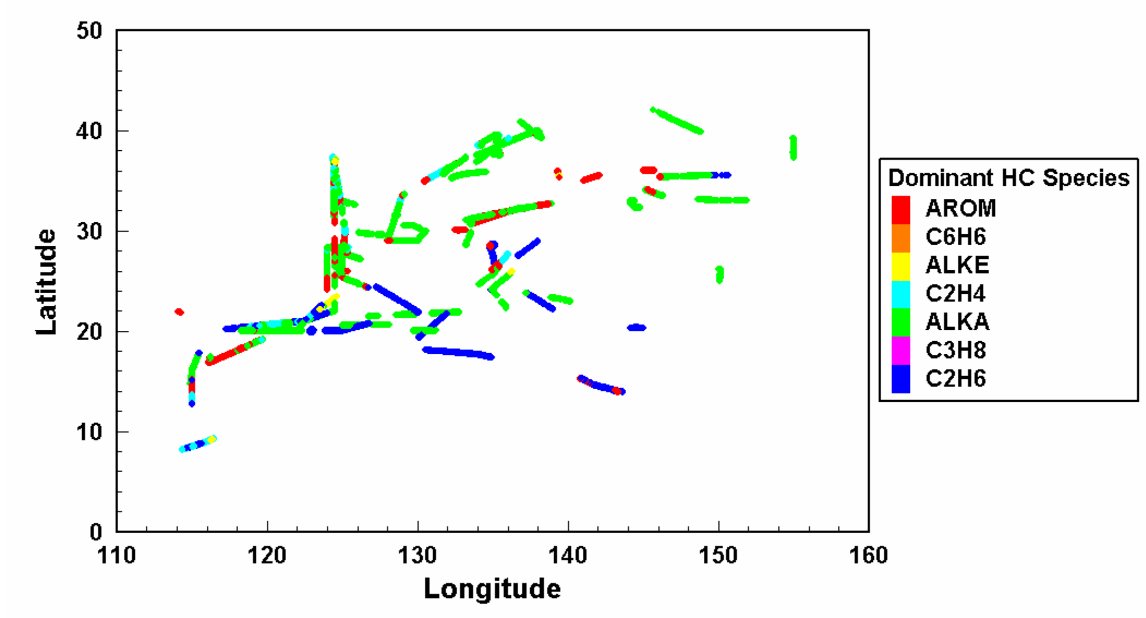

Figure 3.12. Geographic distribution of dominant NMHC species in the BL (0-2 km) during TRACE-P mission.

3.3.4 Major NMHC Species

It is important to know not only how reactive all the NMHCs are in a given sub-region, but also which individual hydrocarbon species is dominant and thus contribute most to the total NMHC reactivity. The identification of the dominant species can not be done by simply comparing the concentration levels of any particular species. Even though some inactive hydrocarbon species, such as ethane and benzene, have relatively high concentrations in the atmosphere, their reactivity is less significant because of their low OH rate coefficients. In order to determine the most reactive hydrocarbon species during TRACE-P, we compared the NMHC reactivity contributions of seven different lumped NMHC species (or families), all of which were explicitly treated in the Lurmann mechanism. These species treated included three alkanes, ethane, propane, and other reactive alkanes (ALKA, C≥4), two alkenes, ethene and other alkenes (ALKE), and two aromatic hydrocarbons, benzene and reactive aromatics (AROM). The distribution of the most dominant hydrocarbon species within the boundary during TRACE-P is that shown in Figure 3.12. From here it can seen that in a majority of the BL areas (especially in region 3) reactive alkanes (ALKA) typically define the total NMHC reactivity to the largest extent. However, ethane (mainly in region 1) and reactive aromatics (AROM) also contribute.

CHAPTER 4

CONTROLLED TESTS OF FOUR NMHC MECHANISMS

As discussed earlier, the four photochemical mechanisms being evaluated in this study have been shown to be different in their NMHC chemistry but are identical in their HO_x-NO_x-CH_4 chemistry. Thus, as the test environment is changed it should primarily reflect the impact from NMHC oxidation for the four mechanisms. To establish these differences, one could start with ambient air parcels. However, here we have elected to first start this evaluation using hypothetical mixtures of trace gases containing different types of hydrocarbons. The gas mixtures used in these runs were selected such that they were similar in structure to those measured in TRACE-P and also that the range in concentration also covered those found in the areas sampled during TRACE-P. The details of these tests are given below. As noted previously, comparisons based on the TRACE-P data will be presented in chapter 5.

4.1 Procedure for Comparing Four NMHC Oxidation Mechanisms Using Specified NMHC/NO_x Gas Mixtures

Although test runs require a specified NMHC/NO_x gas mixture, they are initiated from a basic run involving BL (0-2 km) conditions as well as free tropospheric (2-8 km) conditions. In the basic run, there are no NMHC species present, and the values required for important physical and meteorological parameters as well as photochemical precursors are median values estimated from measurements recorded during the TRACE-P campaign (see Table 4.1). Moreover, these test runs are made using two representative NO_x mixing ratios (e.g., 3.0 ppbv and 90 pptv). This spread in the NO_x concentration level shows the impact of the NO_x level on the concentrations of critical free radicals and/or stable oxidation products. Finally, in each test run, several selected NMHC species are independently added to the initial gas mixture to examine how any single hydrocarbon species might affect the predicted levels of various free radicals. For these runs once again all four NMHC mechanisms are assessed. The NMHC species selected were C_3H_8 (reactive alkane), C_3H_6 (reactive alkene), toluene (moderately reactive aromatic), xylene (very reactive aromatic), and isoprene (very reactive biogenic NMHCs). (Note, for completeness, isoprene was tested even though it was not present in the TRACE-P data set due to its importance in continental NMHC data sets.) The NMHC concentration levels examined were 5 ppbv, 1 ppbv, and 300 pptv for the BL, and 1 ppbv and 300 pptv for the FT. These selected values reflect the NMHC data recorded during the TRACE-P field program. Thus, these initial test runs have a level of relevance when compared to the results from TRACE-P.

It is to be noted, however, that the high levels employed for any single NMHC species (e.g., 5 ppbv) were only occasionally seen in TRACE-P measurements and therefore represent upper limit results. It was decided at the outset that only one hydrocarbon species would be added at a time since this approach permitted a far more detailed look at the relationship between any given NMHC species and the key photochemical free radicals generated from the oxidation of this species.

Table 4.1. Several critical parameters for the basic runs in both BL and FT.

	BL	FT
Altitude (km)	0.3	4.8
Temperature (°C)	15	-10
Dew Point Temperature (°C)	9	-25
Pressure (hPa)	975	600
[O_3] (ppbv)	55	60
[CO] (ppbv)	200	150
[NO_x] (ppbv)	3 & 0.09	3 & 0.09
[CH_4] (ppmv)	1.79	1.79

In these controlled test runs, important photochemical free radicals and/or molecules that were monitored included OH, HO_2, CH_3O_2, CH_2O, other higher aldehydes (e.g., ALD_2), and all organic peroxy radicals, e.g.,RO_2.

4.2 Impact of NMHC Oxidation on Critical Photochemical Species

The results of the controlled NMHC test runs are shown in Tables 4.2 to 4.5. For illustration purposes, we have presented only the case of the highest NMHC addition for both BL (5ppb) and FT (1ppb), but have done so for both NO_x levels (i.e., 90ppt and 3ppb). The impact from several different types of hydrocarbon species is discussed below.

4.2.1 Alkanes (C_3H_8)

As discussed in chapter 3, in terms of OH reactivity, the family "reactive alkanes (≥ C3)" were found to be the dominant family within the BL during TRACE-P field study. Representative of this family, the impact on OH and other radicals as well as the more stable oxidation products CH_2O and ALD2 from C_3H_8 are given in Tables 4.2 to 4.5.

Typically, a saturated hydrocarbon species such as C_3H_8 undergoes an H-atom abstraction reaction with OH to produce the alkyl radical, R· (Atkinson, 2000). This alkyl radical subsequently reacts with O_2 to generate an alkyl peroxy radical, $RO_2\cdot$, as shown in reactions R4.1 and R4.2 below:

(R4.1) $RH + OH \rightarrow R\cdot + H_2O$

(R4.2) $R\cdot + O_2 + M \rightarrow RO_2\cdot$

In the troposphere, alkyl peroxy radicals can be eliminated by several competing reactions, as shown in R4.3 to R4.6. For example, they may react with NO to form alkoxy radicals RO· or alkyl nitrates $RONO_2$, or react with NO_2 to produce alkyl peroxynitrates RO_2NO_2, which can decompose back to its reactants. RO· may also react with molecular oxygen to form critical photochemical species such as HO_2 and CH_2O. In addition, peroxy radicals may react with the hydrogen peroxy radical HO_2, or undergo self-reaction, or react with other alkyl peroxy radicals to produce a variety of oxygenated hydrocarbon species. Typically, the reaction with either NO, NO_2, or HO_2 is the dominant sink for $RO_2\cdot$.

Table 4.2. Model-predicted levels of product species from the BL low NO_x test runs (molecules/cm^3). [HC] = 5 ppbv; [NO_x] = 90 pptv.

Model	HC	OH	HO_2	CH_3O_2	CH_2O	RO_2	ALD2
CB-IV	None	1.5×10^{6}	2.0×10^{8}	9.9×10^{7}	5.0×10^{9}	0	0
	C_3H_8	1.5×10^{6}	2.0×10^{8}	1.1×10^{8}	5.5×10^{9}	2.9×10^{7}	1.3×10^{9}
	C_3H_6	3.1×10^{5}	3.0×10^{8}	6.8×10^{8}	8.7×10^{10}	3.6×10^{8}	3.4×10^{11}
	TOL	8.0×10^{5}	2.3×10^{8}	1.1×10^{8}	7.1×10^{9}	4.8×10^{8}	3.9×10^{7}
	XYL	3.7×10^{5}	3.4×10^{8}	3.2×10^{8}	3.3×10^{10}	3.9×10^{9}	8.0×10^{10}
	ISOP	1.3×10^{5}	2.0×10^{8}	2.5×10^{8}	1.2×10^{11}	1.0×10^{9}	2.7×10^{10}
Lurmann	None	1.5×10^{6}	2.0×10^{8}	9.9×10^{7}	5.0×10^{9}	0	0
	C_3H_8	1.3×10^{6}	1.8×10^{8}	9.4×10^{7}	5.1×10^{9}	5.0×10^{7}	2.5×10^{9}
	C_3H_6	2.2×10^{5}	4.8×10^{8}	7.9×10^{8}	2.3×10^{11}	2.8×10^{8}	1.0×10^{12}
	TOL	4.6×10^{5}	1.6×10^{8}	6.9×10^{7}	5.5×10^{9}	1.5×10^{9}	0
	XYL	4.6×10^{5}	1.6×10^{8}	6.9×10^{7}	5.5×10^{9}	1.5×10^{9}	0
	ISOP	1.2×10^{5}	1.7×10^{8}	1.0×10^{8}	6.2×10^{10}	8.2×10^{8}	1.4×10^{11}
RACM	None	1.5×10^{6}	2.0×10^{8}	9.9×10^{7}	5.0×10^{9}	0	0
	C_3H_8	1.1×10^{6}	1.7×10^{8}	1.4×10^{8}	6.4×10^{9}	6.3×10^{7}	6.8×10^{9}
	C_3H_6	3.2×10^{5}	2.0×10^{8}	3.6×10^{8}	6.0×10^{10}	4.4×10^{8}	1.8×10^{11}
	TOL	7.9×10^{5}	1.5×10^{8}	1.5×10^{8}	9.6×10^{9}	1.9×10^{8}	7.1×10^{9}
	XYL	3.8×10^{5}	1.5×10^{8}	2.0×10^{8}	1.9×10^{10}	3.4×10^{8}	2.4×10^{10}
	ISOP	1.4×10^{5}	2.8×10^{8}	3.0×10^{8}	1.1×10^{11}	6.1×10^{8}	1.7×10^{11}
SAPRC	None	1.5×10^{6}	2.0×10^{8}	9.9×10^{7}	5.0×10^{9}	0	0
	C_3H_8	1.3×10^{6}	1.8×10^{8}	1.1×10^{8}	7.1×10^{9}	3.9×10^{7}	2.2×10^{9}
	C_3H_6	1.3×10^{5}	1.8×10^{8}	2.8×10^{8}	6.0×10^{10}	4.0×10^{8}	4.7×10^{11}
	TOL	5.5×10^{5}	1.3×10^{8}	1.0×10^{8}	8.8×10^{9}	2.0×10^{8}	2.9×10^{10}
	XYL	2.4×10^{5}	1.4×10^{8}	1.5×10^{8}	1.6×10^{10}	3.2×10^{8}	8.9×10^{10}
	ISOP	8.8×10^{4}	1.9×10^{8}	2.5×10^{8}	9.8×10^{10}	8.1×10^{8}	3.7×10^{11}

Table 4.3. Model-predicted levels of product species from the BL high NO_x test runs (molecules/cm^3). [HC] = 5 ppbv; [NO_x] = 3 ppbv.

Model	HC	OH	HO_2	CH_3O_2	CH_2O	RO_2	ALD2
CB-IV	None	3.7×10^6	6.2×10^7	1.7×10^7	9.9×10^9	0	0
	C_3H_8	3.7×10^6	6.5×10^7	2.0×10^7	1.1×10^{10}	3.5×10^6	1.3×10^9
	C_3H_6	2.1×10^6	4.5×10^8	5.3×10^8	3.0×10^{11}	3.5×10^9	2.8×10^{11}
	TOL	3.5×10^6	1.4×10^8	3.9×10^7	2.5×10^{10}	1.4×10^8	3.5×10^7
	XYL	2.6×10^6	6.1×10^8	3.5×10^8	1.9×10^{11}	2.3×10^9	9.5×10^{10}
	ISOP	9.2×10^6	5.2×10^8	3.0×10^8	5.9×10^{11}	8.0×10^8	2.2×10^{11}
Lurmann	None	3.7×10^6	6.2×10^7	1.7×10^7	9.9×10^9	0	0
	C_3H_8	3.6×10^6	6.7×10^7	1.8×10^7	1.1×10^{10}	1.1×10^7	1.4×10^9
	C_3H_6	2.0×10^6	5.6×10^8	5.6×10^8	4.1×10^{11}	2.9×10^8	3.8×10^{11}
	TOL	3.1×10^6	4.0×10^8	9.0×10^7	6.7×10^{10}	6.8×10^8	0
	XYL	3.1×10^6	4.0×10^8	9.0×10^7	6.7×10^{10}	6.8×10^8	0
	ISOP	9.2×10^5	4.8×10^8	1.3×10^8	4.7×10^{11}	2.3×10^9	2.9×10^{11}
RACM	None	3.7×10^6	6.2×10^7	1.7×10^7	9.9×10^9	0	0
	C_3H_8	3.6×10^6	9.5×10^7	7.7×10^7	2.3×10^{10}	4.0×10^7	9.9×10^9
	C_3H_6	1.6×10^6	3.1×10^8	2.9×10^8	2.5×10^{11}	5.3×10^8	2.2×10^{11}
	TOL	3.7×10^6	2.3×10^8	1.5×10^8	6.1×10^{10}	1.6×10^8	8.6×10^9
	XYL	2.1×10^6	3.9×10^8	3.3×10^8	1.8×10^{11}	4.1×10^8	4.9×10^{10}
	ISOP	6.9×10^5	4.7×10^8	3.3×10^8	4.3×10^{11}	8.9×10^8	2.8×10^{11}
SAPRC	None	3.7×10^6	6.2×10^7	1.7×10^7	9.9×10^9	0	0
	C_3H_8	3.8×10^6	7.7×10^7	3.8×10^7	1.7×10^{10}	7.8×10^6	1.8×10^9
	C_3H_6	9.8×10^5	2.4×10^8	2.0×10^8	2.2×10^{11}	3.7×10^8	3.4×10^{11}
	TOL	2.7×10^6	1.5×10^8	8.4×10^7	4.4×10^{10}	8.0×10^7	3.2×10^{10}
	XYL	1.6×10^6	3.2×10^8	2.1×10^8	1.4×10^{11}	2.6×10^8	1.3×10^{11}
	ISOP	5.3×10^5	4.4×10^8	3.0×10^8	4.6×10^{11}	1.1×10^9	6.3×10^{11}

Table 4.4. Model-predicted levels of product species from the FT low NO_x test runs (molecules/cm^3). [HC] = 1 ppbv; [NO_x] = 90 pptv.

Model	HC	OH	HO_2	CH_3O_2	CH_2O	RO_2	ALD2
CB-IV	None	1.2×10^{6}	8.7×10^{7}	2.6×10^{7}	2.0×10^{9}	0	0
	C_3H_8	1.2×10^{6}	8.8×10^{7}	2.7×10^{7}	2.1×10^{9}	2.23×10^{6}	1.4×10^{8}
	C_3H_6	6.5×10^{5}	1.6×10^{8}	2.0×10^{8}	2.1×10^{10}	7.46×10^{7}	3.5×10^{10}
	TOL	1.0×10^{6}	1.0×10^{8}	2.8×10^{7}	2.7×10^{9}	6.13×10^{7}	3.6×10^{6}
	XYL	8.6×10^{5}	2.1×10^{8}	1.3×10^{8}	1.4×10^{10}	4.66×10^{8}	1.1×10^{10}
	ISOP	4.2×10^{5}	1.8×10^{8}	1.0×10^{8}	3.9×10^{10}	3.30×10^{8}	1.2×10^{10}
Lurmann	None	1.2×10^{6}	8.7×10^{7}	2.6×10^{7}	2.0×10^{9}	0	0
	C_3H_8	1.1×10^{6}	8.5×10^{7}	2.5×10^{7}	2.0×10^{9}	4.1×10^{6}	2.2×10^{8}
	C_3H_6	5.8×10^{5}	1.6×10^{8}	1.6×10^{8}	2.4×10^{10}	9.6×10^{7}	4.5×10^{10}
	TOL	8.2×10^{5}	1.3×10^{8}	3.6×10^{7}	4.1×10^{9}	2.7×10^{8}	0
	XYL	8.2×10^{5}	1.3×10^{8}	3.6×10^{7}	4.1×10^{9}	2.7×10^{8}	0
	ISOP	3.4×10^{5}	1.3×10^{8}	5.0×10^{7}	2.0×10^{10}	2.2×10^{8}	3.7×10^{10}
RACM	None	1.2×10^{6}	8.7×10^{7}	2.6×10^{7}	2.0×10^{9}	0	0
	C_3H_8	9.9×10^{5}	8.1×10^{7}	3.0×10^{7}	2.5×10^{9}	1.3×10^{7}	1.4×10^{9}
	C_3H_6	4.6×10^{5}	1.0×10^{8}	1.0×10^{8}	1.3×10^{10}	1.3×10^{8}	3.0×10^{10}
	TOL	8.1×10^{5}	8.8×10^{7}	4.8×10^{7}	4.6×10^{9}	4.8×10^{7}	3.4×10^{9}
	XYL	5.5×10^{5}	1.1×10^{8}	9.6×10^{7}	1.0×10^{10}	1.1×10^{8}	1.5×10^{10}
	ISOP	2.9×10^{5}	1.5×10^{8}	1.5×10^{8}	2.7×10^{10}	2.1×10^{8}	7.1×10^{10}
SAPRC	None	1.2×10^{6}	8.7×10^{7}	2.6×10^{7}	2.0×10^{9}	0	0
	C_3H_8	1.1×10^{6}	8.7×10^{7}	2.7×10^{7}	2.3×10^{9}	3.2×10^{6}	3.2×10^{8}
	C_3H_6	3.3×10^{5}	1.3×10^{8}	9.3×10^{7}	1.7×10^{10}	1.2×10^{8}	7.0×10^{10}
	TOL	6.7×10^{5}	8.3×10^{7}	3.6×10^{7}	4.0×10^{9}	3.8×10^{7}	7.8×10^{9}
	XYL	4.1×10^{5}	1.1×10^{8}	7.2×10^{7}	9.2×10^{9}	9.4×10^{7}	3.4×10^{10}
	ISOP	2.1×10^{5}	2.1×10^{8}	1.7×10^{8}	3.8×10^{10}	2.7×10^{8}	2.3×10^{11}

Table 4.5. Model-predicted levels of product species from the FT high NO_x test runs (molecules/cm^3). [HC] = 1 ppbv; [NO_x] = 3 ppbv.

Model	HC	OH	HO_2	CH_3O_2	CH_2O	RO_2	ALD2
CB-IV	None	7.8×10^5	3.1×10^6	4.7×10^5	1.4×10^9	0	0
	C_3H_8	7.9×10^5	3.2×10^6	5.1×10^5	1.5×10^9	6.8×10^4	1.4×10^8
	C_3H_6	3.6×10^6	7.2×10^7	5.2×10^7	6.2×10^{10}	7.2×10^7	3.7×10^{10}
	TOL	8.9×10^5	5.4×10^6	9.1×10^5	2.4×10^9	1.9×10^6	3.0×10^6
	XYL	5.0×10^6	1.1×10^8	2.9×10^7	4.2×10^{10}	3.8×10^8	1.3×10^{10}
	ISOP	4.7×10^6	3.2×10^8	8.6×10^7	2.5×10^{11}	4.4×10^8	4.0×10^{10}
Lurmann	None	7.8×10^5	3.1×10^6	4.7×10^5	1.4×10^9	0	0
	C_3H_8	7.9×10^5	3.2×10^6	4.9×10^5	1.5×10^9	2.6×10^5	1.1×10^8
	C_3H_6	3.4×10^6	7.5×10^7	6.2×10^7	6.1×10^{10}	3.5×10^7	3.9×10^{10}
	TOL	3.2×10^6	4.2×10^7	7.1×10^6	1.2×10^{10}	4.0×10^7	0
	XYL	3.2×10^6	4.2×10^7	7.1×10^6	1.2×10^{10}	4.0×10^7	0
	ISOP	4.4×10^6	2.1×10^8	3.3×10^7	1.6×10^{11}	1.7×10^8	3.5×10^{10}
RACM	None	7.8×10^5	3.1×10^6	4.7×10^5	1.4×10^9	0	0
	C_3H_8	9.0×10^5	4.3×10^6	8.8×10^5	2.4×10^9	8.0×10^5	1.1×10^9
	C_3H_6	2.9×10^6	5.9×10^7	2.4×10^7	6.0×10^{10}	7.1×10^7	3.1×10^{10}
	TOL	1.9×10^6	1.6×10^7	3.7×10^6	8.9×10^9	8.5×10^6	8.3×10^8
	XYL	3.7×10^6	8.6×10^7	2.1×10^7	4.8×10^{10}	6.1×10^7	6.8×10^9
	ISOP	2.7×10^6	1.9×10^8	4.9×10^7	1.9×10^{11}	2.9×10^8	5.0×10^{10}
SAPRC	None	7.8×10^5	3.1×10^6	4.7×10^5	1.4×10^9	0	0
	C_3H_8	8.4×10^5	3.6×10^6	6.0×10^5	1.8×10^9	1.2×10^5	1.2×10^8
	C_3H_6	1.9×10^6	4.4×10^7	1.8×10^7	4.7×10^{10}	3.7×10^7	3.9×10^{10}
	TOL	1.3×10^6	1.1×10^7	2.5×10^6	5.7×10^9	4.0×10^6	3.6×10^9
	XYL	3.5×10^6	7.1×10^7	1.9×10^7	3.4×10^{10}	2.9×10^7	1.5×10^{10}
	ISOP	2.6×10^6	2.1×10^8	6.5×10^7	2.1×10^{11}	2.2×10^8	9.1×10^{10}

(R4.3a) $RO_2\cdot + NO \rightarrow RO\cdot + NO_2$

(R4.3b) $RO_2\cdot + NO + M \rightarrow RONO_2$

(R4.4) $RO_2\cdot + NO_2 + M \rightarrow RO_2NO_2$

(R4.5) $RO_2\cdot + HO_2 \rightarrow ROOH + O_2$

(R4.6) $RO_2\cdot + R'O_2\cdot \rightarrow$ oxygenated hydrocarbons

As noted earlier, since C_3H_8 was the most abundant reactive alkane in the TRACE-P data set, it was selected to be the representative alkane in our test runs. Figures 4.1 and 4.2 illustrate how the BL concentrations of four most critical species, e.g., OH, HO_2, CH_3O_2, and CH_2O, change with the amount of propane added and the level of NO_x.

From Figures 4.1 and 4.2, it can seen that the addition of propane does not have a large impact on the OH concentration, but is seen to decrease OH levels almost linearly with increasing C_3H_8, especially for the low NO_x case. This can be explained by the fact that propane does not become a major sink for OH, relative to OH+CO or OH+CH_4, until very high concentrations are reached. However, it is to be noted that for high levels of NO_x, the CBIV and SAPRC mechanisms actually predict small increases in the OH concentration at high levels of propane. This occurs because the HO_2 level tends to increase with propane concentration when NO_x is high and thus leads to secondary OH generation from reaction of HO_2 with NO. As for HO_2, only when NO_x is elevated do enhanced levels of propane produce increased HO_2 for all mechanisms examined. The concentration of CH_3O_2, one of the products of propane oxidation, is typically enhanced by the addition of propane regardless of mechanism type, especially for low levels of NO_x. The only exception that CH_3O_2 level was lowered by propane is seen in the low NO_x case shown by the Lurmann mechanism (Figure 4.1). As related to CH_2O, it is not surprising that the same trend is seen for this species with increasing propane concentration. This reflects the fact that the reaction of molecular oxygen with the alkoxy radical $CH_3O\cdot$ is always the largest source of CH_2O under tropospheric conditions. The details of the sources and sinks for these species will be discussed later.

4.2.2 Alkenes (C_3H_6)

Alkenes are significantly more reactive than alkanes. They not only react with OH but also with O_3 and NO_3 in the troposphere. During TRACE-P propene was the only anthropogenic alkene species measured other than ethene, the latter being much less reactive. Thus, propene was selected as the appropriate representative of the alkene family for the NMHC test runs.

Propene may undergo OH addition to either carbon atom of its double C=C bond to produce β-hydroxyalkyl radicals (the dominant pathway), or undergo hydrogen abstraction from a single C-H bond of the alkyl substituent group. β-hydroxyalkyl radicals quickly react with O_2 to form β-hydroxyalkyl peroxy radicals which subsequently go through a series of reactions analogous to those for alkyl peroxy radicals involving the reactants NO, NO_2, HO_2, as well as other peroxy radicals (i.e., see R4.3 to R4.6). However, the alkenes tend to generate more complex products.

Although the reaction rate constants of alkenes with O_3 are much slower compared with OH, O_3 is far more abundant than the OH radical in the troposphere. Therefore, under some circumstances, alkenes such as propene may be consumed at comparable rates by both OH and O_3. O_3 is initially added to the C=C bond of alkenes to form an energized intermediate product which then rapidly breaks down to form two

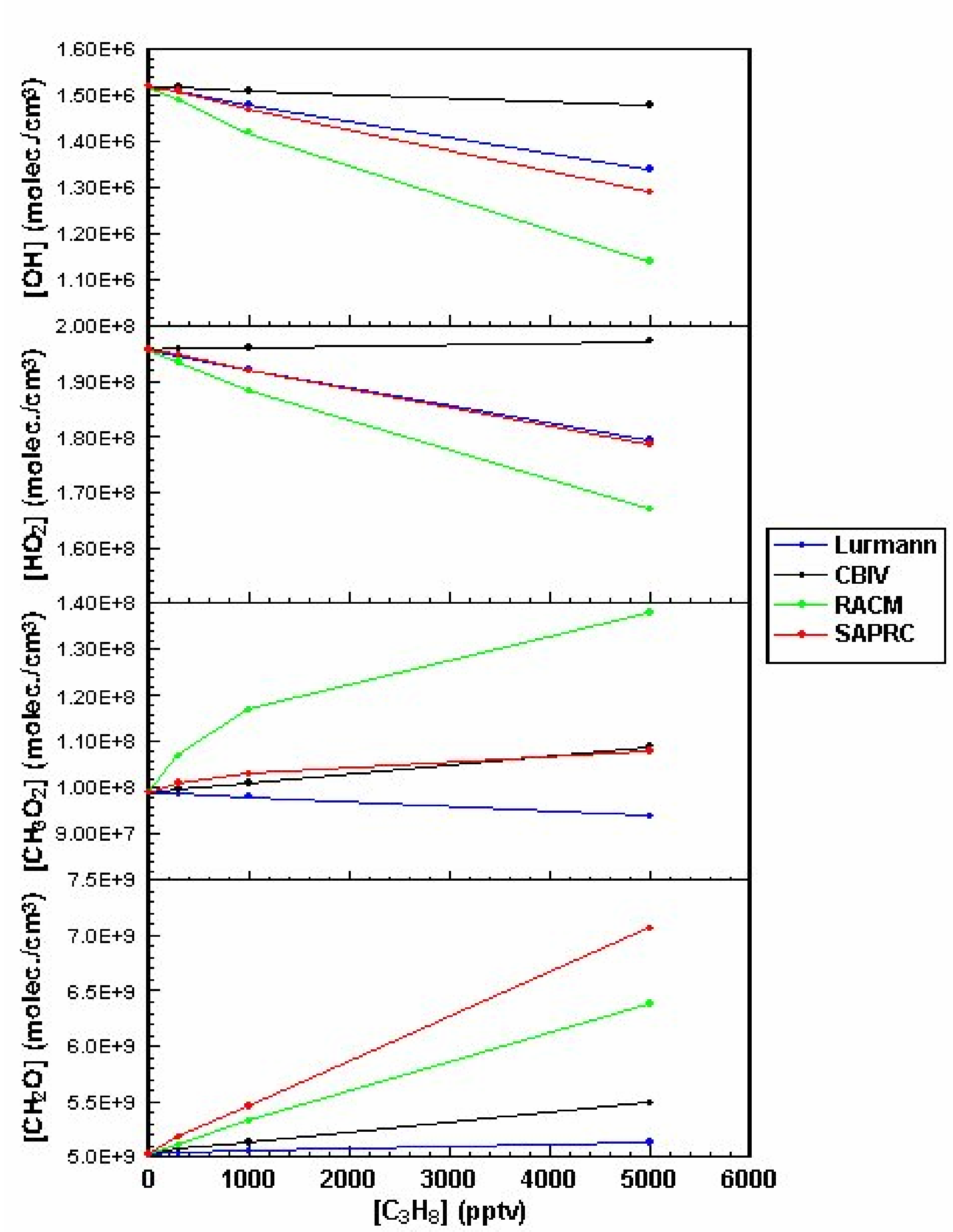

Figure 4.1. Several critical species versus propane for BL low NO_x test runs.

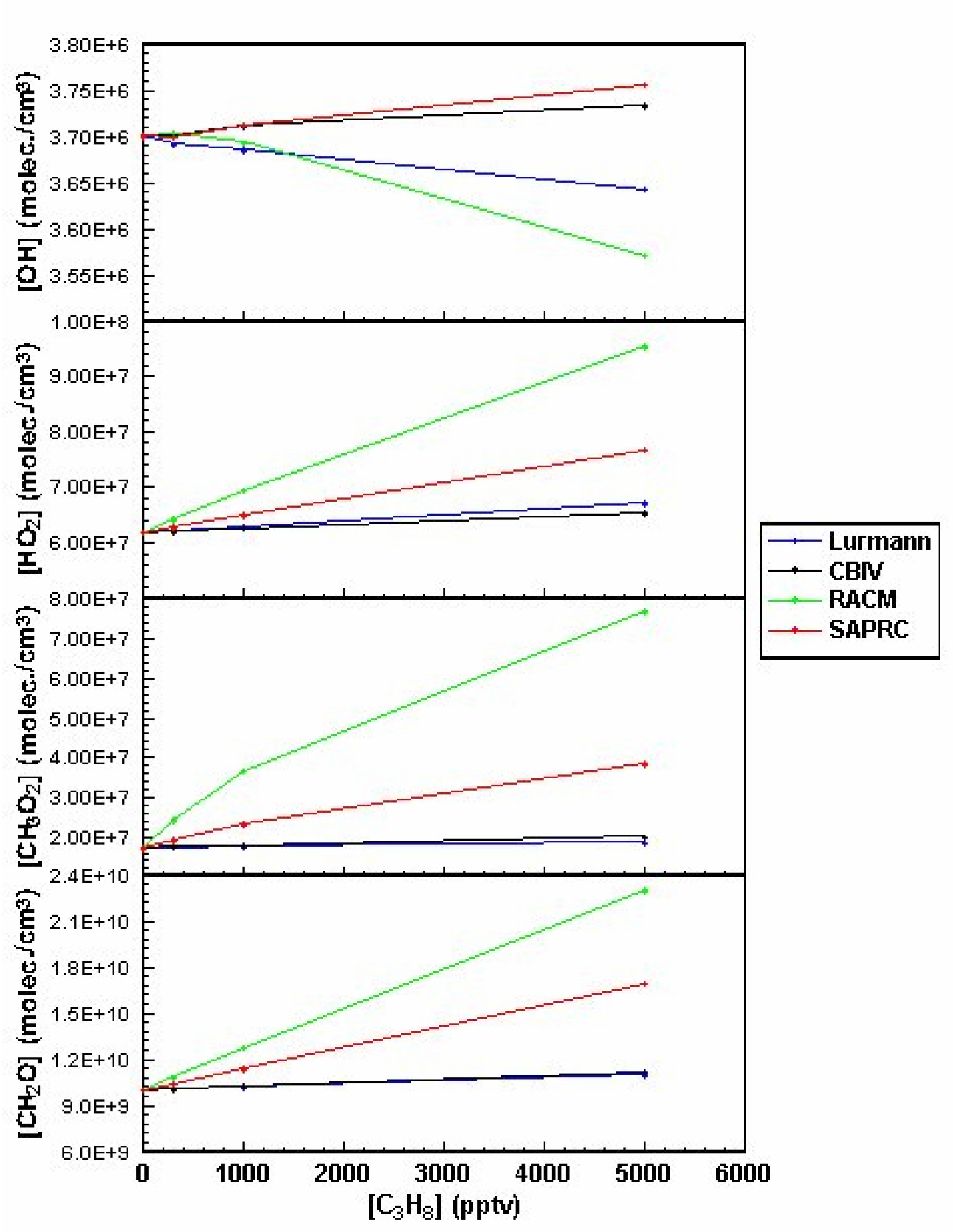

Figure 4.2. Several critical species versus propane for BL high NO_x test runs.

different types of carbonyl species and the Criegee biradical (Martinez et al., 1981; Niki et al., 1987; Paulson and Orlando, 1996; Atkinson, 1997). The relative importance of the two decomposition pathways depends on the structure of the alkene. For propene, it favors the channel that produces a methyl-substituted biradical and CH_2O. The Criegee biradical is not stable enough to live long. Therefore, it may undergo decomposition or isomerization afterwards. Among all the possibilities, the "hydroperoxide" channel can produce both OH and HO_2 radicals, thus becoming a secondary source of these radicals.

The reaction between NO_3 and alkenes begins with the NO_3 adding to the C=C bond, thus generating a β-nitrooxyalkyl radical. This species undergoes an analogous reaction to that involving the β-hydroxyalkyl radical. In this case β-nitrooxyalkyl peroxy radicals are produced which then react with NO_2, NO_3, HO_2, or other peroxy radicals to form a series of different products.

The impact of propene on the levels of OH, HO_2, CH_3O_2, and CH_2O for the four NMHC mechanisms is shown in Figures 4.3 and 4.4. Similar to propane, propene typically results in a lowering of the OH concentration. The only exception is that shown by the Lurmann and CBIV mechanisms when a small amount of propene is added under high NO_x conditions. However, regardless of the NO_x level, the existence of propene effectively increases the HO_2 concentration level. This is partly because of the enhanced level of organic peroxy radicals which can serve as an effective secondary source of HO_2 radicals. Even so, when the concentration of propene is low (less than 1 ppbv), the drop in OH may lead to a major decline in the primary source of HO_2 (OH+CO), and thus, a decrease in the HO_2 level. This is seen for the case of low NO_x for both the RACM and SAPRC mechanisms. Not surprisingly, CH_3O_2 concentrations are also raised to a higher

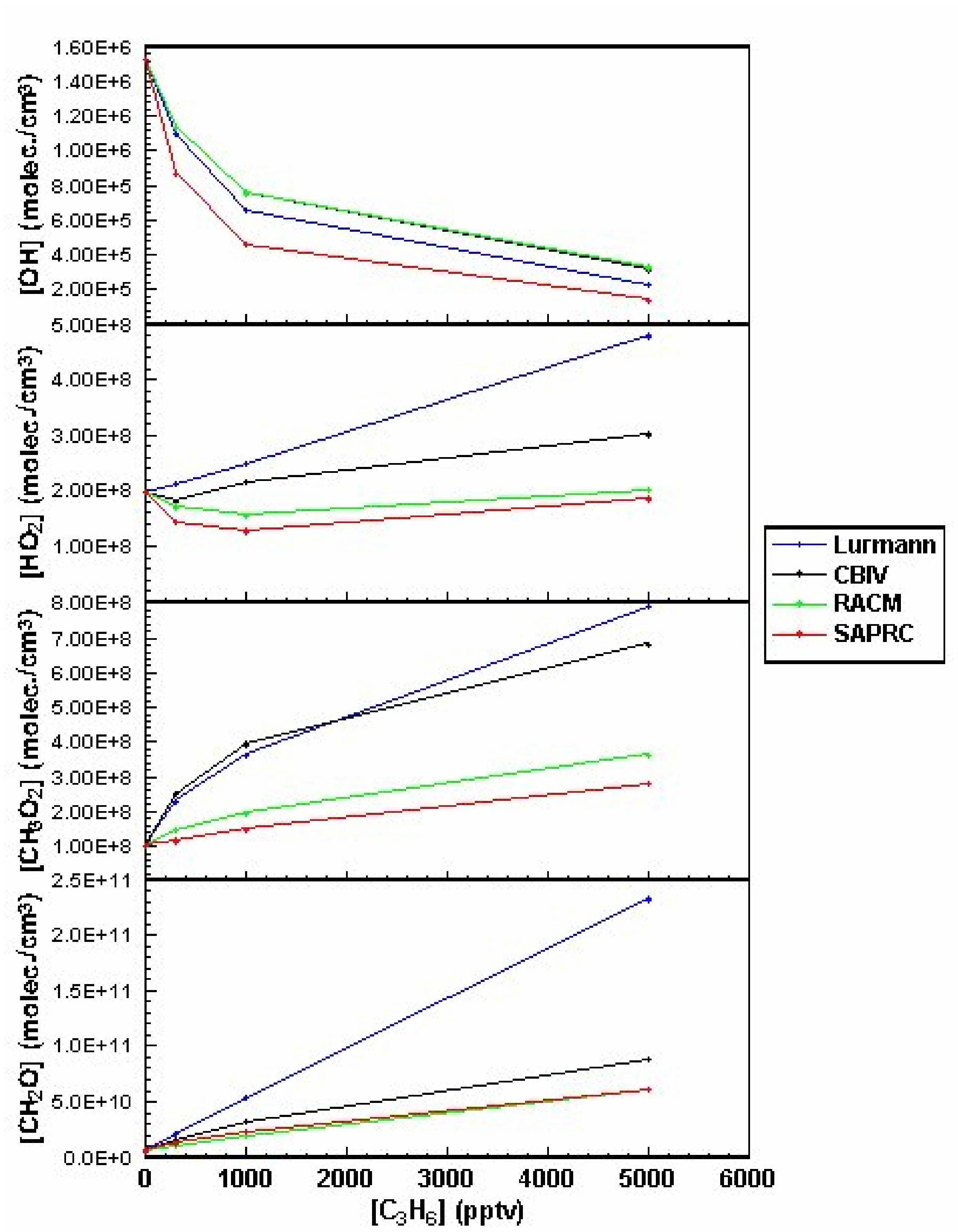

Figure 4.3. Several critical species versus propene for BL low NO_x test runs.

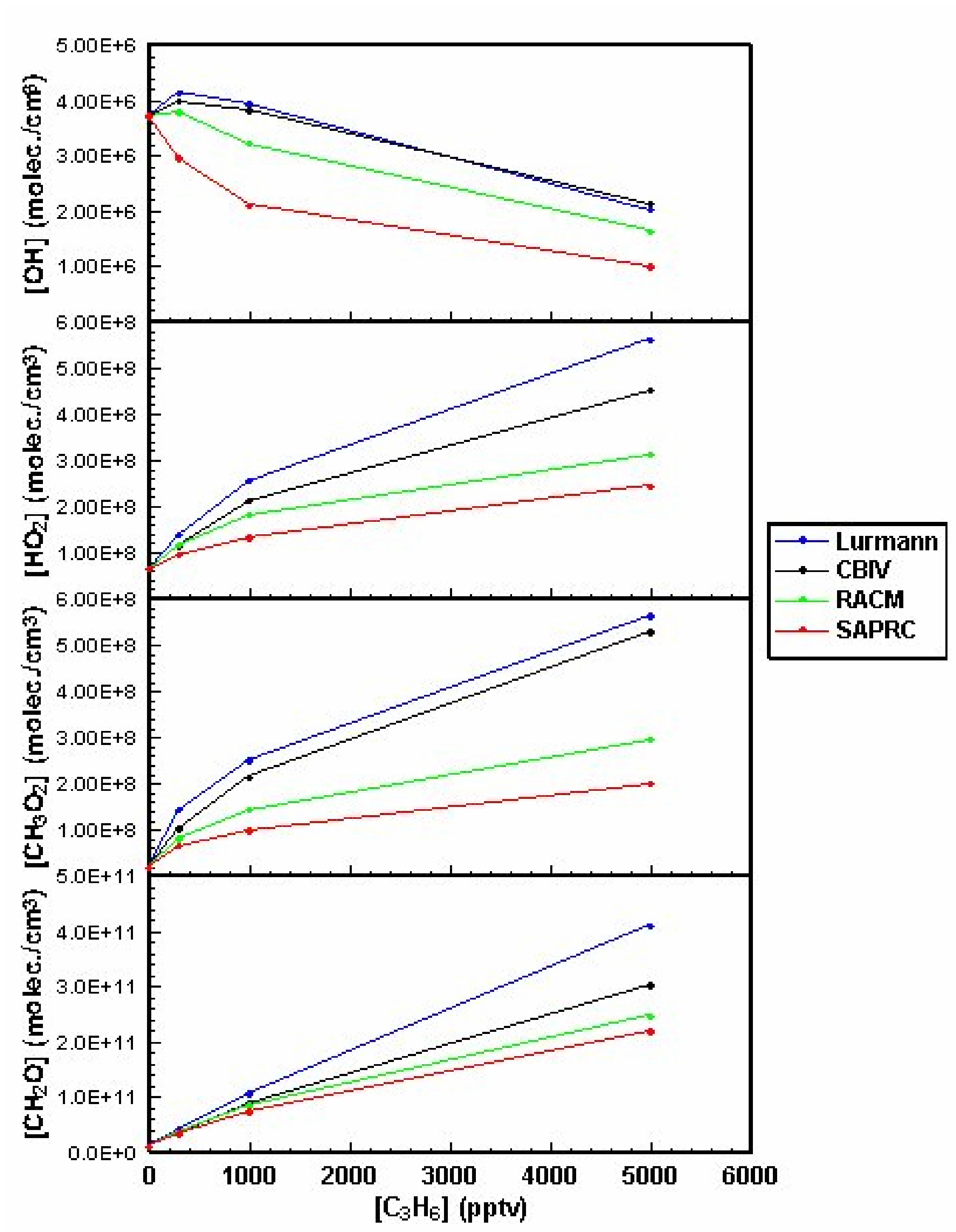

Figure 4.4. Several critical species versus propene for BL high NO_x test runs.

level. This results from the increased production of acetyl peroxy radicals (CH_3CO_3). For the same reason as discussed for propane, increases in CH_2O always result from higher CH_3O_2 levels.

4.2.3 Aromatics (Tolulene, Xylene)

The reaction with OH is the single most important sink for atmospheric aromatics, including benzene and all alkyl-substituted benzenes, e.g., toluene and xylene. Their reactions with OH may proceed via two different channels: OH addition and H-abstraction. Under tropospheric conditions, the H-abstraction channel accounts for less than 10% (Atkinson, 1994). Therefore, the OH-adduction channel is of primary interest. When OH is added to the aromatic ring, an intermediate OH-alkylbenzene adduct is produced, which decomposes by reacting with O_2. The products include phenol, epoxide-alkoxy radicals, bicycloalkyl radicals, peroxy radicals, benzene oxides/oxepins. The subsequent reactions of the radical species typically lead to the formation of unsaturated carbonyls, dicarbonyls, and epoxy-carbonyls.

Benzene is by far the most abundant aromatic hydrocarbon. However, because of its low reactivity it is usually not of major importance in its impact on OH and other radical species. Instead, toluene and xylene typically have much larger impacts and thus have here been chosen to be representative of the aromatic family. The reason both toluene and xylene were selected is that they are quite different in their chemical reactivity. Toluene, to some extent, has the properties of alkanes, while xylene behaves more closely to an alkene under tropospheric conditions. But xylene does not react with either O_3 or NO_3 as the alkenes do.

In Figures 4.5 through 4.8, the concentration levels of four critical photochemical species are shown as influenced by the addition of these two aromatic species. In the case toluene it can be seen that this species has a somewhat similar trend to that of propane; whereas xylene is seen as being similar to propene. And, from the magnitude of the change in the concentration levels of OH, HO_2, CH_3O_2, and CH_2O, it may be concluded that toluene is more reactive than propane; whereas xylene is less active than propene. The only major difference between propane and toluene comes from its effect on OH for the case of high NO_x. When the concentration level of toluene is low (less than 1 ppbv), it either increases OH in the Lurmann and RACM mechanisms or it has no influence. Seemingly, this is because of extra OH radicals generated from increased levels of HO_2 which is large enough to compensate for the OH loss via the reaction with toluene. Except for the Lurmann mechanism, the other three mechanisms give similar trends for all four product species. The unusual character of the Lurmann mechanism is a result of its failure to treat toluene and xylene separately. If we compare the OH part of Figure 4.5 with Figure 4.7, we find that aromatics in the Lurmann mechanism are more reactive than toluene in the other three mechanisms, but less reactive than xylene in the other mechanisms.

4.2.4 Isoprene

Isoprene (2-methyl-1,3-butadiene or $CH_2=C(CH_3)CH=CH_2$) is the simplest diene type compound and is also the dominant NMHC emitted by natural vegetation in the atmosphere (Brewer et al., 1984; Miyoshi et al., 1994; Starn et al., 1998; Nouaime et al.1998; Shallcross and Monks, 2000). Because of its great importance as a highly reactive biogenic alkene with a high emission rate, we have included it here even though

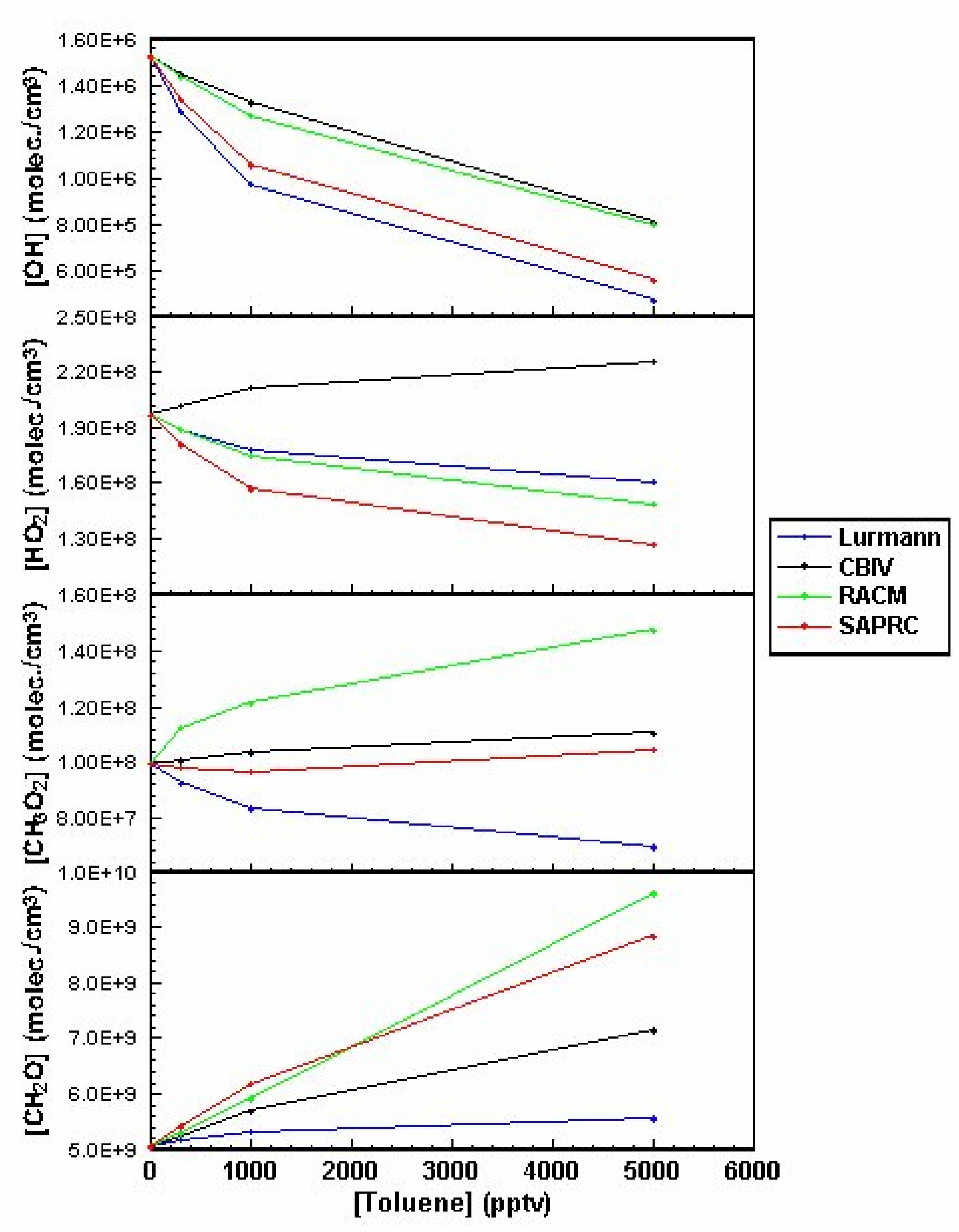

Figure 4.5. Several critical species versus toluene for BL low NO_x test runs.

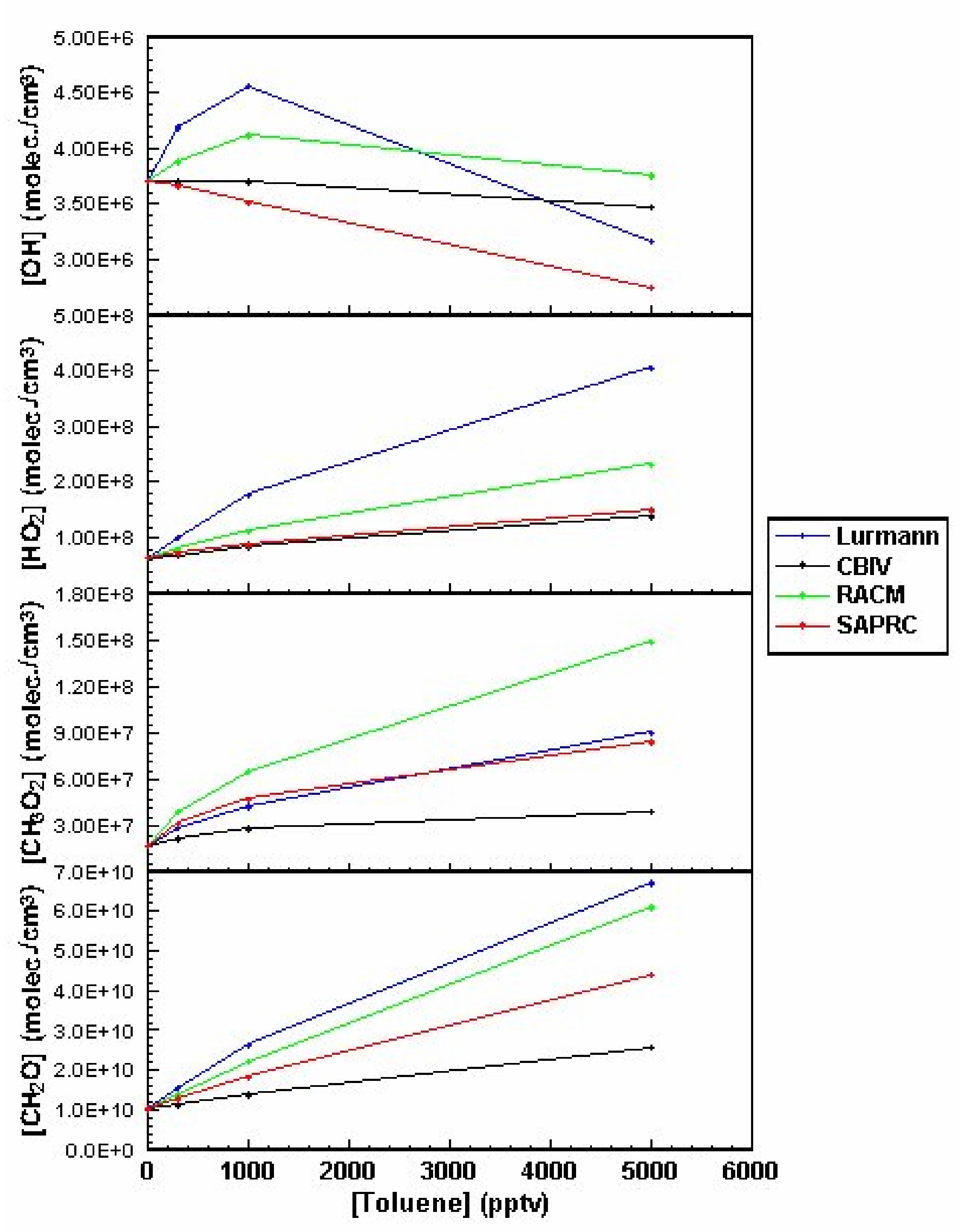

Figure 4.6. Several critical species versus toluene for BL high NO_x test runs.

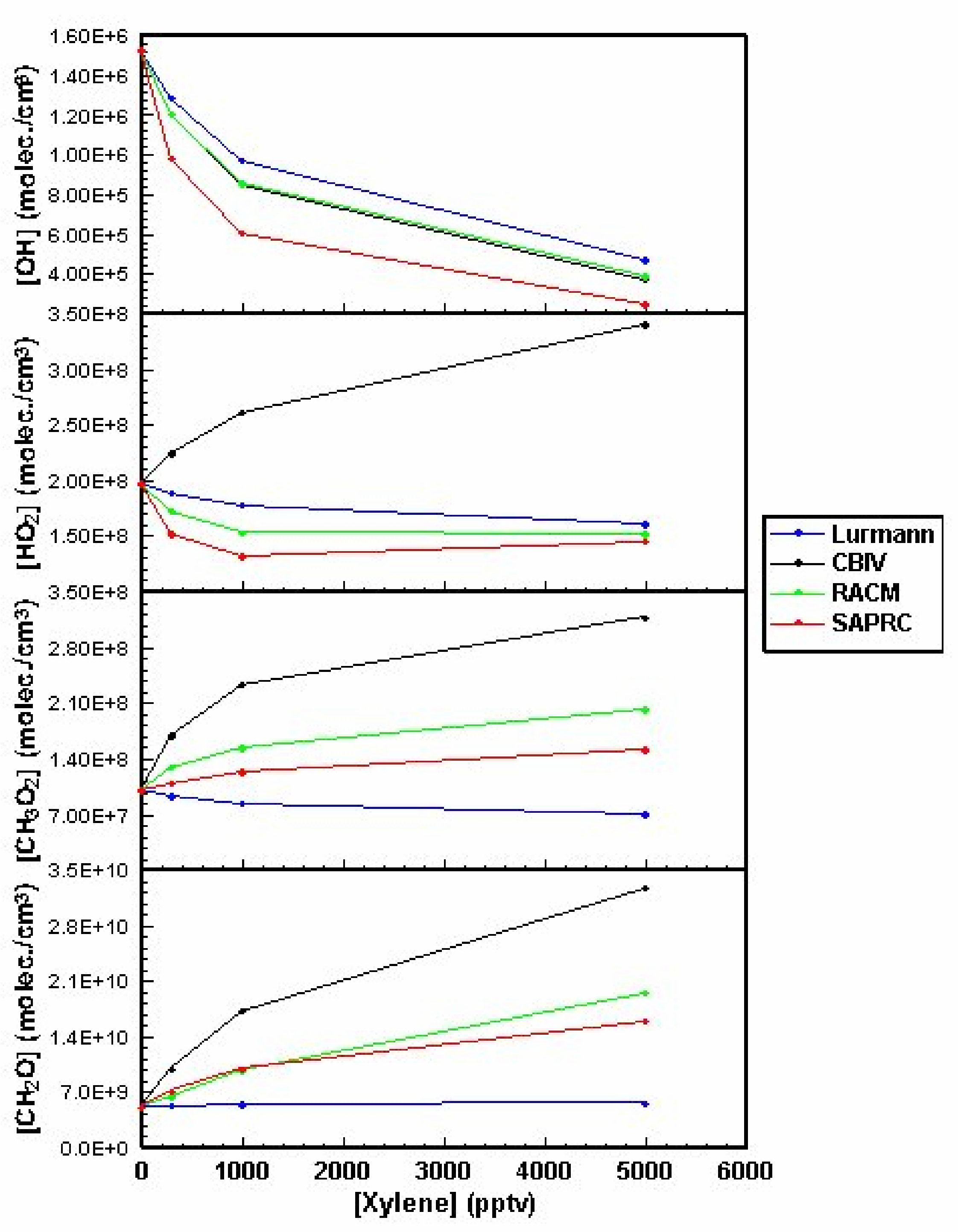

Figure 4.7. Several critical species versus xylene for BL low NO_x test runs.

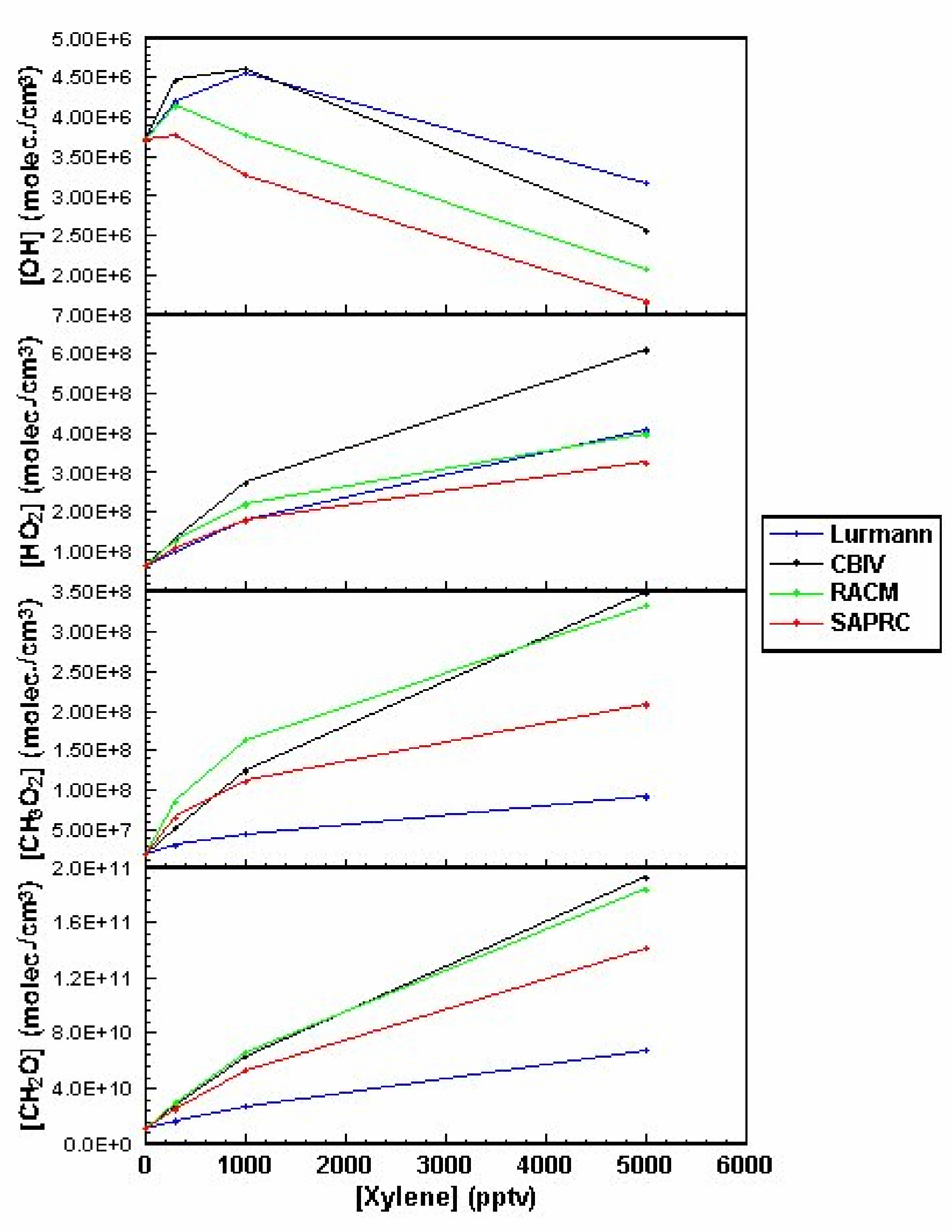

Figure 4.8. Several critical species versus xylene for BL high NO_x test runs.

no measurable concentration of it is reported in the TRACE-P data set due to the dominance of marine sampling. Quite interestingly, isoprene is treated separately in all four NMHC mechanisms because of its unique chemical reactivity.

Isoprene can react with OH, O_3, and NO_3, as reflected in all four NMHC mechanisms. Among these reaction pathways, the reaction with OH is typically the most significant removal pathway for isoprene. Like propene, isoprene also undergoes OH addition at the 1- or 4- position to produce a β-hydroxyalkyl radical which then isomerizes or goes through reactions similar to R4.3 to R4.6. Thus, it generates peroxy radicals, nitrates, aldehydes, peroxides, or other stable products. Generally, the products from the reaction of isoprene with O_3 include formaldehyde, methyl vinyl ketone (MVK), and methacrolein. The reaction of isoprene with NO_3 leads to the formation of NO_2 as well as other peroxy radicals, aldehydes, or peroxides. Because of the complexity of the structure of isoprene, a lot of reactions are involved in isoprene oxidation, and the methods of simplification are also different in various mechanisms. For example, only one peroxy radical is produced from the reaction of OH with isoprene, which then undergoes a series of reactions similar to R4.3 to R4.6 in both the Lurmann and RACM mechanisms. In CBIV, two intermediate products are formed from the same reaction, and they both then react with NO and HO_2 generating different products. In the SAPRC mechanism, however, all final products, including several operator peroxy radicals, formaldehyde, MVK, methacrolein, are formed in one step without any intermediate processes.

The impact from isoprene on several critical photochemical species is shown in Tables 4.9 and 4.10. Similar to propene, the addition of high levels of isoprene (5 ppbv)

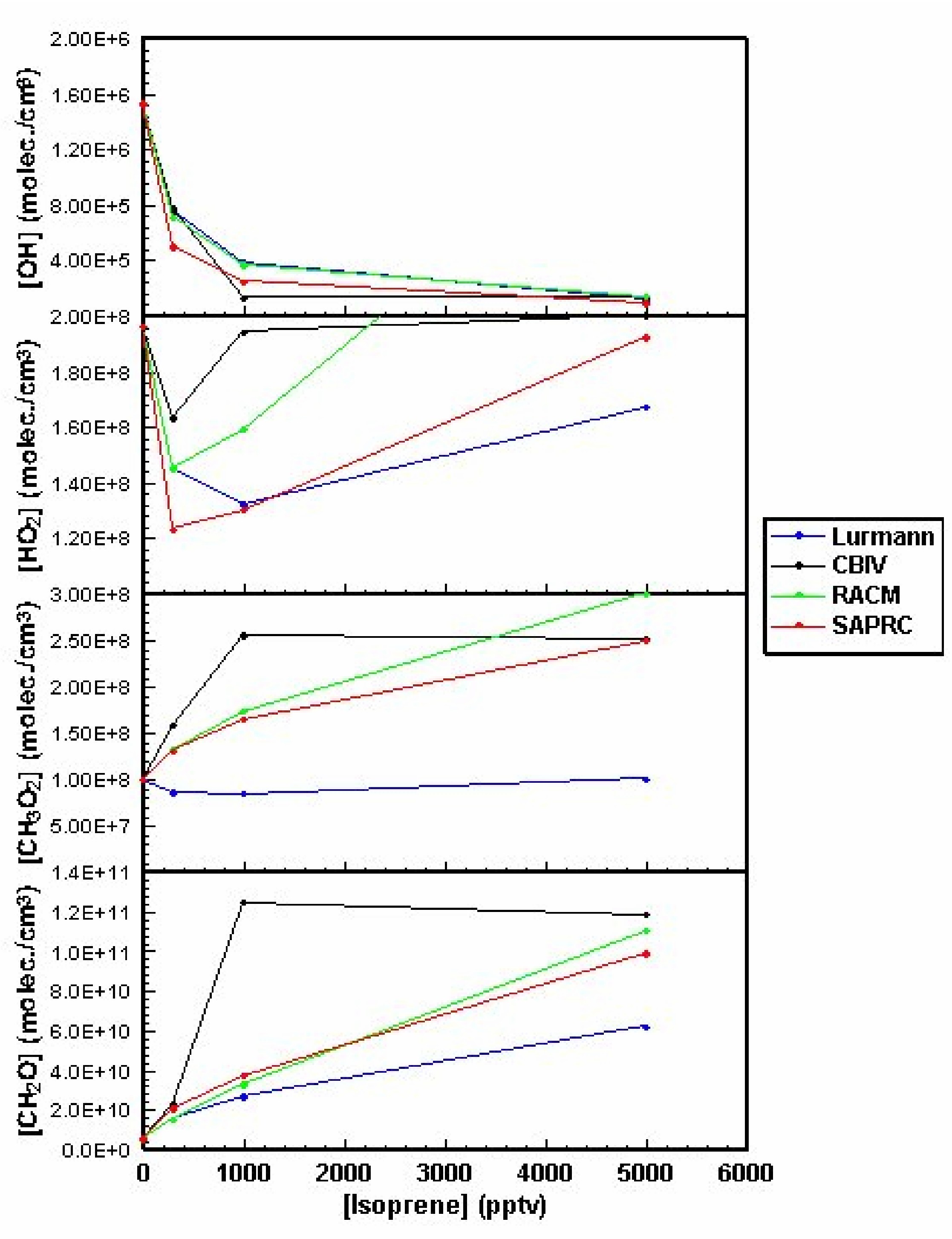

Figure 4.9. Several critical species versus isoprene for BL low NO_x test runs.

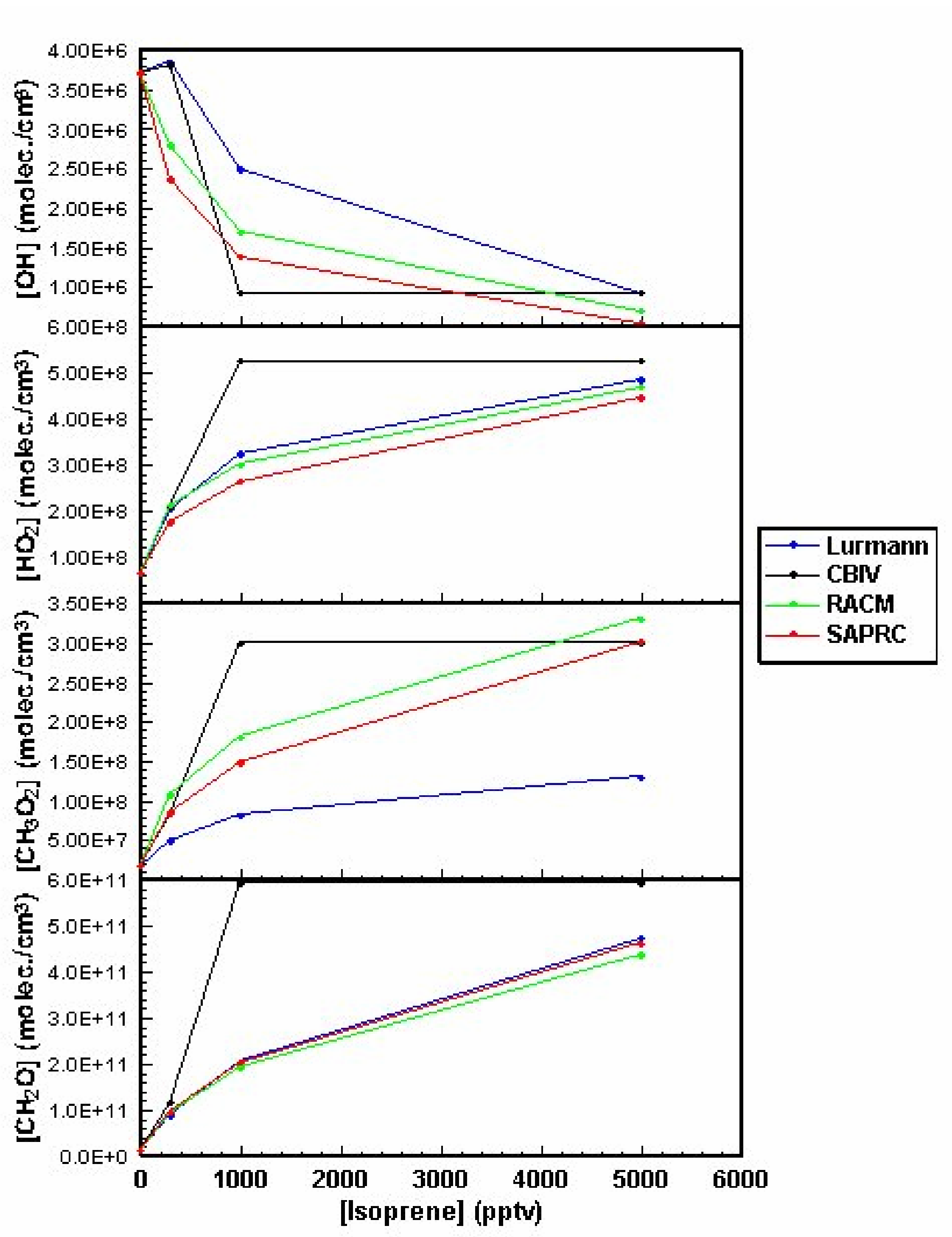

Figure 4.10. Several critical species versus isoprene for BL high NO_x test runs.

decreases the OH level; whereas, it typically increases the levels of HO_2, CH_3O_2, and CH_2O, at both high and low mixing ratios of NO_x. The one exception occurs when NO_x is low. In this case it results in a huge decrease in the primary source of HO_2 (OH+CO) because of the much reduced level of OH in both the Lurmann and SAPRC mechanisms.

4.3 Budget Analysis of Critical Photochemical Species

The purpose of this budget analysis is to focus on the specific sources and sinks of the four critical photochemical by-products resulting from the oxidation of NMHCs under different conditions, e.g., high or low NO_x. Yet another point of this analysis is to show more clearly how the four NMHC mechanisms differ under the same atmospheric conditions. All discussion in the following text is based on the previously cited NMHC test runs made for the BL only since only BL data contained high enough NMHC's to have any influence on the photochemistry of the region.

4.3.1 OH

The relative effects on OH from the four reactive NMHCs are shown in Table 4.6. From here it can be seen that, for all four mechanisms, the addition of any single NMHC species always decreases OH levels when the BL NO_x concentration is low. Thus, the more hydrocarbons added, the lower the OH level. However, at high NO_x, the OH is found to increase at certain concentration levels of NMHCs. Among the four tested hydrocarbons, OH levels are most sensitive to changes in propene and xylene, reflecting their higher reactivity.

For the low NO_x case, the primary production of OH, which is from the reaction of excited oxygen $O(^1D)$ and water vapor, is always the major source of OH. With the

Table 4.6. Relative effect of several NMHCs on OH for test runs. The values in boldface denote the biggest relative change.

$[NO_x]$	HC	[HC]	CB-IV	Lurmann	RACM	SAPRC	Trend
0.09 ppb	C_3H_8	0.3 ppb	-0.1%	-0.8%	**-2.0%**	-0.9%	Decrease
		1 ppb	-0.4%	-2.6%	**-6.4%**	-3.4%	Decrease
		5 ppb	-2.2%	-12%	**-25%**	-15%	Decrease
	C_3H_6	0.3 ppb	-25%	-29%	-25%	**-43%**	Decrease
		1 ppb	-51%	-57%	-51%	**-70%**	Decrease
		5 ppb	-80%	-86%	-79%	**-91%**	Decrease
	TOL	0.3 ppb	-5.1%	**-16%**	-6.0%	-12%	Decrease
		1 ppb	-13%	**-36%**	-17%	-31%	Decrease
		5 ppb	-47%	**-69%**	-48%	-64%	Decrease
	XYL	0.3 ppb	-21%	-16%	-21%	**-36%**	Decrease
		1 ppb	-44%	-36%	-44%	**-61%**	Decrease
		5 ppb	-76%	-69%	-75%	**-84%**	Decrease
3 ppb	C_3H_8	0.3 ppb	0.03%	**-0.2%**	0.1%	-0.03%	Mixed
		1 ppb	0.3%	**-0.4%**	-0.2%	0.3%	Mixed
		5 ppb	0.9%	-1.6%	**-3.5%**	1.5%	Mixed
	C_3H_6	0.3 ppb	7.2%	11%	2.0%	**-20%**	Mixed
		1 ppb	2.8%	5.7%	-13%	**-43%**	Mixed
		5 ppb	-43%	-46%	-56%	**-74%**	Decrease
	TOL	0.3 ppb	-0.2%	**13%**	4.7%	-1.3%	Mixed
		1 ppb	-0.2%	**23%**	11%	-5.3%	Mixed
		5 ppb	-6.5%	-15%	1.2%	**-26%**	Mixed
	XYL	0.3 ppb	**20%**	13%	12%	1.6%	Increase
		1 ppb	**24%**	23%	1.6%	-12%	Mixed
		5 ppb	-31%	-15%	-44%	**-56%**	Decrease

addition of NMHCs, the concentration of HO_2 increases and HO_2 can react with NO or O_3 to produce secondary OH. The more hydrocarbon present, and the more chemically reactive the hydrocarbon, the more important this secondary source of OH becomes. The reaction with the relatively long-lived species CO and CH_4 always defines the major sinks for the OH radical. When substantial hydrocarbons are present, some of these also add to the sink for OH. In addition, there can be some final products from hydrocarbon oxidation that can serve as OH sinks (e.g., formaldehyde, acetaldehyde, higher aldehydes, and peroxides).

The addition of propane does not affect the OH concentrations significantly. Even when its concentration reaches levels of 5 ppbv, the biggest decrease in OH (given in RACM mechanism) is only ~ 25%. The RACM mechanism always lowers the OH level the most regardless of the amount of propane; while the CBIV mechanism shows no effect on OH levels from propane (see Figure 4.1). This is mainly because of the strong sinks for the OH radical in the RACM mechanism. One source of this elevated OH sink in the RACM mechanism is the high reaction rate constant for the OH/propane reaction (e.g., 2.2×10^{-12} cm^3 $(molec.\cdot s)^{-1}$ at 298K) as compared to 1.1×10^{-12} cm^3 $(molec.\cdot s)^{-1}$ for the Lurmann mechanism and 1.0×10^{-12} cm^3 $(molec.\cdot s)^{-1}$ for SAPRC. Another reason for the higher sink rate in the RACM mechanism is the abundance of aldehydes and peroxides produced in this mechanism, all of which further react with OH. Despite these differences, the ratio of OH given by CBIV over that by RACM is only approximately 1.3 when the propane concentration is 5 ppbv.

As mentioned before, the OH level is most sensitive to the change in propene concentration. The overall difference in the propene results as given by the four mechanisms, however, is not as large as might be expected. The CBIV and RACM are quite similar, both of which are ~ 2.5 times higher than given by the SAPRC mechanism. For the SAPRC mechanism, propene seems to have the largest impact on OH. Again, the major reason for the difference in mechanisms is the dissimilarity in the magnitude of their respective OH sinks. The total OH sink rate in the SAPRC mechanism is significantly higher than that in either CBIV or RACM mechanism. This difference is partly a result of the higher reaction rate constant for the OH/propene reaction used in SAPRC which is 3.2×10^{-11} cm^3 $(molec.\cdot s)^{-1}$ at 298K, compared to 2.5×10^{-11} cm^3 $(molec.\cdot s)^{-1}$ in the Lurmann mechanism and 2.8×10^{-11} cm^3 $(molec.\cdot s)^{-1}$ in the CBIV mechanism. Furthermore, as already noted there is a higher production of acetaldehydes and peroxides in the SAPRC mechanism, both of which react with OH.

Concerning toluene, the biggest impact on OH level occurs in the Lurmann mechanism, as shown in Figure 4.5, because of the method of lumping species. For example, the rate constant for the OH/toluene reaction is 1.5×10^{-11} cm^3 $(molec.\cdot s)^{-1}$ at 298K, compared to 6.0×10^{-12} cm^3 $(molec.\cdot s)^{-1}$ in both the RACM and SAPRC mechanisms, and 6.3×10^{-12} cm^3 $(molec.\cdot s)^{-1}$ in CBIV. This higher reactivity assigned to toluene in the Lurmann mechanism leads to a ratio of ~ 1.7 for the absolute OH level given in CBIV over that in Lurmann when the toluene level is 5 ppbv.

For the same reason, in the Lurmann mechanism xylene has the least impact on decreasing the OH concentration (see Figure 4.7). In this case, the rate constant of 1.5×10^{-11} cm^3 $(molec.\cdot s)^{-1}$, at 298K, for the OH/xylene reaction is slower in the Lurmann mechanism, compared to 2.4×10^{-11} cm^3 $(molec.\cdot s)^{-1}$ in RACM, 2.5×10^{-11} cm^3 $(molec.\cdot s)^{-1}$ in CBIV, and 2.6×10^{-11} cm^3 $(molec.\cdot s)^{-1}$ in SAPRC. As a result, the sharpest contrast between the Lurmann and SAPRC mechanisms is seen when the test run involves 5 ppbv of xylene, e.g., ratio of OH equals 1.9. Similar to the propene case, the biggest impact of xylene on OH is found when using the SAPRC mechanism, reflecting a very large OH sink. As before, higher levels of peroxides, acetaldehyde, and higher aldehydes all contribute significantly in the SAPRC mechanism to an excessive large OH sink.

When the NO_x level is high, there is adequate NO to convert substantial amounts of HO_2 to OH. Consequently, the secondary production of OH from HO_2 becomes the dominant OH source, exceeding primary OH production ($O(^1D)+H_2O$). The removal pathways, such as the reactions of OH with CO and CH_4, are still important, but are not as dominant as when the levels of NO_x are low. This is because NO_2 competes with these species in reacting with OH, especially when hydrocarbon concentrations are low. Moreover, in a high NO environment it promotes the rapid oxidation of hydrocarbons, thus leading to the formation of significant levels of peroxides and carbonyls, all of which consume OH. Another distinctive feature of high NO_x levels is that the OH level does not always monotonically change with hydrocarbons, as shown in Figures 4.2, 4.4, 4.6, and 4.8. In many cases, OH levels are unexpectedly elevated with the addition of small amounts of NMHC species (e.g., 0.3 ppbv), but begin to decrease as NMHC mixing ratios reach up to 5 ppbv.

For the high NO_x case, the addition of increasing amounts of propane has only a minor impact on the OH level for all four mechanisms. The biggest change in OH level is seen as a 3.5% decrease, when using the RACM mechanism. Overall, the four mechanisms behave in a similar way at low NO_x levels with added propane. The largest difference between any two mechanisms is only 5% (CBIV vs. RACM).

The increase of OH with additions of propene occurs even in the presence of only small amounts of propene (e.g., less than 1 ppbv). The one exception to this is found in the SAPRC mechanism where the OH level decreases with propene. This is partly due to lower secondary OH production from HO_2 since HO_2 is only slightly increased by additions of propene in the SAPRC mechanism. Another reason for the lower OH level in the SAPRC mechanism is the very large OH sinks inherent in this mechanism, which has been discussed earlier. All factors being considered, the level of OH with additions of propene is 2.2 times higher in the CBIV mechanism than for SAPRC. Because of the higher reactivity of propene, the OH loss via reaction with propene (even under high NO_x conditions) can not be compensated by secondary OH production; thus, leading to lower and lower values with increasing additions of propene.

For the same reasons discussed above, the largest drop in OH with additions of aromatic compounds always occurs with the SAPRC mechanism. As mentioned earlier, toluene is assigned a higher reactivity in the Lurmann mechanism than in the other three mechanisms. Therefore, in the Lurmann mechanism, the HO_2 produced by toluene oxidation can impact on OH by its reaction with NO when NO_x level is high and toluene level is low. However, as the toluene concentration continues to increase, its rapid reaction with OH in the Lurmann mechanism quickly overcomes the secondary source of OH. Thus, the highest OH level with additions of toluene is not given by the Lurmann mechanism but by the RACM mechanism, which is ~ 1.4 times higher than that given by the SAPRC mechanism, with the other two mechanisms being somewhat less this.

As for xylene, the shapes of the curves for the four mechanisms are quite similar to those for propene. Thus, the least impact on OH occurs for the Lurmann mechanism, and the ratio between it and that of the SAPRC mechanism is nearly 1.9 when the xylene concentration is 5 ppbv.

4.3.2 HO_2

The quantitative impact of the four test hydrocarbons on HO_2 is shown in Table 4.7. In all four mechanisms, HO_2 always increases with increasing hydrocarbon levels when the BL NO_x concentration is high. The increase seen is monotonic with the concentration of the test hydrocarbon. However, the impact predicted from the four mechanisms is quite different when the NO_x level is low. HO_2 is found to always increase with the addition of NMHCs based on the CBIV mechanism; whereas, the opposite tendency is typically seen for the other three mechanisms. Again, the reactive hydrocarbons propene and xylene tend to have much more of an impact on HO_2 than propane and toluene.

The major HO_2 production comes directly from reactions of the OH radical with common trace gases in the troposphere. This would include carbon monoxide, which reacts with OH to form atomic H subsequently reacts with molecular oxygen to form a HO_2 radical. It also includes the reaction with O_3 or formaldehyde, the reaction of active methyloxy radical ($CH_3O\cdot$) with molecular oxygen, or the photolysis of peroxide or formaldehyde. HO_2 can also be formed from the decomposition of compounds like peroxynitric acid (HO_2NO_2) or hydroxymethylperoxy radical ($HOCH_2OO\cdot$, the adduct of HO_2 and CH_2O). These compounds, however, are formed from HO_2 and then quickly decompose back to produce HO_2. The net effect from these processes at equilibrium state

Table 4.7. Relative effect of several NMHCs on HO_2 for test runs. The values in boldface denote the biggest relative change.

$[NO_x]$	HC	[HC]	CB-IV	Lurmann	RACM	SAPRC	Trend
0.09 ppb	C_3H_8	0.3 ppb	0.1%	-0.6%	**-1.1%**	-0.5%	Mixed
		1 ppb	0.2%	-1.8%	**-3.8%**	-2.0%	Mixed
		5 ppb	0.8%	-8.4%	**-15%**	-8.7%	Mixed
	C_3H_6	0.3 ppb	-8.6%	7.2%	-14%	**-27%**	Mixed
		1 ppb	9.4%	25%	-22%	**-36%**	Mixed
		5 ppb	53%	**144%**	2.2%	-6.8%	Mixed
	TOL	0.3 ppb	2.7%	-4.0%	-4.0%	**-8.3%**	Mixed
		1 ppb	7.8%	-9.6%	-11%	**-21%**	Mixed
		5 ppb	15%	-18%	-25%	**-36%**	Mixed
	XYL	0.3 ppb	14%	-4.0%	-13%	**-23%**	Mixed
		1 ppb	33%	-9.6%	-22%	**-33%**	Mixed
		5 ppb	**73%**	-18%	-23%	-27%	Mixed
3 ppb	C_3H_8	0.3 ppb	0.4%	0.4%	**3.9%**	1.4%	Increase
		1 ppb	1.2%	1.6%	**12%**	5.0%	Increase
		5 ppb	5.6%	8.6%	**54%**	24%	Increase
	C_3H_6	0.3 ppb	84%	**122%**	86%	50%	Increase
		1 ppb	241%	**313%**	193%	111%	Increase
		5 ppb	631%	**808%**	405%	293%	Increase
	TOL	0.3 ppb	6.6%	**58%**	25%	13%	Increase
		1 ppb	34%	**185%**	78%	39%	Increase
		5 ppb	122%	**555%**	273%	139%	Increase
	XYL	0.3 ppb	**109%**	58%	101%	73%	Increase
		1 ppb	**339%**	185%	250%	185%	Increase
		5 ppb	**886%**	555%	539%	421%	Increase

is nearly zero. Thus, they do not actually increase HO_2 formation. The counterpart in HO_2 sinks includes the association reactions of HO_2 with NO_2, formaldehyde, or methyl peroxy radical (CH_3O_2), which do not really consume HO_2. More importantly, HO_2 may react with NO and O_3, or undergo self-reaction, thus being tied up in a stable form such that elimination from the atmosphere is quite possible.

When the NO_x level is high and there are added NMHCs, the enhanced levels of methyl peroxy radical (CH_3O_2), other peroxy radicals, and formaldehyde all can contribute to increase levels of HO_2. On the other hand, the sinks of HO_2 stay relatively stable because the reactions with NO_x are always the major removal pathways of HO_2, and the total short-lived nitrogen, which is mainly made up of NO and NO_2, is held constant in the model calculation, as stated in chapter 2.1. Consequently, larger sources and nearly constant sinks lead to increasing concentration level of HO_2. How large this increase is depends on the type of hydrocarbon.

As compared with the other three test hydrocarbons, propane does not lift the HO_2 level significantly. The biggest increase in HO_2 is found to be only 50%, based on the RACM mechanism. As discussed in section 4.3.1, OH is also not influenced much by propane. Accordingly, the HO_2 source coming from the reaction of OH with CO remains relatively constant. However, due to the large increase in the levels of both CH_3O_2 and formaldehyde, more HO_2 is produced from the CH_3O/O_2 and OH/CH_2O reactions. Thus, it is the higher production of CH_3O_2 and CH_2O in the RACM mechanism that is the main reason for the enhancement in HO_2 source. In addition, other peroxy radicals generated in the process of propane oxidation can also react with NO to form HO_2. Thus, the extra formation of peroxy radicals other than CH_3O_2 in the RACM mechanism versus other mechanisms tends to generate higher HO_2 levels. As a result, the ratio of HO_2 given by the RACM mechanism over that given by the CBIV or Lurmann mechanisms is ~ 1.5 when BL propane is at 5 ppbv.

For propene, the HO_2 concentration is found to be increased by up to an order of magnitude when the BL mixing ratio of propene approaches 5 ppbv, reflecting the greater reactivity of propene. Here the sharpest contrast is seen between the Lurmann and SAPRC mechanisms which differ by a factor of 2.3. This is a direct result of both lower than average HO_2 sources in the SAPRC mechanism and higher than average sources in the Lurmann mechanism. As discussed earlier, the calculated OH level from the SAPRC mechanism is always lower than that in any other mechanism when the NO_x level is high. This also leads to lower concentrations of both CH_3O_2 and CH_2O. The Lurmann mechanism produces the highest CH_3O_2 and CH_2O, and nearly the highest OH concentrations among the four mechanisms. This is the reason why the highest predicted HO_2 level is found in this mechanism.

Similar to propene, the addition of toluene produces the highest HO_2 formation rate, and thus, the highest HO_2 level in the Lurmann mechanism. This again reflects the higher reactivity of toluene in this mechanism. Not only does the high production of CH_3O_2 and CH_2O enhance the HO_2 level, but considerable HO_2 is also generated from the reactions of NO with aromatic peroxy radicals, such as TO2· and TCO_3 ($CHOCH{=}CHCO_3$). As a result, the HO_2 levels given by the Lurmann mechanism triple that calculated from the SAPRC or CBIV mechanisms at mixing ratio of toluene of 5 ppbv.

Xylene revealed its biggest impact on HO_2 levels when the NO_x level is at its highest. Xylene affects the HO_2 level in a similar way as propene under the high NO_x conditions. However, the highest HO_2 level is calculated when using the CBIV mechanism because of this mechanism's higher production of CH_3O_2 and CH_2O from xylene. The HO_2 concentration in the CBIV mechanism is twice that calculated from the SAPRC mechanism when using mixing ratio of xylene of 5 ppbv.

When the NO_x level is reduced, NO_x is not abundant enough to prevent HO_2 CH_3O_2, and other peroxy radicals from reacting with HO_2. In another words, the reaction with NO_x is not the single most important removal pathway for HO_2. With the addition of NMHCs, the levels of all these competing species increase. Given that the total amount of short-lived nitrogen is fixed in the model calculation, substantial fraction of HO_2 radicals is removed by non-NO_x pathways at low NO_x levels. As a result, the total HO_2 sink rate typically increases with the presence of NMHCs. On the other hand, the HO_2 sources are enhanced by NMHCs in general, regardless of the NO_x levels. Therefore, the addition of NMHCs leads to increases in both HO_2 sources and HO_2 sinks. Consequently, a different impact from NMHCs on HO_2 can be found in the different mechanisms (i.e., Table 4.7).

As discussed in section 4.3.1, propane has little impact on OH under the low NO_x conditions. As a result, the HO_2 levels are not significantly affected by propane. As shown in Table 4.7, the HO_2 levels were changed by less than 15% in all four mechanisms even at high levels of propane. The HO_2 level is typically decreased with the addition of propane, most in the RACM mechanism (i.e., Figure 4.1). However, different impact on HO_2 is found in the CBIV mechanism where the HO_2 level nearly stays constant regardless of the amounts of added propane. This is mainly because propane has almost no effect on the OH levels, which gives a relatively constant HO_2 source in the CBIV mechanism. Despite this difference, in CBIV and RACM, the results given by them only differ by 20%.

The four mechanisms showed different impact on HO_2 levels from propene (see Figure 4.3). As discussed in section 4.2.2, the difference results from the fact that HO_2 levels are decreased at low levels of propene in some of the four mechanisms. Overall, however, HO_2 tends to be increased by propene when its level is high. The biggest increase in HO_2 is found using the Lurmann mechanism, due to the enormously increased levels of CH_3O_2 and CH_2O. With addition of 5 ppbv of propene, the level of HO_2 is 2.6 times higher in the Lurmann mechanism than for SAPRC.

Similar to propane, the addition of toluene decreases the HO_2 level in all the mechanisms except CBIV where the HO_2 level slightly increases with increasing toluene (see Figure 4.5). This is because the toluene-OH adduct $TO_2\cdot$ reacts with NO to generate HO_2, leading to a high HO_2 source in the CBIV mechanism. As a result, the HO_2 levels predicted from the CBIV and SAPRC mechanisms differ by a factor of 1.8 at 5 ppbv of toluene.

Very similar impact of xylene on HO_2 level is seen to that from toluene in all four mechanisms (i.e., Figure 4.7). The only difference is that xylene is reactive enough to affect the HO_2 level to a much higher degree.

4.3.3 CH_3O_2

Besides HO_2, the methyl peroxy radical (CH_3O_2) is the most important organic peroxy radical species in tropospheric chemistry. Because it is a natural by-product of methane oxidation, the chemistry of CH_3O_2 is a part of HO_x-NO_x-CH_4 cycle in all four mechanisms. The impact of the test NMHC species on CH_3O_2 is displayed in Table 4.8.

The major CH_3O_2 formation comes primarily from methane oxidation by OH radicals and, less importantly, from the reaction of the methyl hydroperoxide (CH_3OOH) with OH. With the addition of NMHCs, other channels, such as the reaction of acetyl peroxy radical (CH_3CO_3) with NO, itself, or other peroxy radicals, or the photolysis of aldehydes, also become significant. Although CH_3O_2 can also be generated by the decomposition of methyl peroxy nitrate ($CH_3O_2NO_2$), that reaction is actually at equilibrium. Thus, this channel can not be considered as either source or sink of CH_3O_2. The species that primarily remove CH_3O_2 radicals are NO and HO_2, but CH_3O_2 can also be removed from the atmosphere via the self-reaction with CH_3O_2 or reaction with other peroxy radicals.

Similar to the HO_2 case, the total CH_3O_2 sink remains nearly constant when the NO_x level is high because reaction with NO is always the major removal pathway for CH_3O_2 and, as noted before, the total short-lived nitrogen is held constant in the model calculation. With the addition of NMHCs, however, CH_3CO_3 radicals are produced and they provide a CH_3O_2 source. As a result, the enhancement in sources with a relatively constant sink for CH_3O_2 leads to steady increases in CH_3O_2 with increasing NMHC levels under high NO_x conditions. This tends to be true for all four mechanisms, as shown in Figures 4.2, 4.4, 4.6, and 4.8. Although the same trend with increasing NMHCs is seen for both HO_2 and CH_3O_2 at high NO_x levels, CH_3O_2 is affected by increases in NMHCs to a much higher degree than is HO_2. For example, the addition of 5 ppbv of propene, one

Table 4.8. Relative effect of several NMHCs on CH_3HO_2 for test runs. The values in boldface denote the biggest relative change.

[NO_x]	HC	[HC]	CB-IV	Lurmann	RACM	SAPRC	Trend
0.09 ppb	C_3H_8	0.3 ppb	0.7%	-0.2%	**8.0%**	2.4%	Mixed
		1 ppb	2.2%	-0.9%	**18%**	4.4%	Mixed
		5 ppb	10%	-5.0%	**40%**	9.3%	Mixed
	C_3H_6	0.3 ppb	**151%**	130%	44%	14%	Increase
		1 ppb	**294%**	262%	94%	47%	Increase
		5 ppb	586%	**694%**	264%	179%	Increase
	TOL	0.3 ppb	1.0%	-7.2%	**13%**	-1.4%	Mixed
		1 ppb	4.1%	-17%	**22%**	-2.9%	Mixed
		5 ppb	11%	-30%	**49%**	5.4%	Mixed
	XYL	0.3 ppb	**70%**	-7.2%	29%	8.8%	Mixed
		1 ppb	**134%**	-17%	54%	23%	Mixed
		5 ppb	**220%**	-30%	103%	51%	Mixed
3 ppb	C_3H_8	0.3 ppb	1.5%	0.4%	**42%**	12%	Increase
		1 ppb	4.1%	1.7%	**116%**	35%	Increase
		5 ppb	17%	8.1%	**356%**	126%	Increase
	C_3H_6	0.3 ppb	500%	**746%**	368%	276%	Increase
		1 ppb	1162%	**1380%**	737%	476%	Increase
		5 ppb	3036%	**3241%**	1647%	1074%	Increase
	TOL	0.3 ppb	27%	67%	**132%**	87%	Increase
		1 ppb	67%	152%	**287%**	180%	Increase
		5 ppb	131%	435%	**784%**	398%	Increase
	XYL	0.3 ppb	199%	67%	**399%**	277%	Increase
		1 ppb	631%	152%	**863%**	550%	Increase
		5 ppb	**1969%**	435%	1874%	1128%	Increase

of the most reactive among the test NMHC species, can elevate the CH_3O_2 concentration by factors of 10 to 30, depending on the mechanism chosen.

Similar to the cases for OH and HO_2, propane has the least influence on the CH_3O_2 level. Interestingly, however, the CH_3O_2 concentration can be increased by almost four fold when using the RACM mechanism and propane is increased to 5 ppbv. It is the extremely high level of acetyl peroxy radical CH_3CO_3 produced in the RACM mechanism that leads to a higher CH_3O_2 production due to the reaction of NO with CH_3CO_3.

CH_3O_2 is also increased most by the RACM mechanism when toluene is selected as the test hydrocarbon. In this case the calculated CH_3O_2 concentration from the RACM mechanism is twice as high as that estimated from the Lurmann mechanism at 5 ppbv of toluene.

When the NO_x level is low, the reaction of CH_3O_2 with HO_2 is one of the major loss processes for CH_3O_2. However, other peroxy radical species (e.g., CH_3CO_3) can become important CH_3O_2 sinks with increasing NMHCs. The sources of CH_3O_2 in the absence of significant levels of NMHCs, as noted earlier, include the reactions of the OH radical with CH_4 and CH_3OOH. When NMHC levels become elevated, reactions involving CH_3CO_3 and the photolysis of aldehydes contribute substantially to the CH_3O_2 production but meanwhile may also contribute to the total CH_3O_2 sink. As discussed in section 4.3.1, the OH level is always lowered by any of the four test NMHC species in all four mechanisms when the NO_x level is low, and it leads to the decline in CH_3O_2 production from the OH/CH_4 reaction. If the loss is too much to be compensated by the CH_3O_2 production from other sources, e.g., reactions involving CH_3CO_3, this reduced total CH_3O_2 production will result in a drop in the CH_3O_2 level. That is exactly what happens in the Lurmann mechanism with the addition of propane, toluene, and xylene. In conclusion, CH_3O_2 levels are typically increased with the addition of NMHCs when the NO_x level is low. This increase is, however, much less when compared to that resulting from high NO_x case, as shown in Table 4.8.

As seen in Table 4.2, the biggest impact from propene on CH_3O_2 is based on the Lurmann mechanism due to the extremely high CH_3O_2 production from the reaction of propene with O_3 as well as the photolysis of aldehydes in this mechanism. The ratio between the CH_3O_2 levels given by the Lurmann and SAPRC mechanisms is 2.8 at 5 ppbv of propene. The calculated CH_3O_2 levels in the CBIV and Lurmann mechanisms differ by a factor of 4.6 at 5 ppbv of xylene.

4.3.4 CH_2O

Formaldehyde (CH_2O) being the most important and the lowest aliphatic aldehyde in the tropospheric chemistry is primarily a product of the reaction of CH_3O with O_2. The former species is generated from the reaction of CH_3O_2 with NO. As noted earlier, CH_2O is part of HO_x-NO_x-CH_4 chemistry in all the four mechanisms used here. In all cases, the CH_3O/O_2 reaction is the dominant source of CH_2O in the troposphere. CH_2O may also be formed from other peroxy radicals such as CH_3CO_3 in the presence of high levels of NMHCs, especially alkenes. Concerning CH_2O sinks, it is mainly removed form the atmosphere via reaction with OH or by photolysis. There are two pathways for the photolysis, with the ratio of their quantum yield being close to 2 to 1, as shown in reactions R4.7 and R4.8.

(R4.7) $CH_2O + h\nu \rightarrow CO + H2$

(R4.8) $CH_2O + h\nu \rightarrow CHO + H$

Both CHO and H go on to react to produce HO_2. When the NO_x level is low and NMHCs are present in the atmosphere, photolysis becomes the dominant loss pathway for CH_2O. Additionally, CH_2O is continually removed from the atmosphere by washout or rainout because of its moderate solubility.

As discussed earlier, the OH level is typically decreased by the addition of NMHCs, especially when the hydrocarbon level is high. This decrease leads to a drop in the CH_2O sink because the other sinks for CH_2O are not significantly affected by enhanced hydrocarbon oxidation. However, because of the dominance of the reaction of CH_3O with O_2 as a source of CH_2O, the CH_2O level is defined by the CH_3O_2 level. This is elevated by the addition of NMHCs. Therefore, because of an increased CH_2O source and only a slightly lower CH_2O sink, the net result is an increase in CH_2O levels with increasing amounts of NMHCs. As seen in Table 4.9, regardless of the NO_x level, the addition of hydrocarbons always leads to an increase in CH_2O, and this level monotonically increase with increasing NMHCs in all four mechanisms. Similar to HO_2 and CH_3O_2, the CH_2O level is most sensitive to changes in the concentration of propene, and least sensitive to propane changes.

When the NO_x level is high, as noted above, the total CH_2O sink tends to remain relatively constant with the addition of NMHCs. This means that the CH_2O level is mostly decided by its sources, i.e., the CH_3O_2 level. This is why the shift in the level of CH_2O follows the CH_3O_2 concentration with added NMHCs in all four mechanisms when the NOx level is high, i.e., see Figures 4.2, 4.4, 4.6, and 4.8.

Table 4.9. Relative effect of several NMHCs on CH_2O for test runs. The values in boldface denote the biggest relative change.

$[NO_x]$	HC	[HC]	CB-IV	Lurmann	RACM	SAPRC	Trend
0.09 ppb	C_3H_8	0.3 ppb	0.9%	0.2%	1.9%	**3.1%**	Increase
		1 ppb	2.1%	0.6%	5.9%	**8.7%**	Increase
		5 ppb	9.4%	2.1%	27%	**41%**	Increase
	C_3H_6	0.3 ppb	195%	**293%**	79%	130%	Increase
		1 ppb	516%	**952%**	260%	330%	Increase
		5 ppb	1631%	**4506%**	1097%	1093%	Increase
	TOL	0.3 ppb	3.8%	2.4%	5.1%	**7.4%**	Increase
		1 ppb	13%	5.5%	17%	**23%**	Increase
		5 ppb	42%	10.1%	**91.0%**	76%	Increase
	XYL	0.3 ppb	**96%**	2.4%	27%	40%	Increase
		1 ppb	**240%**	5.5%	91%	95%	Increase
		5 ppb	**549%**	10%	287%	214%	Increase
3 ppb	C_3H_8	0.3 ppb	0.8%	0.5%	**8.5%**	4.2%	Increase
		1 ppb	2.7%	1.9%	**28%**	14%	Increase
		5 ppb	12%	10%	**132%**	70%	Increase
	C_3H_6	0.3 ppb	244%	**302%**	255%	225%	Increase
		1 ppb	786%	**960%**	743%	638%	Increase
		5 ppb	2941%	**4024%**	2381%	2096%	Increase
	TOL	0.3 ppb	11%	**53%**	37%	26%	Increase
		1 ppb	36%	**163%**	120%	81%	Increase
		5 ppb	157%	**574%**	514%	342%	Increase
	XYL	0.3 ppb	168%	53%	**190%**	144%	Increase
		1 ppb	531%	163%	**557%**	425%	Increase
		5 ppb	**1839%**	574%	1749%	1322%	Increase

At lower NO_x levels, both OH and HO_2 drop simultaneously, which leads to a significant decrease in the total CH_2O sink. In this case, the decrease in the CH_2O sink also contributes to enhance the CH_2O level. In another words, the CH_2O level is not exclusively controlled by the CH_3O_2 level. For example, although the CH_3O_2 level drops with the addition of propane or aromatics in the Lurmann mechanism, it always increases, as shown in Figures 4.1, 4.5, and 4.7.

4.3.5 ALD2

The lumped species ALD2 does not represent exactly the same compounds in all four mechanisms of interest here. In the CBIV, Lurmann, and RACM mechanisms, ALD2 stands for all ≥C2 aldehydes, beginning with acetaldehyde. In the SAPRC mechanism, however, it exclusively represents acetaldehyde, and the other higher aldehydes are lumped into another species, RCHO. Similar to formaldehyde, ALD2 is the intermediate product resulting from NMHC oxidation, but it can not be formed from CH_4. Thus, it is less important of these two species in tropospheric chemistry. Additionally, ALD2 is treated in a different way in the four different oxidation mechanisms, making it a most difficult to compare them in the different mechanisms. For example, no ALD2 is produced by the oxidation of aromatic compounds in the Lurmann mechanism, whereas a great deal is formed in the other three mechanisms, e.g., Tables 4.2 through 4.5. Thus, the sources and sinks of ALD2 are not here analyzed in as much detail as done on CH_2O and CH_3O_2.

As mentioned above, ALD2 does not come from methane oxidation. It is produced via the oxidation of NMHCs by their reaction with OH or O_3. As a result, additions of NMHCs increase the ALD2 level. Its formation pathways include the reaction of NO with various higher molecular weight peroxy radicals, reaction of O_3 with alkenes, and the photolysis or oxidation of higher peroxides. It is removed by the reaction with OH radicals or from photolysis, with the former always being the dominant channel under tropospheric conditions. As a result, the total ALD2 sink is controlled by the OH level.

Not surprisingly, the ALD2 concentration is increased most by the addition of propene and its reaction with OH. The direct production of ALD2 from the reaction of propene with O_3 is also significant. The biggest increase in ALD2 from propene is that calculated from the Lurmann mechanism due to the ALD2 production from the reaction of O_3 with propene. The latter is much greater in the Lurmann mechanism than in any other mechanism. The largest impact from propane on ALD2 is seen in the RACM mechanism results because of its exceptionally high production of ALD2 from the propane/OH reaction. Concerning the aromatic hydrocarbons, both toluene and xylene show the highest calculated ALD2 levels when using the SAPRC mechanism. In this mechanism, there are two particularly strong ALD2 sources that do not exist in the other mechanisms. The first one is the photolysis of the higher aldehydes (RCHO), and the second one is the reaction of NO with higher peroxy acyl radicals (RCO_3).

4.3.6 RO_2

RO_2 means the ensemble of all peroxy radicals other than methyl peroxy radical. Same as CH_3O_2, RO_2 is one of the intermediate products resulting from NMHC oxidation. It can thus undergo a series of reactions similar to R4.3 through R4.6, but it can not be generated from methane and is therefore less important in tropospheric chemistry. Since there are numerous types of peroxy radical species in the atmosphere, they have to be somehow generalized to make the model calculation possible. As discussed in chapter 2, the methods of grouping the peroxy radicals are quite different in different mechanisms. Among the four mechanisms used in this study, RO_2 is highly generalized in the CBIV and SAPRC mechanisms, in which case only nine RO_2 species are employed. The introduction of several operator RO_2 species is the main form of the simplification. On the contrary, RO_2 is treated in considerable detail in the RACM mechanism where each NMHC species reacts with OH to produce a specific RO_2. This results in a total of 19 RO_2 species in the mechanism. All of these RO_2 react with NO, HO_2, CH_3O_2, NO_3, and CH_3CO_3. Thus, it is difficult to compare any single RO_2 species in the four mechanisms. Alternatively, one can compare the total amount of RO_2 in the four mechanisms to give somewhat of a qualitative look, e.g., see Tables 4.2 through 4.5. Here it can be seen that RO_2 is mostly increased with the addition of propene. More importantly, the total RO_2 level is basically of the same order of magnitude as that for HO_2 and CH_3O_2. And sometimes, with the addition of reactive NMHCs such as xylene or propene, it is actually higher than HO_2 or CH_3O_2. Consequently, even when using an average rate constant for the reaction of RO_2 with NO (which is less than that for reaction with HO_2 or CH_3O_2), the ability of RO_2 to convert NO to NO_2 and thus lead to ozone formation is comparable to that from HO_2 or CH_3O_2.

CHAPTER 5

TRACE-P DATA ANALYSIS AND DISCUSSION

As shown in chapter 4, the chemical consequences of the four mechanisms under the same ambient conditions can be significant. However, the differences shown in chapter 4 were all based on test runs involving specified tropospheric gas mixtures. In chapter 5, these same four photochemical mechanisms have been applied to the field data recorded during the TRACE-P campaign in order to assess the impact from these four different mechanisms under actual atmospheric conditions.

5.1 Separation of TRACE-P BL Based on NMHC Reactivity

As discussed in section 3.3.2, the median level of total reactive NMHCs in the BL during TRACE-P was found to be far lower than the test mixture values cited in chapter 4. For example, the median levels of propane were 630 pptv which is a factor of 8 times lower than the 5 ppbv cited in chapter 4. At 630 pptv, propane is hardly a factor in determining the OH concentration regardless of the NO_x level, as shown in Figures 4.1 and 4.2. Thus, the differences among the mechanisms for the BL data of TRACE-P only give a modest hint as to what the differences might be as one approaches a more urban environment. This is why we have further sub-divided the BL into three sub-regions according to the total NMHC reactivity with OH, as displayed in Figure 3.11. The median NMHC reactivity and dominant HC species in these regions are quite different, as shown in Table 5.1.

Table 5.1. Median NMHC reactivity and dominant NMHC species for different TRACE-P BL regions (s^{-1}).

Region	Median NMHC reactivity (s^{-1})	Dominant NMHC species
Entire BL	0.084	ALKA
Region 1	0.021	ALKA/Ethane
Region 2	0.054	ALKA/Ethane/AROM
Region 3	0.12	ALKA

Among the three moderate size regions identified, region 3 was found to be the most reactive one with a median total NMHC-OH reactivity of 0.12 s^{-1}, and the dominant NMHC species in this region were the reactive alkanes, ALKA ($C \geq 4$), and occasionally reactive aromatic hydrocarbons, AROM. Region 1 is seen as the least reactive one with a median total NMHC reactivity of only 0.021 s^{-1}. The dominant NMHC species in region 1 were ethane and ALKA. In region 2 there was no clearly dominant hydrocarbon species, and it was found to be moderately reactive with a median total NMHC reactivity of 0.054 s^{-1}.

5.2 A Detailed Examination of the NMHC Impact on OH, HO_2, CH_3O_2, and CH_2O

The GT time-dependent model used in this study has been previous employed to analyze other GTE data sets. Included in this number are PEM-West-A and B and PEM-Tropics-A and B. In the latter two cases model-predicted results were compared against observations for several selected species (e.g., NO_2, OH, HO_2, and CH_2O) [Crawford et al., 1999a; Davis et al., 2001, 2003; Chen et al., 2001; Olson et al., 2001]. Generally, the agreement between model calculations and observations was within a factor of 1.5. For the more recent TRACE-P field data, the overall agreement between model predictions and observations was also shown to be within a factor of 1.5 for HO_x species. This suggests that the model used in this study reasonably well simulates atmospheric variability in what are normally considered to be critical atmospheric species.

The BL median model-calculated concentrations of OH, HO_2, CH_3O_2, and CH_2O for the three BL regions selected for study here are shown in Table 5.2. For each region investigated the results from all four mechanisms are shown. In order to reveal the impact from NMHCs, we have also provided in this table the "background" situation as controlled by NO_x-HO_x-CH_4 chemistry only. These are displayed in the first column of this table. Note also, because of the very low concentrations of NMHCs in the FT, all results discussed in this chapter are exclusively for the BL.

As shown in Table 5.2, the four mechanisms generally gave similar results, especially for HO_x. However, this is not that surprising considering the low average levels of NMHCs found in the study region.. The biggest difference is seen between CBIV and RACM, as related to OH and HO_2 levels, which is 20% or less in all three regions. The difference in CH_2O was one of the largest between mechanisms which. This was ~ 30% and involved the difference between CBIV and SAPRC in region 3. Overall, the highest CH_2O concentration was that produced by the SAPRC mechanism and the lowest was given by CBIV. The overall result for CH_3O_2 revealed that the RACM mechanism as being moderately higher than those predicted by CBIV and Lurmann by ~ 70% in region 3. Overall, the CBIV and Lurmann mechanisms tended to perform in a similar manner. And it also appears that the results given by the RACM and SAPRC mechanisms were often close to each other.

Table 5.2. Model-predicted median concentrations of several critical photochemical species during TRACE-P (molecules/cm^3).

Region	Species	W/O NMHCs	CBIV	Lurmann	RACM	SAPRC
Region 1	OH	1.9×10^6	1.9×10^6	1.9×10^6	1.8×10^6	1.8×10^6
	HO_2	1.9×10^8	1.9×10^8	1.8×10^8	1.8×10^8	1.8×10^8
	CH_3O_2	1.8×10^8	1.8×10^8	1.7×10^8	1.8×10^8	1.7×10^8
	CH_2O	5.7×10^9	6.0×10^9	6.0×10^9	6.0×10^9	6.2×10^9
Region 2	OH	2.3×10^6	2.3×10^6	2.1×10^6	2.0×10^6	2.0×10^6
	HO_2	2.3×10^8	2.3×10^8	2.2×10^8	2.1×10^8	2.1×10^8
	CH_3O_2	1.2×10^8	1.2×10^8	1.2×10^8	1.5×10^8	1.3×10^8
	CH_2O	7.6×10^9	8.3×10^9	8.5×10^9	8.9×10^9	9.1×10^9
Region 3	OH	1.1×10^6	1.1×10^6	1.0×10^6	9.1×10^5	9.3×10^5
	HO_2	1.1×10^8	1.2×10^8	1.2×10^8	1.1×10^8	1.1×10^8
	CH_3O_2	3.5×10^7	4.2×10^7	4.6×10^7	7.3×10^7	5.9×10^7
	CH_2O	5.1×10^9	7.2×10^9	8.6×10^9	8.7×10^9	9.5×10^9

As seen from Table 5.2, in order to more clearly see the trends and differences between mechanisms we have presented the results from the region having the lowest NMHC levels on up to the region having the highest. This reflects the reactivity scale shown in Table 5.1. To further emphasize the differences between the four NMHC oxidation mechanisms, however, we also shown in Table 5.3 the relative impact from the NMHCs as related specifically to the levels of OH, HO_2, CH_3O_2, and CH_2O.

Table 5.3. Relative impact from NMHCs on several critical photochemical species during TRACE-P.

Region	Species	CBIV	Lurmann	RACM	SAPRC	Trend
Region 1	OH	-0.7%	-3%	-7%	-5%	Decrease
	HO_2	0.5%	-3%	-5%	-5%	Mixed
	CH_3O_2	0.7%	-1%	-0.7%	-4%	Mixed
	CH_2O	3%	3%	5%	7%	Increase
Region 2	OH	-2%	-8%	-15%	-12%	Decrease
	HO_2	1%	-3%	-8%	-7%	Mixed
	CH_3O_2	5%	0.9%	25%	6%	Increase
	CH_2O	11%	15%	20%	26%	Increase
Region 3	OH	-2%	-11%	-21%	-18%	Decrease
	HO_2	5%	0.8%	-7%	-5%	Mixed
	CH_3O_2	17%	22%	87%	57%	Increase
	CH_2O	33%	61%	58%	78%	Increase

5.2.1. OH

In all three regions (1, 2, and 3) the same trend was found for the impact of NMHCs on the level of OH, e.g., Tables 5.2 and 5.3. In all cases OH levels were lowered by all four mechanisms; and the magnitude of the change for each mechanism became larger as NMHCs levels increased. As expected, however, the magnitude of the change in OH was very much dependent on the NMHC mechanism chosen. The maximum impact was seen when using the RACM mechanism and the minimum was found for CBIV. For instance, OH was down by 21% and 2% in region 3 for RACM and CBIV mechanisms, respectively.

It should be noticed that the above stated percentages matches rather closely that of the test mixture results from propane under the low-NO_x case in chapter 4 (see Table 4.2). We note that the median NO_x mixing ratio in the BL during TRACE-P was ~120 pptv. This number is much closer to 90 pptv, representative of the low-NO_x case in the test runs in chapter 4, than that of the high-NO_x case (3 ppbv). Quite significant is the fact that only ~ 110 out of 2700 plus model runs in the BL had NO_x mixing ratios higher than 1 ppbv. This means that most of the model runs based on TRACE-P field data should be simulated best by low NO_x levels. Consequently, the results from NMHCs involving model runs with high-NO_x are greatly overshadowed by those involving a low-NO_x environment.

As illustrated in Figure 3.12, the alkanes were the dominant NMHC family for the altitude range of 0-2 km during TRACE-P. As a result, the difference in the reactivity of the alkanes with respect to OH is the major basis for the differences appearing between the four NMHC mechanisms. Due to the relatively high reactivity and concentration levels, propane and butane combine to account for about 90% of the total reactive NMHCs, and thus define the major NMHC reactivity as measured in terms of OH. Of these two alkane species, propane is the more abundant one. As discussed in chapter 2, propane is represented by a lumped alkane species HC3 in the RACM mechanism, and the rate constant for reaction with OH is 2.2×10^{-12} cm^3 $(molec.\cdot s)^{-1}$ at 298K. This number is significantly larger than the value of 1.7×10^{-13} cm^3 $(molec.\cdot s)^{-1}$ used in the CBIV mechanism, in which propane is represented as a 1.5 C-C single bond species, PAR; but it is also twice the value used in both the Lurmann and SAPRC mechanisms.. In the Lurmann mechanism, propane is explicitly treated and its OH oxidation rate constant is 1.1×10^{-12} cm^3 $(molec.\cdot s)^{-1}$ at 298K. In SAPRC, propane is also lumped into an alkane species ALK2, but its reaction rate constant with OH is only 1.0×10^{-12} cm^3 $(molec.\cdot s)^{-1}$. As for butane, its rate constant with OH is the highest in the Lurmann mechanism where butane is placed into a lumped species that represents all alkanes higher than propane. Its value of 3.7×10^{-12} cm^3 $(molec.\cdot s)^{-1}$ is moderately higher than the value of 2.3×10^{-12} cm^3 $(molec.\cdot s)^{-1}$ used in both the RACM and SAPRC mechanisms though butane is represented by a different lumped species in these two mechanisms. In the CBIV mechanism, butane is assigned as 4 PAR, and the rate constant with OH is only 4.5×10^{-13} cm^3 $(molec.\cdot s)^{-1}$, again significantly lower than that employed in the other three mechanisms. Therefore, based on rate constant differences and mechanism differences, it is not surprising to see that, among the four mechanisms, RACM gives the highest total NMHC reactivity in the BL during TRACE-P, whereas CBIV gives the lowest as related to OH.

As abundant as alkanes are in the BL during TRACE-P, their concentration levels were not high enough to have a major impact on OH. However, with the separation of the BL into three sub-regions (regions 1, 2, and 3), a gradient can clearly be seen with increasing NMHC levels. For example, the median propane levels for regions 1, 2, and 3 are 170, 410, and 800 pptv, respectively. The relative changes in OH due to NMHCs for regions 1 through 3 are shown in Figure 5.1.

In Table 5.3 and Figure 5.1, we can see that OH decreases with increasing NMHCs and that the median OH decline given by the four mechanisms follows the order RACM, SAPRC, Lurmann, and CBIV, with CBIV being the least influenced. This order is perfectly consistent with the test runs when using propane as the test NMHC species (e.g., see Figure 4.1). In region 3, on average, OH decreases by 21% using RACM, making it the most influenced mechanism. On the other hand, the OH decrease predicted by the RACM mechanism in regions 2 and 1 drop to 15% and 7%, respectively. Thus, the monotonic decrease in OH with increasing NMHC reactivity and the absolute magnitude of the decrease for the different mechanisms suggests that the alkane family was the most likely NMHC family affecting the OH concentration level during TRACE-P.

It should be noted that reactive aromatic hydrocarbons, mainly toluene and xylene, were occasionally the dominant species in specific runs for both regions 2 and 3 during TRACE-P, as shown in Figure 3.12. Of these two aromatics, the former is much more abundant with a median concentration level of almost an order of magnitude higher than that of the latter. Thus, toluene should be the major aromatic species of interest during TRACE-P. Therefore, the difference in the treatment of toluene by the four mechanisms also resulted in some impact on OH, though not to the same degree as the

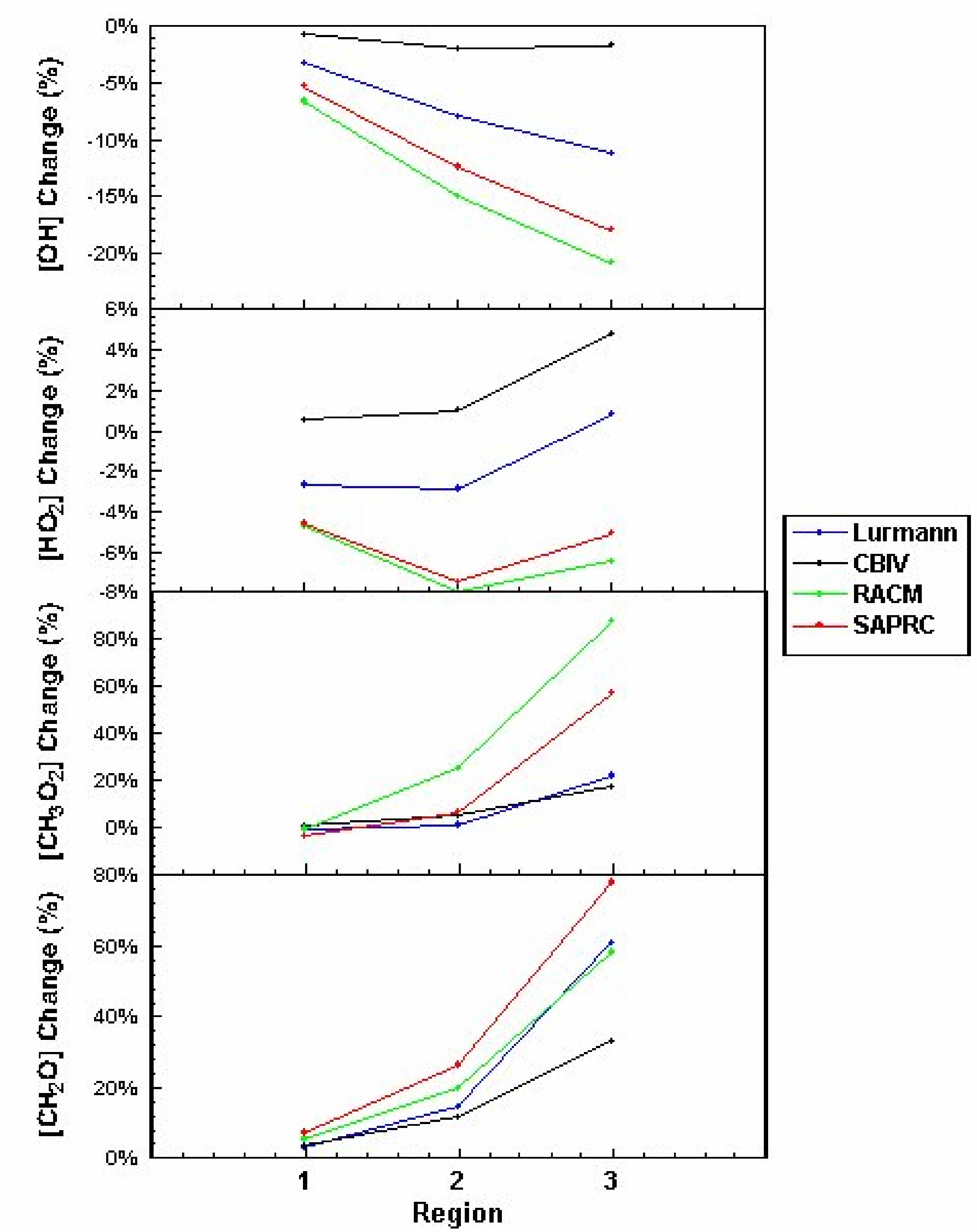

Figure 5.1. Impact from NMHCs on several critical species for the BL data during TRACE-P.

alkanes. As discussed in chapter 2, toluene and xylene are handled in the same manner in the Lurmann mechanism, making toluene as reactive as xylene. Thus, the reaction rate constant for the toluene oxidation by OH in the Lurmann mechanism is 1.5×10^{-11} cm^3 $(molec.\cdot s)^{-1}$ at 298K. This is more than twice the value of 6.0×10^{-12} cm^3 $(molec.\cdot s)^{-1}$ used in both the RACM and SAPRC mechanisms, and approximately twice the value used in the CBIV mechanism.

For this reason, the biggest OH decrease is expected to be given by the Lurmann mechanism (see Figure 4.5) for those regions dominated by aromatics during TRACE-P. Unfortunately, the aromatic-dominated model runs made up only about 15% of the total for the BL. In the most reactive sub-region (i.e., region 3), the percentage of the aromatic-driven model runs was less than 20%. As a result, the impact from aromatic hydrocarbons on OH and other free radical species from TRACE-P does not reveal itself as clearly as those resulting from the alkanes.

Concerning the alkene, propene, the only alkene measured during TRACE-P, so few measurements were recorded (less than 3% of the total model runs) that it was not possible to conclude anything about its role in the tropospheric chemistry of the TRACE-P study regions.

5.2.2 HO_2

As seen in Table 5.3, with the exception of the CBIV mechanism, the other NMHC mechanisms show an initial trend of lower HO_2 values in the presence of NMHCs. However, the biggest decrease in HO_2, 7~8% was seen only in the results from the RACM mechanism. Thus, the major finding here as in the test mixtures is that HO_2 levels seem to be buffered by a mixture of positive and negative feedbacks that tend to give HO_2 levels that are relatively unchanged over a substantial range of NMHC concentrations.

In general, HO_2 seems to be influenced by NMHCs to a somewhat lesser extent in the SAPRC and Lurmann mechanisms. As for CBIV, the median value of the relative HO_2 change is slightly positive, which is opposite the results of the other three mechanisms. However, this trend is consistent with that seen from the test results when using propane under low NO_x conditions as discussed in chapter 4. This again suggests that the TRACE-P field data fall into the category of a low-NO_x region and that reactive alkanes were the major NMHCs species having an impact on HO_x. The fact that the impact from NMHCs on HO_2 versus OH is much less for a given NMHC level is in good agreement with the earlier cited test run results, as shown in Figure 4.1.

As shown in Figure 5.1, HO_2 is influenced by NMHCs in a similar manner in both CBIV and Lurmann mechanisms. The relative change in HO_2 tends to increase with increasing NMHC levels for both mechanisms. The difference between them is that HO_2 appears to always increase with increasing NMHCs levels when using the CBIV mechanism, whereas the median HO_2 change is only positive for the Lurmann mechanism in region 3 when NMHC levels are very low. At present**,** it is difficult to explain the HO_2 increase given by the Lurmann mechanism under low-NO_x conditions. In chapter 4, the only test NMHC species that resulted in an increase in HO_2 in the Lurmann mechanism was propene, as shown in Figure 4.3. But, as mentioned before, propene was not often detected during TRACE-P. Thus, one would not expect it to substantially change the general impact of NMHCs' on HO_2. It now seems more probable that free radicals produced by all NMHC species interact in ways which lead to some very weak positive feedbacks.

As for the RACM and SAPRC mechanisms, the biggest relative decrease in HO_2 from NMHCs was unexpectedly found to be in region 2 (see Figure 5.1). Again, from the results of the test runs in chapter 4, one is hard pressed to explain this fact since HO_2 levels tend to monotonically decrease with increasing NMHC concentration for these two mechanisms. In the test runs, HO_2 concentrations increased with increasing levels of either propene or xylene only under high NMHC levels (> 1 ppbv), as shown in Figures 4.3 and 4.7. But neither of these two species was abundant enough during TRACE-P to have a significant impact on HO_2 during TRACE-P. So this uncharacteristic HO_2 change due to NMHCs for these two mechanisms may also be a consequence of the mutual effects of several hydrocarbon species, which can not be reproduced in the tests made involving only a single NMHC species. However, it must be kept in mind also that the changes being discussed above are at the 2-4 % level and therefore do not constitute a major deviation from some expected trend.

5.2.3 CH_3O_2

CH_3O_2 radicals are shown increasing with increasing levels of NMHCs for all three TRACE-P regions examined and for all four mechanisms tested, i.e., see Table 5.3. Due to extremely high levels of the acetyl peroxy radical CH_3CO_3 produced from NMHC oxidation (yielding high levels of CH_3O_2), the RACM mechanism was found to yield by far the largest relative increase in CH_3O_2, e.g., ~ 90% for region 3. The smallest change in CH_3O_2 levels were those given by the Lurmann and CBIV mechanisms (regions 2 and 3). In magnitude, therefore, this result is more consistent with that from the test runs based on the test species propane and toluene for low-NO_x conditions, e.g., see Figures 4.1 and 4.5. However, it is to be noted that CH_3O_2 levels typically decreased with additions of propane and aromatic hydrocarbons under low-NO_x test conditions when using the Lurmann mechanism. This, of course, is contrary to the small increase in CH_3O_2 seen here in the TRACE-P field data (i.e., regions 2 and 3 in Table 5.3). The only NMHC species that was found to increase CH_3O_2 levels when using this mechanism was propene. But, as mentioned above, propene measurements suggest that levels were so low during TRACE-P that they should not have made a significant impact on the HO_x or CH_3O_2 distributions. Thus, the small increase in CH_3O_2 found when using the Lurmann mechanism may be due to a combination of effects, one being the loss in CH_3O_2 production from OH/CH_4 reaction (e.g., lower levels of OH) which might have been compensated by CH_3O_2 production from peroxy radicals generated via the oxidation of other hydrocarbon species. Again, the change being addressed is very small.

It is to be noted that the RACM mechanism always gives larger CH_3O_2 increases than the other three mechanisms in regions 2 and 3 where NMHC concentration levels are relatively high. In region 1, however, the median CH_3O_2 changes given by the four mechanisms are all close to zero. This reflects the fact that very few peroxy radicals are produced from NMHC oxidation when NMHC levels are low, and thus, the gain in CH_3O_2 production from the NO/RO_2 reaction is offset by the loss in CH_3O_2 production from the OH/CH_4 reaction, due to the decrease in OH from NMHC oxidation. In the case of the CBIV mechanism, the OH level remains nearly the same in the presence of NMHCs while the NO_x level is low, and this leads to a nearly constant contribution to CH_3O_2 production from the OH/CH_4 reaction. Thus, only a slight increase in CH_3O_2

concentration occurs. On the other hand, it shows that CH_3O_2 is much more sensitive to changes in NMHC levels than HO_x is. Ethane is seen as the dominant hydrocarbon species in region 1, (Figure 3.12), but it was not selected as a test species here because of its low reactivity compared to the higher alkanes. Even so, the small change in CH_3O_2 in region 1 may partly reflect the impact from ethane.

5.2.4 CH_2O

Similar to the trends in CH_3O_2, CH_2O is shown as enhanced by the addition of NMHCs when using all four NMHC mechanisms for all three BL sub-regions of TRACE-P, see Table 5.3. The biggest CH_2O increase, 80% for region 3, is given by the SAPRC mechanism, and the second biggest increase was for RACM. This order matches that given by the test runs when using propane under low-NO_x condition. However, the smallest impact from NMHCs on CH_2O was not found for the Lurmann mechanism, as indicated in Figures 4.1 and 4.5, but rather for the CBIV mechanism. As discussed in chapter 4, the source of CH_2O is increased when CH_3O_2 levels are elevated with the addition of NMHCs. At the same time, the sink for CH_2O is lowered because of decreases in the levels of both OH and HO_2 when the NO_x level is low. The combination of these two factors thus leads to the cited increases in CH_2O when NMHCs are present. Although the relative change on CH_3O_2 in the CBIV mechanism is higher than that in the Lurmann mechanism, the higher predicted HO_x levels in CBIV seem to be more important in determining the CH_2O level when using TRACE-P data.

As in the case of CH_3O_2 radicals one sees almost the same trend in CH_2O for the three sub-regions 1, 2, and 3. That is, the CH_2O level is always enhanced by the addition of NMHCs and it monotonically increases with increasing hydrocarbon levels for all four mechanisms, see Figure 5.1. Region 1 shows no significant CH_2O change for all four mechanisms, reflecting what happens to CH_3O_2, which is the major source for CH_2O.

5.2.5 The Evaluation of the Four Mechanisms

Based on the comparison made on several product species for the four mechanisms, a reasonable question that could be raised is which of these four mechanisms is the preferred one. Said slightly differently, given the differences seen in the TRACE-P analysis, is there any basis for choosing one mechanism over the others?

Typically, an evaluation of different mechanisms can be completed by comparing the model-predicted results against observations. This becomes particularly convenient when the test analysis involves the use of smog chamber data. Concerning the TRACE-P campaign, however, the question that must first be addressed in such a comparison is that of the accuracy of the field observations. For example, during TRACE-P, the measurement of OH was performed by using a multi-channel Selected Ion Chemical Ionization Mass Spectrometer (SICIMS) system [Eisele and Tanner, 1991; Eisele et al., 1994, 1997; Mount et al., 1997] and by a laser-induced fluorescence (LIF) technique [Brune et al., 1995, 1998]. These instruments were mounted two different aircraft, a P-3B and DC-8 aircraft, respectively. The reported instrument uncertainty was ±35% for SICIMS and ±40% for LIF. However, the two instruments disagreed with each other nearly 50% of the time by factors lying outside their combined stated uncertainties. Furthermore, looking back at earlier efforts to compare these experimental observations with model predictions (using the modified Lurmann mechanism) one finds that the agreement between them was typically in the range of a factor of 1.5 (Davis et al., 2001, 2003). Thus, from all accounts (i.e., instrument to instrument comparisons and instrument to model predictions), the uncertainties found are all significantly larger than the OH differences found between mechanisms during TRACE-P, ~20%. This means that the difference in predicted OH levels given by the four mechanisms in relationship to the observational data can not currently be used to determine the preferred mechanism.

However, bigger differences were shown when the mechanisms were used to predict levels of species such as CH_2O and CH_3O_2, which are more sensitive to NMHC levels than HO_x. The biggest differences between mechanisms (in region 3) were 30% and 70% for CH_2O and CH_3O_2, respectively. Therefore, if highly accurate observational data were available for these two species one could select a preferred mechanism. As with the case of OH, this is not the case. The instrumental accuracy, based on the results of comparing two or more instruments against each other, is at best a factor of 2 and more likely a factor of 3. Thus significant improvements will be needed in the instrumentation before this mechanism selection process can take place. What will further help this effort is that of caring out an analysis on a data set containing much higher levels of NMHCs. It is expected that much larger differences would emerge thus making the testing procedure more tractable.

5.3 Photochemical O_3 Budget

As discussed in chapter 1, tropospheric photochemistry is triggered by the absorption of UV radiation which produces excited state atomic oxygen, $O(^1D)$. Most of the $O(^1D)$ formed this way is quenched to ground state atomic oxygen, $O(^3P)$, by collision with N_2 or O_2 at which point the resulting $O(^3P)$ can combine with O_2 to form ozone again. A very small percentage of the $O(^1D)$, however, reacts with water vapor to produce two OH radicals. This process can be summarized as follows:

(R5.1) $O_3 + h\nu \rightarrow O(^1D) + O_2$

(R5.2) $O(^1D) + M \rightarrow O(^3P)$

(R5.3) $O(^3P) + O_2 + M \rightarrow O_3$

(R5.4) $O(^1D) + H_2O \rightarrow 2OH$

The reaction of $O(^1D)$ with water vapor actually leads to the loss of ozone; whereas, the formation of the OH free radical can result in either formation and/or destruction of O_3. O_3 can also be removed via other channels such as its direct reaction with OH, HO_2, or hydrocarbons, e.g., alkenes:

(R5.5) $O_3 + OH \rightarrow HO_2 + O_2$

(R5.6) $O_3 + HO_2 \rightarrow OH + 2O_2$

(R5.7) O_3 + Alkene → products

Therefore, the loss of O_3 can be expressed as:

$$D(O_3) = k_4[O(^1D)][H_2O] + [O_3](k_5[OH] + k_6[HO_2] + k_7[Alkene]) \quad (5.1)$$

For O_3 production, as we have already seen from reaction 5.3, it is formed via the combination of $O(^3P)$ and O_2 molecule. However, the most important source of $O(^3P)$ in the net production of O_3 typically involves reactions with NO, where the NO is converted to NO_2 without the consumption of O_3, unlike the case of reactions 5.8, 5.9, and 5.3:

(R5.8) $O_3 + NO \rightarrow NO_2 + O_2$

(R5.9) $NO_2 + h\nu \rightarrow O(^3P) + NO$

(R5.3) $O(^3P) + O_2 + M \rightarrow O_3$

Thus, any species that can compete with O_3 by reacting with NO to generate NO_2 is potentially a source of O_3. These species include HO_2, CH_3O_2, and other peroxy radicals, and their reactions with NO include:

(R5.10) $HO_2 + NO \rightarrow NO_2 + OH$

(R5.11) $CH_3O_2 + NO \rightarrow NO_2 + CH_3O$

(R5.12) $RO_2 + NO \rightarrow NO_2 + RO$

Thus, O_3 formation can be defined as:

$$F(O_3) = [NO](k_{10}[HO_2] + k_{11}[CH_3O_2]+ k_{12}[RO_2]) \quad (5.2)$$

It should be noticed that, when the NO_x level is high, the NO_x cycle could be affected by other channels via which NO_2 is efficiently removed. For example,

(R5.13) $NO_2 + OH + M \rightarrow HNO_3$

This leads to the additional O_3 destruction, which should be added to formula 5.1 and can be expressed as:

$$k_8[NO][O_3] \ (k_{13}[NO_2][OH] / (k_{13}[NO_2][OH] + J_9[NO_2])) \quad (5.3)$$

Finally, the photochemical ozone tendency can be defined as the difference between O_3 formation and O_3 destruction:

$$P(O_3) = F(O_3) - D(O_3) \quad (5.4)$$

5.3.1 O_3 Production

The diurnal average rates for photochemical formation given by all four mechanisms are shown in Table 5.4. We can see that the Lurmann mechanism always gives the highest average ozone production for the BL data recorded during TRACE-P. The difference between the results from the Lurmann mechanism and those from the other three mechanisms increases with increasing NMHC levels. The biggest difference, about 30%, is found between the Lurmann and CBIV mechanisms in region 3.

Table 5.4. Diurnal average rates for ozone formation, destruction, and tendency during TRACE-P (ppbv/day).

Region	Mechanism	CBIV	Lurmann	RACM	SAPRC
Region 1	$F(O_3)$	0.9	0.9	0.8	0.8
	$D(O_3)$	2.8	2.8	2.7	2.7
	$P(O_3)$	-2.0	-1.9	-1.9	-1.9
Region 2	$F(O_3)$	2.7	3.0	2.7	2.7
	$D(O_3)$	3.7	3.6	3.6	3.6
	$P(O_3)$	-1.0	-0.6	-0.9	-0.9
Region 3	$F(O_3)$	3.5	4.5	4.0	3.8
	$D(O_3)$	1.7	1.7	1.6	1.6
	$P(O_3)$	1.8	2.7	2.4	2.2

As seen in formula 5.2, the O_3 formation should be determined by the levels of both NO and peroxy radicals (i.e., HO_2, CH_3O_2, and RO_2). As mentioned in chapter 2, the total short-lived nitrogen is held constant in the model calculation. As a result, NO levels in all four mechanisms are nearly identical. That leaves the peroxy radicals as the decisive chemical species factor for O_3 formation. Therefore, it is not surprising to see that, in the three sub-regions, the highest average O_3 formation rate takes place in the most NMHC-abundant region 3 (see Table 5.4).

Tables 5.5 and 5.6 show the average absolute and relative contribution to $F(O_3)$ from the three formation channels, as given by the four mechanisms using TRACE-P data, respectively. For the largest of these, the Lurmann mechanism, the results have also been displayed in the form of Figure 5.2 for regions 1 – 3. Clearly, the reaction of NO with HO_2 is always the single most important contributor to O_3 production in all four NMHC mechanisms. In any of the BL sub-regions, the contribution from the NO/HO_2 pathway accounts for at least 50% of the O_3 formation. Besides the NO/HO_2 channel, the reaction of CH_3O_2 with NO is also of some importance, especially in those regions where the NO level is extremely low. For example, these two pathways are almost of equal importance for the O_3 production in region 1 where the NO mixing ratio is typically below 20 pptv (i.e., Figure 3.5). The third channel, NO/RO_2, may have considerable contribution to the O_3 production only in high-NMHC areas (e.g., region 3). In this situation, the organic peroxy radicals generated via NMHC oxidation could become comparable in importance to CH_3O_2 in converting NO to NO_2.

In Table 5.5, it is also seen that the absolute contributions from the first two channels to the total O_3 formation given by all four mechanisms are very similar in each of the three sub-regions. In another words, the difference in O_3 formation mainly results from the third channel, NO/RO_2. In region 3, the contributions from this channel for the Lurmann and CBIV channels differ by nearly a factor of 4. This accounts for 60% of the difference in total O_3 formation.

Table 5.5. Average contribution from different channels to ozone formation during TRACE-P (ppbv/day).

Region	Mechanism	CBIV	Lurmann	RACM	SAPRC
Region 1	$k[HO_2][NO]$	0.5	0.5	0.4	0.4
	$k[CH_3O_2][NO]$	0.3	0.3	0.3	0.3
	$k[RO_2][NO]$	0.1	0.1	0.1	0.1
Region 2	$k[HO_2][NO]$	1.8	1.8	1.7	1.7
	$k[CH_3O_2][NO]$	0.8	0.8	0.8	0.8
	$k[RO_2][NO]$	0.2	0.4	0.2	0.2
Region 3	$k[HO_2][NO]$	2.7	3.0	2.7	2.6
	$k[CH_3O_2][NO]$	0.6	0.7	0.7	0.7
	$k[RO_2][NO]$	0.2	0.8	0.6	0.5

Table 5.6. Average relative contribution from different channels to ozone formation during TRACE-P.

Region	Mechanism	CBIV	Lurmann	RACM	SAPRC
Region 1	$k[HO_2][NO]$	54%	50%	53%	53%
	$k[CH_3O_2][NO]$	40%	39%	41%	41%
	$k[RO_2][NO]$	6%	11%	6%	6%
Region 2	$k[HO_2][NO]$	65%	59%	61%	62%
	$k[CH_3O_2][NO]$	29%	27%	29%	29%
	$k[RO_2][NO]$	6%	14%	10%	9%
Region 3	$k[HO_2][NO]$	78%	67%	68%	69%
	$k[CH_3O_2][NO]$	16%	16%	18%	18%
	$k[RO_2][NO]$	6%	17%	14%	13%

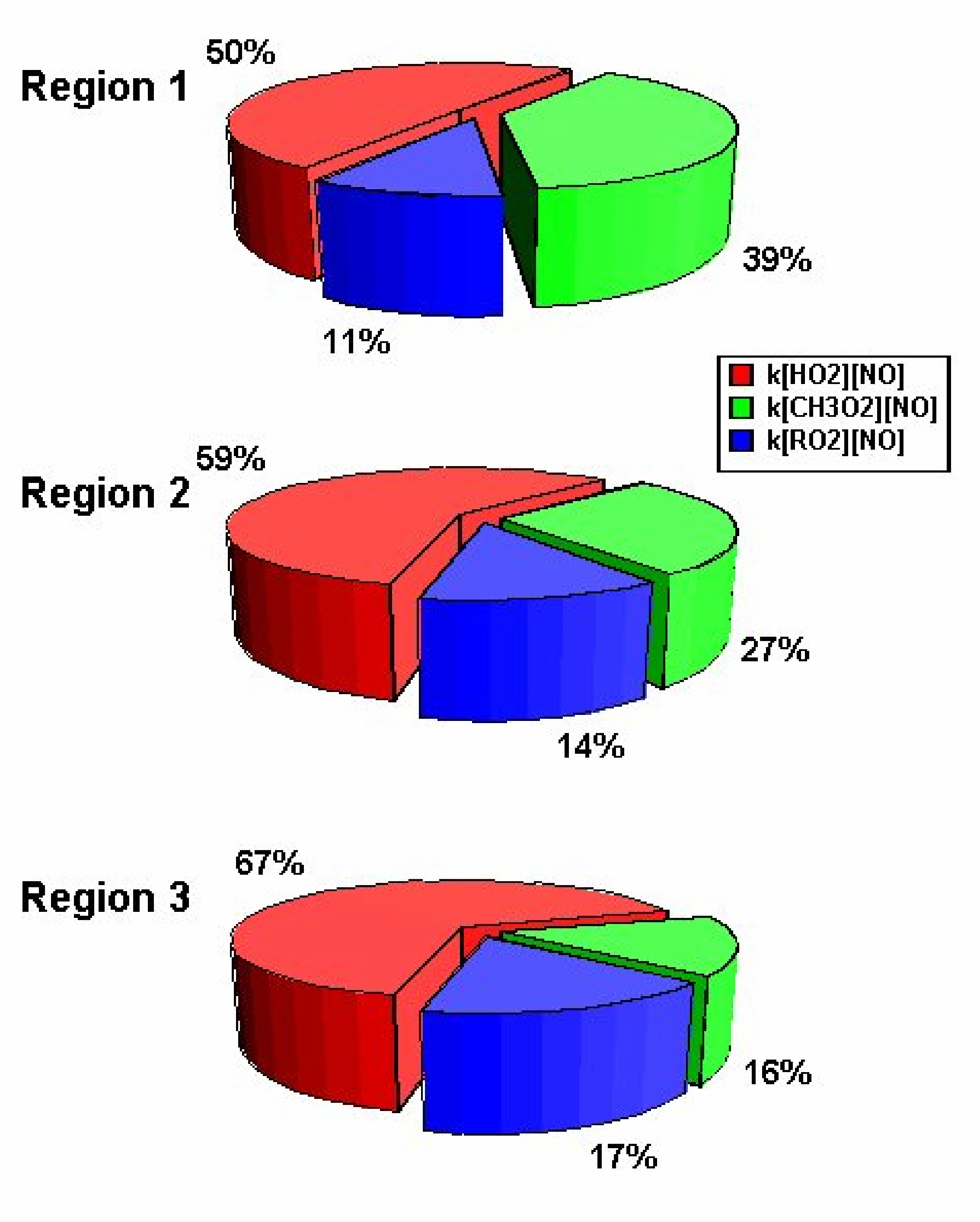

Figure 5.2. Relative contribution from different channels to the O_3 formation in regions 1, 2, and 3 during TRACE-P based on the Lurmann mechanism.

To further understand the basis of this difference, both the total RO_2 concentration and k_{12} (in formula 5.2) for region 3 are here compared for the Lurmann and CBIV mechanisms. What one finds is that, on average, the total RO_2 concentrations for these two mechanisms are 6.1×10^7 and 3.6×10^7 molecules/cm^3, respectively. This is consistent with the test run results when using propane under low-NO_x conditions in chapter 4 (see Table 4.2). Moreover, the weighted average k_{12} for these two mechanisms in region 3 are 1.1×10^{-11} and 9.7×10^{-12} cm^3 (molec.·s)$^{-1}$, respectively, with the former being higher by 10~15%. Thus, it is these two factors that combine to lead to the major difference in RO_2 contribution to O_3 formation for the two mechanisms. In fact, this difference becomes much bigger for high-NO_x model runs (i.e., above 200 pptv).

Note from Table 4.2 the highest RO_2 level when using propane as the test species is given by the RACM mechanism. This also applies to the TRACE-P data. However, the average k_{12} is much lower for this mechanism. For example, it is only ~ 5.0×10^{-12} (molec.·s)$^{-1}$ in region 3, which is less than half of that for the Lurmann mechanism. As a result, the biggest RO_2 contribution to O_3 formation is still found using the Lurmann mechanism.

5.3.2 O_3 Destruction

The average diurnal rates of O_3 destruction, as given by the four mechanisms using TRACE-P data, are shown in Table 5.4. Tables 5.7 and 5.8 show the average absolute and relative contribution to $D(O_3)$ from five channels, respectively. Again, for the Lurmann mechanism, the results have also been displayed in the form of Figure 5.3 for regions 1 – 3.

Of some interest is the fact that the O_3 loss rate in region 3, where NMHC levels were the highest, shows the lowest rate. But as indicated in Table 5.6, it is clear that this unusual situation tends to be caused by the low levels of water vapor in this region. Compared to the difference in O_3 formation rates given by the four mechanisms, they performed quite similarly by producing nearly the same O_3 destruction values. Overall, the biggest difference in the average O_3 destruction rate is seen as occurring between the CBIV and RACM mechanisms**,** but this difference is typically less than 5%.

As seen in Table 5.8, the $O(^1D)$ reaction with water vapor is on average the primary contributor to O_3 loss within the BL because of the high abundance of water vapor in this region. Meanwhile, the reaction of O_3 with HO_2 can also be a key factor to the O_3 destruction at the low altitude. In areas where both NO and NMHCs are plentiful, e.g., region 3, this pathway is of even slightly greater significance than the $O(^1D)/H_2O$ reaction. Collectively, these two channels combine to contribute about 80% of the ozone loss during TRACE-P. As we know, the $O(^1D)/H_2O$ term is calculated exactly the same way in each of the four mechanisms. Moreover, the O_3 mixing ratio is considered constant in the model calculation, and as shown in Table 5.1 HO_2 levels given by the different mechanisms do not differ by much when using the TRACE-P dataset.

Therefore, the similarity of these two major contributors to O_3 destruction tends to minimize the difference seen on average O_3 in the loss rate given by the four mechanisms.

Table 5.7. Average contribution from different channels to ozone destruction during TRACE-P (ppbv/day).

Region	Mechanism	CBIV	Lurmann	RACM	SAPRC
Region 1	$k[O(^1D)][H_2O]$	1.9	1.9	1.9	1.9
	$k[O_3][HO2]$	0.7	0.7	0.6	0.6
	$k[O_3][OH]$	0.2	0.2	0.2	0.2
	$k[NO_2][OH]$	0	0	0	0
	$k[O_3][NMHC]$	0	0	0	0
Region 2	$k[O(^1D)][H_2O]$	2.4	2.4	2.4	2.4
	$k[O_3][HO2]$	0.9	0.9	0.8	0.8
	$k[O_3][OH]$	0.3	0.3	0.3	0.3
	$k[NO_2][OH]$	0.1	0.1	0.1	0.1
	$k[O_3][NMHC]$	0	0	0	0
Region 3	$k[O(^1D)][H_2O]$	0.6	0.6	0.6	0.6
	$k[O_3][HO2]$	0.8	0.7	0.7	0.7
	$k[O_3][OH]$	0.2	0.2	0.2	0.2
	$k[NO_2][OH]$	0.1	0.2	0.1	0.1
	$k[O_3][NMHC]$	0	0	0	0

Table 5.8. Average relative contribution from different channels to ozone destruction during TRACE-P.

Region	Mechanism	CBIV	Lurmann	RACM	SAPRC
Region 1	$k[O(^1D)][H_2O]$	67%	68%	69%	68%
	$k[O_3][HO_2]$	25%	24%	23%	23%
	$k[O_3][OH]$	8%	8%	7%	8%
	$k[NO_2][OH]$	0%	0%	1%	1%
	$k[O_3][NMHC]$	0%	0%	0%	0%
Region 2	$k[O(^1D)][H_2O]$	65%	66%	67%	67%
	$k[O_3][HO_2]$	25%	24%	23%	23%
	$k[O_3][OH]$	8%	8%	8%	8%
	$k[NO_2][OH]$	2%	2%	2%	2%
	$k[O_3][NMHC]$	0%	0%	0%	0%
Region 3	$k[O(^1D)][H_2O]$	34%	35%	37%	36%
	$k[O_3][HO_2]$	44%	43%	42%	42%
	$k[O_3][OH]$	13%	12%	11%	12%
	$k[NO_2][OH]$	8%	9%	9%	9%
	$k[O_3][NMHC]$	1%	1%	1%	1%

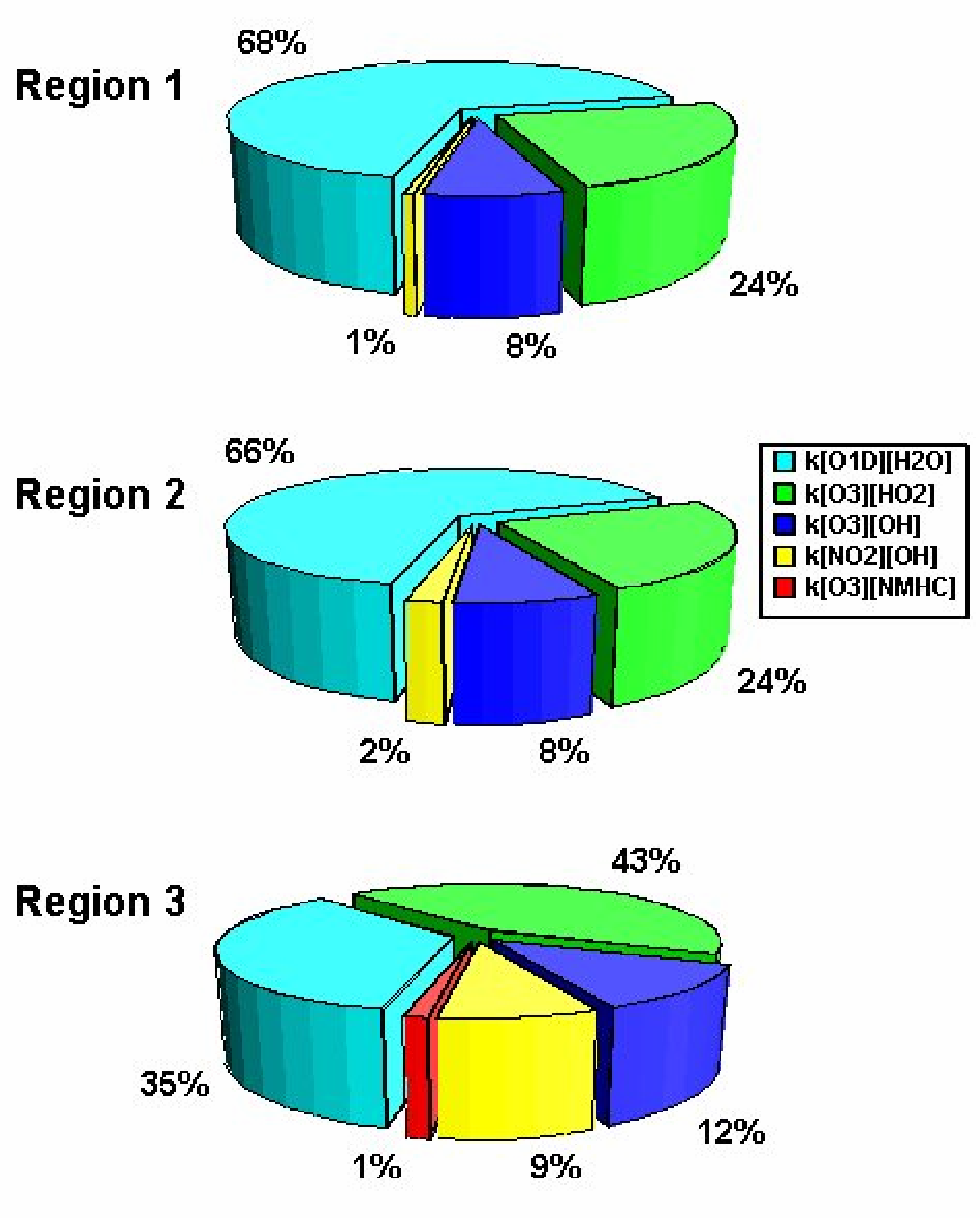

Figure 5.3. Relative contribution from different channels to the O_3 destruction in regions 1, 2, and 3 during TRACE-P based on the Lurmann mechanism.

In addition to the two channels discussed above, the reaction of O_3 with OH can also be important under certain conditions. The lower the H_2O level is, the more important the contribution of this pathway to the O_3 destruction. However, it never competes with the O_3/HO_2 channel during TRACE-P. As for the other two terms, the reaction of O_3 with alkenes is virtually negligible, and the additional O_3 destruction because of the NO_2 reaction with OH generally accounts for less than 5% during TRACE-P.

5.3.3 O_3 Tendency

The net effect of all photochemical reactions on ozone, i.e., the ozone tendency, during TRACE-P is shown in Table 5.4**.** As discussed in section 5.3.2, the O_3 destruction terms given by the four mechanisms are very similar. Consequently, the difference in O_3 tendency for the different mechanisms is mainly determined by the ozone formation term. As stated earlier, the Lurmann mechanism tends to produce the highest O_3 formation rate. For that reason, this mechanism also gives the biggest O_3 increase in all regions.

Generally, the net O_3 tendency increases with increasing NMHC reactivity because the O_3 production rate increases faster than the O_3 destruction rate in the presence of high levels of NMHCs. This trend is reflected in the sub-regions within the BL. The O_3 tendency in sub-regions 1 and 2 is seen as negative for all four mechanisms due to the low NMHC reactivity. In region 1, it is negative because of low values of NO in this region. In region 2, both O_3 production and O_3 destruction are strong, and the net effect is slight O_3 decrease. Only in region 3 is the tendency seen as going positive. This primarily reflects the contribution from NO/RO_2 reactions. To a lesser extent there is also a reduction in $D(O_3)$ in sub-region 3 due to the low H_2O level in this region. Quite significant is the fact that the Lurmann mechanism results in nearly a factor of 1.5 times greater net O_3 production in sub-region 3 than does CBIV. Even the RACM and SAPRC mechanisms delivery substantially higher net O_3 than does CBIV. As discussed earlier in section 5.3.1, the big difference in the CBIV and Lurmann mechanisms as regards $P(O_3)$ were the differences that surfaced in RO_2 levels and rate coefficients for reaction with NO, both of which were favored by Lurmann.

CHAPTER 6

CONCLUSIONS AND FUTURE WORK

This work has focused on showing the differences among four different NMHC oxidation mechanisms: GT (Georgia Tech) version of the Lurmann mechanism, CBIV (Carbon Bond IV) mechanism, RACM mechanism (Regional Atmospheric Chemistry Mechanism), and SAPRC (Statewide Air Pollution Research Center) mechanism. Each of these mechanisms uses a different approach to give simplified representation of the rather complex NMHC degradation process by use of surrogated/lumped species to represent real species and parameterized chemical reactions describing the interactions between these species. The major differences between these mechanisms are reflected in the way that the surrogated species are assigned and in the number of surrogated species and parameterized chemical reactions. Furthermore, even the rate coefficients for similar reactions can be quite different. This investigation was carried out to characterize the mechanisms using specified NO_x/NMHC gas mixtures and to examine their atmospheric impact based on observations from a NASA airborne field study, TRACE-P.

6.1 Mechanism Characterization with Specified NMHC/NO_x Gas Mixtures

Test runs are set up to examine the sensitivity of each of the four NMHC oxidation mechanisms in terms of NMHC impact on HO_x, peroxy radical production,

CH_2O and acetaldehyde yield. All of the test runs were set up using hypothetical NMHC/NO_x mixtures but were initiated from a basic run where all NMHCs were absent. The test mixture runs were carried out under both high and low NO_x (3 ppbv and 90 pptv, respectively) conditions due to the importance of NO_x in tropospheric photochemistry. The mixing ratios of NMHCs varied from 0.3 to 5.0 ppbv for BL conditions. The NMHC species selected for the specified gas mixtures included propane, propene, toluene, xylene, and isoprene. These species were chosen because they covered the types of hydrocarbons measured during TRACE-P. They were also selected for their range of reactivity and thus included a represent reactive alkane, a reactive alkene, a moderately reactive aromatic, a very reactive aromatic, and a very reactive biogenic NMHC.

In this study the impact from a single NMHC species on the levels of the reactive product species OH, HO_2, CH_3O_2, CH_2O, ALD_2, and RO_2 was examined. For all four mechanisms, the test run results show that the magnitude of the impact on these product species is highly dependent on the reactivity of a given NMHC species as well as its absolute concentration level. Not surprisingly, these product species were affected more by highly reactive species such as propene and xylene rather than by the less reactive compounds like propane and toluene. Interestingly, propane's impact had a similar dependence on its concentration level as that of toluene, likewise, propene and xylene were found to be similar, even though their reactivities are different.

The differences among the mechanisms can mainly be summarized in two areas. First, different mechanisms use different values of rate constants even for the same reactions. Second, different mechanisms use different approaches for simplifying and in making approximations for the same photochemical processes, i.e., the oxidation schemes themselves. These differences can be seen in the numbers of lumped or surrogate species used, treatment of reactants, intermediates, and products, all of which can affect the modeling results. In the test runs, both of the above cited factors play important roles. Their respective relative importance depends on the levels of NO_x and NMHC, and the type of NMHC species used.

OH is the major oxidant of NMHCs in the troposphere. To a large extent, the differences in predicted OH levels resulting from the different mechanisms can be assigned to the use of different rate constants for OH/NMHC reactions. In the test runs, differences in OH levels given by different mechanisms are the smallest among all product species. By contrast, HO_2 has numerous interactions with many of the NMHC oxidation intermediates. For example, it can be produced from OH reactions with NMHC as well as RO_2 reactions with NO, while it can also be consumed by reactions with RO_2. As a result, the differences in HO_2 are larger than for OH levels. For similar reason, the differences in the levels of CH_3O_2 and CH_2O, direct products of NMHC oxidation, are more significant than those in HO_x. The similarity between these two species reflects the fact that CH_3O_2 is the dominant source of CH_2O. The largest mechanism differences are shown in model predictions of ALD2 and RO_2. These differences represent the differences in the simplifications and approximations made by each of the four mechanisms as well as difference in definitions and lumping methods adopted by the mechanisms. For this reason, the intercomparison studies involving these two species were mostly qualitative. Typically, the impact from NMHCs on these product species was found to be larger at higher level of NO_x.

Propane is the least reactive test NMHC species. The OH level was decreased by the addition of 5 ppbv of propane by less than 25% in all four mechanisms. Therefore, the difference among the predicted OH levels from the four mechanisms was small, within a factor of 1.3. The lowest predicted OH level was found using the RACM mechanism because of the stronger OH sinks caused by the highest OH/propane reaction rate constant and high levels of aldehydes and peroxides generated in this mechanism. The predicted OH levels from the other three mechanisms were similar. CH_3O_2 was most sensitive to the presence of propane among the four major product species. Its level was increased by propane by nearly 3.5 times when using the RACM mechanism. This high CH_3O_2 level was the result of extremely high CH_3O_2 sources produced in the RACM mechanism. The ratio between the predicted CH_3O_2 level by RACM and those by the other three mechanisms was about 3.

As one of the most reactive test NMHC species, propene had a much stronger impact on OH than did propane. With the addition of 5 ppbv of propene, OH levels were lowered by at least 80% in all four mechanisms. The lowest OH level was found using the SAPRC mechanism due to the stronger OH sink resulting from this mechanism having the highest OH/propene reaction rate constant, higher production of ALD2 and peroxides, and the extra production of ketones and other aldehydes. As a result, the predicted OH level based on the SAPRC mechanism and those from the other three mechanisms differed by a factor of nearly 2. The biggest impact from propene on the product species was seen on CH_2O. The largest CH_2O increase caused by propene, which was a factor of 40, was found using the Lurmann mechanism; whereas the value for the other three mechanisms was 10. This high CH_2O level based on the Lurmann mechanism can be explained by its very strong CH_2O sources caused by both much higher yields of CH_3O_2 and the much bigger O_3/propene reaction rate constant.

6.2 Mechanism Analysis with TRACE-P Field Data

The consistency level of the four mechanisms was also examined under ambient conditions based on field data recorded during the NASA TRACE-P campaign. These data generally reflected near coast conditions. The comparative analysis was focused on BL data because of the rapid fall-off in NMHC levels with altitude. According to a scale developed in this study designed to show NMHC-OH reactivity, it was possible to further divide these BL data into three sub-regions. Of these sub-regions, region 1 was the lowest in reactivity and region 3 the highest. Region 1 had ethane and higher alkanes (C4 and above) as the dominant species; region 2 had no clear dominant species, however, the NMHC levels were clearly higher than those of region 1; and region 3 had the highest NMHC levels and the reactivity was dominated by higher alkanes (C4 and above). NO_x levels for the three regions had a trend similar to the NMHC reactivity scale, with the highest in region 3 (median = 210 pptv), lower values in region 2 (75 pptv), and still lower values in region 1 (15 pptv). However, most of the TRACE-P test runs, even the ones in Region 3, are in the low NO_x regime discussed in the section 6.1.

Because of the generally low levels of NMHCs recorded during TRACE-P, the levels of OH, HO_2, CH_3O_2, and CH_2O predicted by the four oxidation mechanisms were not dramatically different. For region 1 and 2, the differences between the mechanisms were generally small, i.e., less than 20%. By contrast, there were some larger differences seen in the model runs representing region 3. As discussed earlier, the largest differences typically corresponded to the highest NO levels. Among the major species analyzed, again, CH_3O_2 and CH_2O were the most sensitive ones in terms of differences between the four mechanisms, reflecting what was found in the controlled test NMHC runs.

Based on the analysis of the TRACE-P database, the alkanes were the dominant NMHC family and most of the model runs involved relatively low NO_x levels in comparison with test cases cited in section 6.1. Aromatic hydrocarbons may also have had some impact on OH levels in regions 2 and 3. Overall, however, importance of this family of hydrocarbons was not comparable to that of the alkanes.

In general, it was found that OH levels were not sensitive to the presence of NMHCs, being decreased by less than 20% for all four mechanisms in region 3. (Note, however, in the controlled studies 5 ppbv of propane caused only a 25% decrease in OH.) The largest difference in median OH levels between mechanisms was ~ 20%. This occurred in the difference between CBIV and RACM mechanisms. Predicted OH levels based on RACM were the lowest among these mechanisms (similar to the controlled results cited for propane). This difference was again mainly a result of the higher rate constants for the OH/propane and OH/butane reactions used in this mechanism.

Different from the test runs results, the difference in HO_2 between mechanisms during TRACE-P was found to be quite small. HO_2 levels were mostly decreased in TRACE-P runs, however, the biggest relative decrease was only 7~8% for regions 2 and 3, and this occurred in runs using the RACM mechanism. Declines in HO_2 levels of a similar magnitude were also found using the SAPRC mechanism. These small changes in HO_2 suggest that HO_2 levels seem to be buffered by a mixture of positive and negative feedbacks that tend to give relatively unchanged HO_2 levels over a substantial range of

NMHC concentrations during TRACE-P. These most likely result from their being present an extensive mixture of many different NMHCs

Concerning the impact of different NMHC mechanisms on O_3 formation and destruction, it was found that the largest difference between mechanisms occurs when dealing with formation (e.g., 30% in region 3). In this case it was the difference between the Lurmann and CBIV mechanisms. By comparison, in the evaluation of the O_3 destruction term the maximum difference between mechanisms was only ~5%. As a result, the net O_3 tendency comparison produced the largest difference between mechanisms (a factor of 1.5) which reflects the difference calculated for the Lurmann and CBIV mechanisms.

The fact that the O_3 formation in the Lurmann mechanism is higher than any other would seem to be inconsistent with the fact that neither the level of HO_2 nor CH_3O_2 was the highest for this mechanism. Actually, the absolute contributions from NO/HO_2 and NO/CH_3O_2 channels to the total O_3 formation given by all four mechanisms were very similar. Most of the differences (over 60%) in O_3 formation can be explained by the different contributions from the NO/RO_2 channel in the different mechanisms. In region 3, the average contribution from this channel for the Lurmann mechanisms was nearly 4 times that for CBIV.

A net O_3 increase during TRACE-P was found only in region 3 where the NMHC reactivity was high. Because of the similar O_3 destruction rates given by all four mechanisms, the difference in O_3 tendency among these mechanisms was mainly determined by the O_3 formation rate. As a result, the biggest O_3 increase (or the least O_3

decrease in certain areas) during TRACE-P was always found to be favored by the Lurmann mechanism.

6.3 Future Work

The present study has included four established photochemical mechanisms which have been widely used during the past several years. With new developments in NMHC oxidation schemes, more mechanisms should be included in any future study.

One of the major uncertainties associated with each mechanism is the incompleteness with which atmospheric photochemical processes are understood. If some critical processes are ignored in the oxidation mechanisms, it is obviously difficult for the mechanisms to accurately reproduce the observations. One possible missing component in the current mechanisms is halogen chemistry. This type of chemistry in the marine BL has been addressed recently by Vogt et al. (1999), von Glasow et al. (2002), and Bloss et al. (2005). Thus, halogen chemistry should be seriously considered in the future version of mechanism testing especially if the data are those being collected over marine areas.

The test runs using the hypothetical NMHC/NO_x mixtures have been shown to be an insightful approach for carrying out intercomparison studies involving different mechanisms. The selected NMHC species have been limited in this study to only ones with relatively high reactivity. However, as seen in the TRACE-P database, despite their low reactivity, species like ethane could become the major contributors to the total NMHC reactivity because of their high concentration. Thus, a greater spectrum of NMHC species (including ethane) should be examined in the future research.

Most importantly, it must be recognized the comparison of mechanisms in this study has been limited to a relatively clean atmosphere, e.g., the marine boundary layer with very modest inputs of anthropogenic NMHC and NO_x pollutants. Thus, in the future, it will be imperative that a much more extensive intercomparison be made involving a much boarder range of both NMHCs and NO_x levels.

Finally, as discussed in chapter 5, the lack of highly accurate measurements of the many product species predicted by the model limits ones ability to select a preferred mechanism. With continued improvements in these measuring techniques in the future, a far better analysis should be possible. Species such as CH_3O_2 and CH_2O should be chosen as the standard of evaluation due to the large divergence in predicted levels of them among the four different mechanisms. They also show the highest sensitivity to NMHC levels.

APPENDIX

LIST OF REACTIONS AND SPECIES FOR THE FOUR NMHC OXIDATION MECHANISMS

Table A.1. HO_x-NO_x-CH_4 chemistry (identical for all four mechanisms).

NO.	Reaction
1	$O(^1D) + N_2 \rightarrow O(^3P)$
2	$O(^1D) + O_2 \rightarrow O(^3P)$
3	$O(^1D) + H_2O \rightarrow 2OH$
4	$O(^1D) + CH_4 \rightarrow CH_3O_2 + OH$
5	$O(^1D) + CH_4 \rightarrow CH_2O + H_2$
6	$O(^1D) + H_2 \rightarrow HO_2 + OH$
7	$OH + CO \rightarrow CO_2 + HO_2$
8	$HO_2 + NO \rightarrow NO_2 + OH$
9	$HO_2 + O_3 \rightarrow OH + 2O_2$
10	$HO_2 + HO_2 \rightarrow H_2O_2 + O_2$
11	$OH + HO_2 \rightarrow H_2O + O_2$
12	$HO_2 + NO_2 + M \rightarrow HO_2NO_2$
13	$HO_2NO_2 \rightarrow HO_2 + NO_2$
14	$HO_2 + NO_3 \rightarrow OH + NO_2 + O_2$
15	$H_2O_2 + OH \rightarrow HO_2 + H_2O$
16	$H_2O_2 \rightarrow$ Rainout/Washout
17	$CH_4 + OH \rightarrow CH_3O_2 + H_2O$
18	$CH_3O_2 + NO \rightarrow CH_3O + NO_2$

Table A.1 (continued).

NO.	Reaction
19	$CH_3O_2 + HO_2 \rightarrow CH_3OOH + O_2$
20	$CH_3O_2 + CH_3O_2 \rightarrow 2CH_3O + O_2$
21	$CH_3O_2 + CH_3O_2 \rightarrow CH_2O + CH_3OH$
22	$CH_3O_2 + NO_2 + M \rightarrow CH_3O_2NO_2$
23	$CH_3O_2NO_2 + M \rightarrow CH_3O_2 + NO_2$
24	$CH_3OOH + OH \rightarrow CH_3O_2 + H_2O$
25	$CH_3OOH + OH \rightarrow CH_2O + OH + H_2O$
26	$CH_3OOH \rightarrow$ Rainout/Washout
27	$CH_2O + OH \rightarrow HO_2 + H_2O + CO$
28	$CH_2O + NO_3 \rightarrow HNO_3 + HO_2 + CO$
29	$CH_2O + HO_2 \rightarrow FROX$
30	$CH_2O \rightarrow$ Rainout/Washout
31	$FROX \rightarrow HO_2 + CH_2O$
32	$FROX + HO_2 \rightarrow CH_3OOH$
33	$FROX + NO \rightarrow NO_2 + HO_2 + HCOOH$
34	$CH_3O + O_2 \rightarrow CH_2O + HO_2$
35	$CH_3O + NO + M \rightarrow MNIT$
36	$CH_3O + NO \rightarrow CH_2O + HO_2 + NO$
37	$CH_3O + NO_2 + M \rightarrow MEN3$
38	$MEN3 + OH \rightarrow CH_2O + NO_2 + H_2O$
39	$MNIT + OH \rightarrow CH_2O + NO + H_2O$
40	$OH + CH_3OH \rightarrow CH_2O\ H + H_2O$
41	$CH_3OH \rightarrow$ Rainout/Washout
42	$CH_2OH + O_2 \rightarrow CH_2O + HO_2$
43	$OH + H_2 \rightarrow H_2O + HO_2$

Table A.1 (continued).

NO.	Reaction
44	$O_3 + OH \rightarrow HO_2 + O_2$
45	$O_3 + NO \rightarrow NO_2 + O_2$
46	$O_3 + NO_2 \rightarrow NO_3 + O_2$
47	$OH + NO + M \rightarrow HONO$
48	$OH + NO_2 + M \rightarrow HNO_3$
49	$OH + NO_3 \rightarrow HO_2 + NO_2$
50	$OH + HNO_3 \rightarrow H_2O + NO_3$
51	$OH + HONO \rightarrow NO_2 + H_2O$
52	$OH + HO_2NO_2 \rightarrow NO_2 + H_2O + O_2$
53	$NO + NO_3 \rightarrow 2NO_2$
54	$NO + NO \rightarrow 2NO_2$
55	$NO + NO_2 + H_2O \rightarrow 2HONO$
56	$NO_3 + CO \rightarrow NO_2 + CO_2$
57	$NO_3 + DMS \rightarrow HNO_3$
58	$NO_3 + NO_2 \rightarrow NO + NO_2 + O_2$
59	$NO_2 + NO_3 + M \rightarrow N_2O_5$
60	$HONO + HONO \rightarrow NO + NO_2 + H_2O$
61	$N_2O_5 + M \rightarrow NO_2 + NO_3$
62	$N_2O_5 + H_2O \rightarrow 2HNO_3$
63	$HNO_3 \rightarrow$ Rainout/Washout
64	$HONO \rightarrow$ Rainout/Washout
65	$HO_2NO_2 \rightarrow$ Rainout/Washout
66	$O_3 + h\nu \rightarrow O(^1D) + O_2$
67	$H_2O_2 + h\nu \rightarrow 2OH$
68	$CH_3OOH + h\nu \rightarrow CH_3O + OH$

Table A.1 (continued).

NO.	Reaction
69	$CH_2O + h\nu \rightarrow 2HO_2 + CO$
70	$CH_2O + h\nu \rightarrow CO + H_2$
71	$NO_2 + h\nu \rightarrow NO + O(^3P)$
72	$NO_3 + h\nu \rightarrow NO_2 + O(^3P)$
73	$N_2O_5 + h\nu \rightarrow NO_2 + NO_3$
74	$HNO_3 + h\nu \rightarrow OH + NO_2$
75	$HO_2NO_2 + h\nu \rightarrow HO_2 + NO_2$
76	$HO_2NO_2 + h\nu \rightarrow OH + NO_3$
77	$HONO + h\nu \rightarrow OH + NO$

Table A.2. List of species in HO_x-NO_x-CH_4 chemistry.

Abbreviation	Species
CH_2O	Formaldehyde
CH_2OH	Hydroxy Methyl Radical
CH_3O	Methoxy Radical
CH_3O_2	Methyl Peroxy Radical
$CH_3O_2NO_2$	Methyl Peroxy Nitrate
CH_3OH	Methanol
CH_3OOH	Methyl Peroxide
CH_4	Methane
DMS	Dimethyl Sulfide
FROX	Hydroxymethylperoxy Radical ($HOCH_2OO\cdot$)
$H2O_2$	Hydrogen Peroxide
HNO_3	Nitric Acid
HO_2	Hydroperoxyl Radical
HO_2NO_2	Pernitric Acid
HONO	Nitrious Acid
MEN3	Methyl Nitrate (CH_3ONO_2)
MNIT	Methyl Nitrite (CH_3ONO)
N_2O_5	Dinitrogen Pentoxide
NO	Nitrogen Oxide
NO_2	Nitrogen Dioxide
NO_3	Nitrage Radical
$O(^1D)$	Excited State Oxygen Atom
$O(^3P)$	Ground State Oxygen Atom
OH	Hydroxyl Radical

Table A.3. NMHC chemistry of the GT Lurman mechanism.

NO.	Reaction
78	$ACET + OH \rightarrow ATO_2 + H_2O$
79	$MEK + OH \rightarrow KO_2 + H_2O$
80	$MEK + NO_3 \rightarrow KO_2 + HNO_3$
81	$ATO_2 + NO \rightarrow 0.04RAN2 + 0.96NO_2 + 0.96MGLY + 0.96HO_2$
82	$KO_2 + NO \rightarrow 0.07RAN2 + 0.93NO_2 + 0.93ALD_2 + 0.93MCO_3$
83	$ATO_2 + HO_2 \rightarrow MCO_3 + CH_3O_2 + H_2O$
84	$KO_2 + HO_2 \rightarrow MGLY + CH_3O_2 + H_2O$
85	$C_2H_6 + OH \rightarrow ETO_2 + H_2O$
86	$ETO_2 + NO \rightarrow ALD_2 + HO_2 + NO_2$
87	$ETO_2 + HO_2 \rightarrow ETP + O_2$
88	$ETO_2 + ETO_2 \rightarrow 1.6ALD_2 + 1.2HO_2$
89	$C_3H_8 + OH \rightarrow nR_3O_2 + H_2O$
90	$C_3H_8 + OH \rightarrow iR_3O_2 + H_2O$
91	$nR_3O_2 + NO \rightarrow ALD_2 + NO_2 + HO_2$
92	$iR_3O_2 + NO \rightarrow ACET + NO_2 + HO_2$
93	$nR_3O_2 + HO_2 \rightarrow nR3P + O_2$
94	$iR_3O_2 + HO_2 \rightarrow iR3P + O_2$
95	$nR_3O_2 + nR_3O_2 \rightarrow 1.5ALD_2 + 0.5nC_3H_7OOH + HO_2$
96	$iR_3O_2 + iR_3O_2 \rightarrow 1.5ACET + 0.5iC_3H_7OOH + HO_2$
97	$ALKA + OH \rightarrow RAO_2 + H_2O$
98	$ALKA + NO_3 \rightarrow RAO_2 + HNO_3$
99	$RAO_2 + NO \rightarrow \beta 1NO_2 + \beta 2NO + \beta 3RAN2 + \beta 4ALD_2 + \beta 5MEK + \beta 6ETO_2 + \beta 7CH_3O_2 + \beta 8HO_2 + \beta 9nR_3O_2 + 0.06RAO_2$
100	$RAO_2 + HO_2 \rightarrow RAP + O_2$
101	$RAN2 + OH \rightarrow RAN1 + H_2O$
102	$RAN1 + NO \rightarrow NO_2 + CH_2O + RANO_2$

Table A.3 (continued).

NO.	Reaction
103	$RAN1 + HO_2 \rightarrow RANP$
104	$RANO_2 + HO_2 \rightarrow RANP2$
105	$RANO_2 + NO \rightarrow 2NO_2 + 2ALD_2$
106	$ISOP + OH \rightarrow RIO_2$
107	$ISOP + O_3 \rightarrow 0.5CH_2O + 0.2MVK + 0.3MACR + 0.2CHO_2 + 0.06HO_2 + 0.2MVKO + 0.3MAOO$
108	$ISOP + NO_3 \rightarrow INO_2$
109	$RIO_2 + NO \rightarrow 0.9NO_2 + 0.9HO_2 + 0.9CH_2O + 0.45MVK + 0.45MACR$
110	$RIO_2 + HO_2 \rightarrow XAP1 + O_2$
111	$INO_2 + NO \rightarrow 2NO_2 + CH_2O + 0.5MVK + 0.5MACR$
112	$INO_2 + NO_2 \rightarrow IPN4$
113	$INO_2 + HO_2 \rightarrow PROD$
114	$MVK + OH \rightarrow VRO_2$
115	$MVK + O_3 \rightarrow 0.5MGGY + 0.5CH_2O + 0.2CHO_2 + 0.2CRO_2 + 0.21HO_2 + 0.15ALD_2 + 0.15MCO_3$
116	$MVK + NO_3 \rightarrow MVN2$
117	$VRO_2 + NO \rightarrow 0.9NO_2 + 0.6MCO_3 + 0.6ALD_2 + 0.3HO_2 + 0.3CH_2O + 0.3MGLY$
118	$VRO_2 + HO_2 \rightarrow RP + O_2$
119	$MVN2 + NO \rightarrow 2NO_2 + CH_2O + 0.5MCO_3 + 0.5MGGY + 0.5HO_2$
120	$MVN2 + HO_2 \rightarrow PROD$
121	$MACR + OH \rightarrow MAO_3$
122	$MACR + OH \rightarrow MRO_2$
123	$MACR + O_3 \rightarrow 0.65CH_2O + 0.5MGGY + 0.36HO_2 + 0.2CHO_2 + 0.2CRO_2 + 0.15NO_2 + -0.15NO$
124	$MACR + NO_3 \rightarrow MAO_3 + HNO_3$
125	$MACR + NO_3 \rightarrow MAN2$
126	$MAO_3 + NO_2 \rightarrow MPAN$

Table A.3 (continued).

NO.	Reaction
127	$MPAN \rightarrow MAO_3 + NO_2$
128	$MAO_3 + NO \rightarrow NO_2 + PO_2 + CO_2$
129	$MAO_3 + HO_2 \rightarrow DAP + O_2$
130	$MRO_2 + NO \rightarrow 0.9NO_2 + 0.9HO_2 + 0.9CO + 0.9HACO$
131	$MRO_2 + HO_2 \rightarrow XAP2 + O_2$
132	$MAN2 + NO \rightarrow 2NO_2 + CH_2O + MGGY$
133	$MAN2 + HO_2 \rightarrow PROD$
134	$MVKO + NO \rightarrow MVK + NO_2$
135	$MVKO + NO_2 \rightarrow MVK + NO_3$
136	$MVKO + H_2O \rightarrow PROD$
137	$MVKO + HO_2 \rightarrow PROD$
138	$MVKO + SO_2 \rightarrow MVK + SO4$
139	$MAOO + NO \rightarrow MACR + NO_2$
140	$MAOO + NO_2 \rightarrow MACR + NO_3$
141	$MAOO + H_2O \rightarrow PROD$
142	$MAOO + HO_2 \rightarrow PROD$
143	$MAOO + SO_2 \rightarrow MACR + SO4$
144	$MGGY + OH \rightarrow MCO_3$
145	$ETHE + OH \rightarrow EO_2$
146	$ETHE + O_3 \rightarrow CH_2O + 0.4CHO_2 + 0.12HO_2 + 0.42CO + 0.06CH_4$
147	$EO_2 + NO \rightarrow NO_2 + 2CH_2O + HO_2$
148	$EO_2 + HO_2 \rightarrow EP + O_2$
149	$EO_2 + EO_2 \rightarrow 2.4CH_2O + 1.2HO_2 + 0.4ALD_2$
150	$ALKE + OH \rightarrow PO_2$
151	$ALKE + O_3 \rightarrow 0.525CH_2O + 0.5ALD_2 + 0.2CHO_2 + 0.2CRO_2 + 0.23HO_2 + 0.215CH_3O_2 + 0.095OH + 0.33CO$

Table A.3 (continued).

NO.	Reaction
152	$ALKE + NO_3 \rightarrow PRN1$
153	$PO_2 + NO \rightarrow NO_2 + ALD_2 + CH_2O + HO_2$
154	$PO_2 + HO_2 \rightarrow PP + O_2$
155	$PO_2 + PO_2 \rightarrow 2.2ALD_2 + 1.2HO_2$
156	$PRN1 + NO_2 \rightarrow PRN2$
157	$PRN1 + HO_2 \rightarrow PRPN + O_2$
158	$PRN1 + NO \rightarrow 2NO_2 + CH_2O + ALD_2$
159	$CHO_2 + NO \rightarrow CH_2O + NO_2$
160	$CHO_2 + NO_2 \rightarrow CH_2O + NO_3$
161	$CHO_2 + H_2O \rightarrow HCOOH$
162	$CHO_2 + SO_2 \rightarrow CH_2O + SO4$
163	$CHO_2 + CH_2O \rightarrow OZID$
164	$CHO_2 + ALD_2 \rightarrow OZID$
165	$CRO_2 + NO \rightarrow ALD_2 + NO_2$
166	$CRO_2 + NO_2 \rightarrow ALD_2 + NO_3$
167	$CRO_2 + H_2O \rightarrow CH_3COOH$
168	$CRO_2 + SO_2 \rightarrow ALD_2 + SO4$
169	$CRO_2 + CH_2O \rightarrow OZID$
170	$CRO_2 + ALD_2 \rightarrow OZID$
171	$BENZ + OH \rightarrow ADDB$
172	$ADDB + NO \rightarrow NO_2 + HO_2 + GLYX + DIAL$
173	$AROM + OH \rightarrow 0.84 + TO_2 + 0.16CRES + 0.16HO_2$
174	$TO_2 + NO \rightarrow NO_2 + HO_2 + 0.72MGLY + 0.18GLYX + DIAL$
175	$TO_2 + HO_2 \rightarrow TP + O_2$
176	$CRES + OH \rightarrow \beta 12HO_2 + 0.9ZO_2 + 0.9TCO_3 + -0.9OH + \beta 13NO_2$

Table A.3 (continued).

NO.	Reaction
177	$CRES + NO_3 \rightarrow HNO_3 + \beta 10NO_2 + \beta 10OH$
178	$MGLY + OH \rightarrow MCO_3 + H_2O + CO$
179	$GLYX + OH \rightarrow HO_2 + 2CO + H_2O$
180	$DIAL + OH \rightarrow TCO_3 + H_2O$
181	$ZO_2 + NO \rightarrow NO_2$
182	$ZO_2 + HO_2 \rightarrow ZP + O_2$
183	$TCO_3 + NO \rightarrow NO_2 + 0.92HO_2 + 0.89GLYX + 0.11MGLY + 0.05MCO_3 + 0.95CO + 0.79CO_2 + 2ZO_2$
184	$TCO_3 + HO_2 \rightarrow TCP + O_2$
185	$TCO_3 + NO_2 \rightarrow TPAN$
186	$TPAN \rightarrow TCO_3 + NO_2$
187	$ALD_2 + OH \rightarrow MCO_3 + H_2O$
188	$ALD_2 + NO_3 \rightarrow MCO_3 + HNO_3$
189	$MCO_3 + NO \rightarrow CH_3O_2 + NO_2 + CO_2$
190	$MCO_3 + HO_2 \rightarrow 0.33MCP + 0.33O_2 + 0.67CH_3COOH + 0.67^{o}_{3}$
191	$MCO_3 + NO_2 \rightarrow PAN$
192	$PAN \rightarrow MCO_3 + NO_2$
193	$MCO_3 + CH_3O_2 \rightarrow CH_3COOH + CH_2O + O_2$
194	$MCO_3 + CH_3O_2 \rightarrow CH_3O_2 + CH_2O + HO_2 + CO_2$
195	$PAN + OH \rightarrow 0.5NO_2 + PROD$
196	$CH_3COOH + OH \rightarrow CH_3O_2 + CO_2 + H_2O$
197	$CH_3COOH \rightarrow$ Rainout/Washout
198	$C_2H_5OH \rightarrow$ Rainout/Washout
199	$ETP + OH \rightarrow 0.5ETO_2 + 0.5ALD_2 + 0.5OH + H_2O$
200	$ETP \rightarrow$ Rainout/Washout
201	$nR3P + OH \rightarrow 0.5nR_3O_2 + 0.5ALD_2 + 0.5OH + H_2O$

Table A.3 (continued).

NO.	Reaction
202	iR3P + OH → 0.5iR_3O_2 + 0.5ALD_2 + 0.5OH + H_2O
203	iR3P → Rainout/Washout
204	nR3P → Rainout/Washout
205	RAP + OH → 0.5RAO_2 + 0.5ALD_2 + 0.5OH + H_2O
206	RAP → Rainout/Washout
207	MCP + OH → 0.5MCO_3 + 0.5CH_2O + 0.5OH + H_2O
208	MCP → Rainout/Washout
209	EP + OH → 0.5EO_2 + CH_2O + 0.5OH + H_2O
210	EP → Rainout/Washout
211	PP + OH → 0.5PO_2 + 0.5ALD_2 + 0.5OH + H_2O
212	PP → Rainout/Washout
213	TP + OH → TO_2 + H_2O
214	TP → Rainout/Washout
215	TCP + OH → TCO_3 + H_2O
216	TCP → Rainout/Washout
217	ZP + OH → ZO_2 + H_2O
218	ZP → Rainout/Washout
219	XAPOH → 0.5RIO_2 + 0.5ALD_2 + 0.5OH + H_2O
220	XAP1 → Rainout/Washout
221	RP + OH → 0.5VRO_2 + 0.5ALD_2 + 0.5OH + H_2O
222	RP → Rainout/Washout
223	DAP + OH → 0.5MAO_3 + 0.5ALD_2 + 0.5OH + H_2O
224	DAP → Rainout/Washout
225	XAP2 + OH → 0.5MRO_2 + 0.5ALD_2 + 0.5OH + H_2O
226	XAP2 → Rainout/Washout

Table A.3 (continued).

NO.	Reaction
227	HACO + NO_2 → IIPAN
228	IIPAN → HACO + NO_2
229	HACO + NO → NO_2 + HO_2 + CH_2O
230	HACO + HO_2 → HEP
231	HEP + OH → 0.5HACO + CH_2O + 0.5OH + H_2O
232	HEP → Rainout/Washout
233	ACET + hν → MCO_3 + CH_3O_2
234	MEK + hν → MCO_3 + ETO_2
235	MGGY + hν → MCO_3 + HO_2
236	MGLY + hν → MCO_3 + HO_2 + CO
237	GLYX + hν → PROD
238	DIAL + hν → 0.98 + HO_2 + 0.02 + MCO_3 + TCO_3
239	ALD_2 + hν → CH_3O_2 + HO_2 + CO
240	ALD_2 + hν → CH_4 + CO
241	PAN + hν → MCO_3 + NO_2
242	ETP + hν → OH + HO_2 + ALD_2
243	nR3P + hν → OH + HO_2 + ALD_2
244	iR3P + hν → OH + HO_2 + ALD_2
245	RAP + hν → OH + HO_2 + ALD_2
246	MCP + hν → OH + HO_2 + CH_2O
247	EP + hν → OH + HO_2 + $2CH_2O$
248	PP + hν → OH + HO_2 + ALD_2
249	XAP1 + hν → OH + HO_2 + ALD_2
250	RP + hν → OH + HO_2 + ALD_2
251	DAP + hν → OH + HO_2 + ALD_2

Table A.3 (continued).

NO.	Reaction
252	XAP2 + hν → OH + HO_2 + ALD_2
253	HEP + hν → OH + HO_2 + $2CH_2O$
254	MNIT + hν → CH_3O + NO

Table A.4. List of Species in NMHC chemistry of the GT Lurman mechanism.

Abbreviation	Species
ADDB	$C_6H_6(OH)OO$
ALD_2	≥ C2 Aldehydes
ALKA	≥ C4 Alkanes
ALKE	≥ C3 Alkenes
AROM	Aromatics Other Than Benzene
ATO_2	$CH_3COCH_2O_2\cdot$
BENZ	Benzene
C_2H_5OH	Ethanol
C_2H_6	Ethane
C_3H_8	Propane
CH_3COOH	Acetic Acid
CHO_2	CH_3CHO_2 Criegee Biradical
CRES	Cresol
CRO_2	CH_2O_2 Criegee Biradical
DAP	Peroxide for MAO_3 Radical
DIAL	Unsaturated Dicarbonyl
EO_2	Ethene RO_2
EP	Peroxide for EO_2
ETHE	Ethene
ETO_2	$C_2H_5O_2\cdot$
ETP	Peroxide for ETO_2
GLYX	Glyoxal $(CHO)_2$
HACO	$HOCH_2C(O)OO\cdot$
HEP	Peroxide for HACO
IIPAN	Nitrate for HACO

Table A.4 (continued).

Abbreviation	Species
INO_2	Isoprene-NO_3-O_2 Adduct
iR_3O_2	i-$C_3H_7O_2$·
iR_3P	Peroxide for iR_3O_2
ISOP	Isoprene
KO_2	MEK RO_2
MACR	Methacrolein
MAN2	MACR + NO_3 Product
MAO_3	CH_2=C(CH_3)C(O)OO·
MAOO	MACR Criegee Biradical
MCO_3	≥ C2 Aldehyde RO_2s
MCP	Peroxide for MCO_3
MEK	Methyl Ethyl Ketone
MGGY	α-dicarbonyl
MGLY	Methyl Glyoxal
MPAN	Nitrate for MAO_3
MRO_2	MACR RO_2
MVK	Methyl Vinyl Ketone
MVKO	MVK Criegee Biradical
MVN2	MVK + NO_3 Product
nR_3O_2	n-$C_3H_7O_2$·
nR_3P	Peroxide for nR_3O_2
PAN	Peroxyacetyl Nitrate
PO_2	ALKE RO_2
PP	Peroxide for PO_2
PRN1	Alkene + NO_3 Product

Table A.4 (continued).

Abbreviation	Species
RAN1	Nitrate for RAO_2
RAN2	Nitrite for RAO_2
$RANO_2$	RAN1 + NO Product
RAO_2	ALKA RO_2
RAP	Peroxide for RAO_2
RIO_2	Isoprene RO_2
RP	Peroxide for RIO_2
TCO_3	$CHOCH{=}CHCO_3$
TCP	Peroxide for TCO_3
TO_2	AROM RO_2
TP	Peroxide for TO_2
TPAN	Nitrate for TCO_3
VRO_2	MVK RO_2
XAP1	Peroxide for RIO_2
XAP2	Peroxide for MRO_2
ZO_2	Cresol RO_2
ZP	Peroxide for ZO_2

Table A.5. NMHC chemistry of the CBIV mechanism.

NO.	Reaction
78	$ALD_2 + OH \rightarrow MCO_3 + H_2O$
79	$ALD_2 + NO_3 \rightarrow MCO_3 + HNO_3$
80	$MCO_3 + NO \rightarrow CH_3O_2 + NO_2 + CO_2$
81	$MCO_3 + NO_2 + M \rightarrow PAN$
82	$PAN \rightarrow MCO_3 + NO_2$
83	$CH_3O_2 + MCO_3 \rightarrow CH_3O_2 + CH_3O + O_2$
84	$MCO_3 + MCO_3 \rightarrow 2CH_3O_2 + O_2$
85	$MCO_3 + HO_2 \rightarrow CH_3OOH + O_2$
86	$MCO_3 + HO_2 \rightarrow CH_3O_2 + OH + O_2$
87	$AONE + OH \rightarrow ANO_2$
88	$ANO_2 + NO \rightarrow MCO_3 + CH_2O + NO_2$
89	$PARA + OH \rightarrow RO_2$
90	$PARA + OH \rightarrow RO_2R$
91	$RO_2 + NO \rightarrow NO_2 + HO_2 + ALD_2 + X$
92	$RO_2 + NO \rightarrow NTR$
93	$RO_2R + NO \rightarrow NO_2 + ROR$
94	$RO_2R + NO \rightarrow NTR$
95	$ROR + NO_2 \rightarrow NTR$
96	$ROR \rightarrow KET + HO_2$
97	$ROR \rightarrow KET + D$
98	$ROR \rightarrow ALD_2 + D + X$
99	$ROR \rightarrow AONE + D + 2X$
100	$X + PARA \rightarrow PROD$
101	$D + PARA \rightarrow RO_2$
102	$D + PARA \rightarrow AO_2 + 2X$

Table A.5 (continued).

NO.	Reaction
103	$D + PARA \rightarrow RO_2R$
104	$D + KET \rightarrow MCO_3 + X$
105	$AO_2 + NO \rightarrow NO_2 + AONE + HO_2$
106	$OH + OLE \rightarrow CH_3O_2 + ALD_2 + X$
107	$O_3 + OLE \rightarrow ALD_2 + CRIG + X$
108	$O_3 + OLE \rightarrow CH_2O + MCRG + X$
109	$O_3 + OLE \rightarrow ALD_2 + HOTA + X$
110	$O_3 + OLE \rightarrow CH_2O + HTMA + X$
111	$NO_3 + OLE \rightarrow PNO_2$
112	$PNO_2 + NO \rightarrow DNIT$
113	$PNO_2 + NO \rightarrow CH_2O + ALD_2 + X + 2NO_2$
114	$OH + ETH \rightarrow ETO_2$
115	$ETO_2 + NO \rightarrow NO_2 + 2CH_2O + HO_2$
116	$ETO_2 + NO \rightarrow NO_2 + ALD_2 + HO_2$
117	$O_3 + ETH \rightarrow HCHO + CRIG$
118	$O_3 + ETH \rightarrow HCHO + HOTA$
119	$HOTA \rightarrow CO_2 + H_2$
120	$HOTA \rightarrow CO + H_2O$
121	$HOTA \rightarrow 2HO_2 + CO_2$
122	$HTMA \rightarrow CH_4 + CO_2$
123	$HTMA \rightarrow CH_3O_2 + CO + OH$
124	$HTMA \rightarrow CH_3O_2 + HO_2 + CO_2$
125	$HTMA \rightarrow CH_2O + CO + 2HO_2$
126	$HTMA \rightarrow CH_3O_2 + HO_2 + CO_2$
127	$CRIG + NO \rightarrow NO_2 + CH_2O$

Table A.5 (continued).

NO.	Reaction
128	$CRIG + H_2O \rightarrow FACD + H_2O$
129	$CRIG + CH_2O \rightarrow OZD$
130	$CRIG + ALD_2 \rightarrow OZD$
131	$MCRG + NO \rightarrow NO_2 + ALD_2$
132	$MCRG + H_2O \rightarrow ACAC + H_2O$
133	$MCRG + CH_2O \rightarrow OZD$
134	$MCRG + ALD_2 \rightarrow OZD$
135	$OH + TOL \rightarrow BO2$
136	$OH + TOL \rightarrow CRES + HO_2$
137	$OH + TOL \rightarrow TO_2$
138	$BO2 + NO \rightarrow NO_2 + BZA + HO_2$
139	$OH + BZA \rightarrow BZO_2$
140	$BZO_2 + NO \rightarrow NO_2 + PHO_2 + CO$
141	$BZO_2 + NO_2 \rightarrow PBZN$
142	$PBZN \rightarrow BZO_2 + NO_2$
143	$PHO_2 + NO \rightarrow NO_2 + PHO$
144	$PHO + NO_2 \rightarrow NPHN$
145	$OH + CRES \rightarrow CRO$
146	$OH + CRES \rightarrow CRO_2$
147	$NO_3 + CRES \rightarrow CRO + HNO_3$
148	$CRO + NO_2 \rightarrow NCRE$
149	$CRO_2 + NO \rightarrow NO_2 + OPEN + HO_2$
150	$CRO_2 + NO \rightarrow NO_2 + ACID + HO_2$
151	$TO_2 + NO \rightarrow NO_2 + OPEN + HO_2$
152	$TO_2 + NO \rightarrow NTR$

Table A.5 (continued).

NO.	Reaction
153	$TO_2 \rightarrow HO_2 + CRES$
154	$OH + XYL \rightarrow XLO_2$
155	$OH + XYL \rightarrow CRES + PARA + HO_2$
156	$OH + XYL \rightarrow TO_2$
157	$OH + XYL \rightarrow XINT$
158	$XLO_2 + NO \rightarrow NO_2 + HO_2 + BZA + PARA$
159	$XINT + NO \rightarrow NO_2 + HO_2 + 2MGLY + 2PARA$
160	$OH + MGLY \rightarrow MGPX$
161	$MGPX + NO \rightarrow NO_2 + MCO_3$
162	$OH + OPEN \rightarrow OPPX + MCO_3 + HO_2 + CO$
163	$OPPX + NO \rightarrow NO_2 + CH_2O + HO_2 + CO$
164	$O_3 + OPEN \rightarrow ALD_2 + MGPX + CH_2O + CO$
165	$O_3 + OPEN \rightarrow CH_2O + CO + OH + 2HO_2$
166	$O_3 + OPEN \rightarrow MGLY$
167	$O_3 + OPEN \rightarrow MCO_3 + CH_2O + HO_2 + CO$
168	$O_3 + OPEN \rightarrow$ Product
169	$OH + ISOP \rightarrow ISO3$
170	$OH + ISOP \rightarrow ISO4$
171	$O_3 + ISOP \rightarrow CH_2O + MACR$
172	$O_3 + ISOP \rightarrow CH_2O + MVK$
173	$O_3 + ISOP \rightarrow CH_2O + OZD + CO$
174	$O_3 + ISOP \rightarrow CH_2O + OZD + CO$
175	$NO_3 + ISOP \rightarrow ISNT$
176	$ISO1 + NO \rightarrow NO_2 + HO_2 + MVK$
177	$ISO2 + NO \rightarrow NO_2 + HO_2 + MACR$

Table A.5 (continued).

NO.	Reaction
178	$ISO3 + NO \rightarrow NO_2 + HO_2 + CH_2O + MVK$
179	$ISO3 + NO \rightarrow ISN$
180	$ISO3 + HO_2 \rightarrow CH_3OOH$
181	$ISO4 + NO \rightarrow NO_2 + HO_2 + CH_2O + MACR$
182	$ISO4 + NO \rightarrow ISN$
183	$ISO4 + HO_2 \rightarrow CH_3OOH$
184	$ISNT + NO \rightarrow DISN$
185	$O_3 + MVK \rightarrow MGLY + CH_2O$
186	$O_3 + MVK \rightarrow PROD$
187	$OH + MVK \rightarrow MV1$
188	$OH + MVK \rightarrow MV2$
189	$O_3 + MACR \rightarrow MGLY + CH_2O$
190	$O_3 + MACR \rightarrow PROD$
191	$OH + MACR \rightarrow MAC1$
192	$OH + MACR \rightarrow MAC2$
193	$MV1 + NO \rightarrow NO_2 + CH_2O + MGLY + HO_2$
194	$MV1 + NO \rightarrow MVNT$
195	$MV1 + HO_2 \rightarrow CH_3OOH$
196	$MV2 + NO \rightarrow NO_2 + MCO_3 + ALD_2$
197	$MV2 + HO_2 \rightarrow CH_3OOH$
198	$MAC1 + NO \rightarrow NO_2 + ETH + CH_3O_2 + CO_2$
199	$MAC1 + HO_2 \rightarrow CH_3OOH$
200	$MAC2 + NO \rightarrow NO_2 + CH_2O + MGLY + HO_2$
201	$MAC2 + HO_2 \rightarrow CH_3OOH$
202	$ALD_2 + h\nu \rightarrow CH_3O_2 + HO_2 + CO$

Table A.5 (continued).

NO.	Reaction
203	MNIT + hν → CH_3O + NO
204	AONE + hν → MCO_3 + CH_3O_2
205	KET + hν → MCO_3 + RO_2 + 2X
206	BZA + hν → PROD
207	MGLY + hν → MCO_3 + CO + HO_2
208	OPEN + hν → MCO_3 + CO + HO_2
209	MVK + hν → MCO_3 + ETH + HO_2
210	MACR + hν → CH_3O_2 + ETH + HO_2 + CO

Table A.6. List of Species in NMHC chemistry of the CBIV mechanism.

Abbreviation	Species
ALD_2	$\geq C_2$ Aldehydes
ACAC	Acetic Acid
ACID	Aromatic Ring Fragment Acid
ANO_2	Acetylmethylperoxy Radical ($CH_3C(O)CH_2OO\cdot$)
AO_2	Dimethyl Secondary Organic Peroxide Radical
AONE	Acetone
BO2	Benzylperoxy Radical
BZA	Benzaldehyde
BZO_2	Peroxybenzoyl Radical
CRES	Cresol and Higher Molecular Weight Phenols
CRIG	Criegee Biradical (H_2COO)
CRO	Methylphenoxy Radical
CRO_2	Methylphenylperoxy Radical
D	Paraffin-to-Peroxy Radical Operator
DISN	Dinitrate of Isoprene
DNIT	C_2 Dinitrate Group
ETH	Ethene
ETO_2	Ethanol Peroxide Radical (CH_2OH-$CH_2OO\cdot$)
FACD	Formic Acid
HOTA	Excited Formic Acid
HTMA	Excited Acetic Acid
ISN	Nitrate of Isoprene
ISNT	Nitrate of Isoprene
ISO1	Isoprene-O Adduct
ISO2	Isoprene-O Adduct

Table A.6 (continued).

Abbreviation	Species
ISO3	Isoprene-OH Adduct
ISO4	Isoprene-OH Adduct
ISOP	Isoprene
KET	Ketone Carbonyl Group (-C(O)-)
MAC1	MACR-OH Adduct
MAC2	MACR-OH Adduct
MACR	Methacrolein
MCO_3	Peroxyacyl Radical
MCRG	Methyl Criegee Biradical (CH_3(H)COO)
MGLY	Methyl Glyoxal
MGPX	Peroxide Radical of MGLY (CH_3C(O)C(O)OO·)
MV1	MVK-OH Adduct
MV2	MVK-OH Adduct
MVK	Methyl Vinyl Ketone
MVNT	Nitrate of MVK
NCRE	Nitrocresol
NPHN	Nitrophenol
NTR	Nitrate
OLE	Olefinic Carbon Bond (C=C)
OPEN	High Molecular Weight Aromatic Oxidation Ring Fragment
OPPX	Peroxide Radical of OPEN
OZD	Ozonide and Further Products
PAN	Peroxyacetyl Nitrate
PARA	Paraffin Carbon Bond (C-C)
PBZN	Peroxybenzoyl Nitrate

Table A.6 (continued).

Abbreviation	Species
PHO	Phenoxy Radical
PHO_2	Phenylperoxy Radical
PNO_2	Nitrated Organic Peroxy Radical (-CH(ONO_2)-CH(OO)·-)
RO_2	Primary Organic Peroxy Radical
RO_2R	Secondary Organic Peroxy Radical
ROR	Secondary Organic Oxy Radical
TO_2	Toluene-OH Adduct
TOL	Toluene
X	Paraffin Loss Operator
XINT	Xylene-OH Adduct
XLO_2	Methylbenzylperoxy Radical
XYL	Xylene

Table A.7. NMHC chemistry of the RACM mechanism.

NO.	Reaction
78	$ETH + OH \rightarrow ETHP + H_2O$
79	$HC3 + OH \rightarrow 0.583HC3P + 0.381HO_2 + 0.335ALD_2 + 0.036ORA1 + 0.036CO + 0.036GLY + 0.036OH + 0.01CH_2O + H_2O$
80	$HC5 + OH \rightarrow 0.75HC5P + 0.25KET + 0.25HO_2 + H_2O$
81	$HC8 + OH \rightarrow 0.951HC8P + 0.025ALD_2 + 0.024HKET + 0.049HO_2 + H_2O$
82	$ETE + OH \rightarrow ETEP$
83	$OLT + OH \rightarrow OLTP$
84	$OLI + OH \rightarrow OLIP$
85	$DIEN + OH \rightarrow ISOP$
86	$ISO + OH \rightarrow ISOP$
87	$API + OH \rightarrow APIP$
88	$LIM + OH \rightarrow LIMP$
89	$TOL + OH \rightarrow 0.9ADDT + 0.1XO_2 + 0.1HO_2$
90	$XYL + OH \rightarrow 0.9ADDX + 0.1XO_2 + 0.1HO_2$
91	$CSL + OH \rightarrow 0.85ADDC + 0.1PHO + 0.05HO_2$
92	$ALD_2 + OH \rightarrow MCO_3 + H_2O$
93	$KET + OH \rightarrow KETP + H_2O$
94	$HKET + OH \rightarrow HO_2 + MGLY + H_2O$
95	$GLY + OH \rightarrow HO_2 + 2CO + H_2O$
96	$MGLY + OH \rightarrow MCO_3 + H_2O + CO$
97	$MACR + OH \rightarrow 0.51\ TCO_3 + 0.41HKET + 0.08MGLY + 0.41CO + 0.08CH_2O + 0.49HO_2 + 0.49XO_2$
98	$DCB + OH \rightarrow 0.5\ TCO_3 + 0.5HO_2 + 0.5XO_2 + 0.35UDD + 0.15GLY + 0.15MGLY$
99	$UDD + OH \rightarrow 0.88ALD_2 + 0.12KET + HO_2$
100	$OP2 + OH \rightarrow 0.44HC3P + 0.08ALD_2 + 0.41KET + 0.49OH + 0.07XO_2$
101	$PAA + OH \rightarrow 0.35CH_2O + 0.65MCO_3 + 0.35HO_2 + 0.35XO_2$

Table A.7 (continued).

NO.	Reaction
102	$PAN + OH \rightarrow CH_2O + XO_2 + H_2O + NO_3$
103	$TPAN + OH \rightarrow 0.6HKET + 0.4CH_2O + 0.4HO_2 + XO_2 + 0.4PAN + 0.6NO_3$
104	$ONIT + OH \rightarrow HC3P + NO_2 + H_2O$
105	$ALD_2 + NO_3 \rightarrow MCO_3 + HNO_3$
106	$GLY + NO_3 \rightarrow HNO_3 + HO_2 + 2CO$
107	$MGLY + NO_3 \rightarrow HNO_3 + MCO_3 + CO$
108	$MACR + NO_3 \rightarrow 0.2TCO_3 + 0.2HNO_3 + 0.8OLNN + 0.8CO$
109	$DCB + NO_3 \rightarrow 0.5TCO_3 + 0.5HO_2 + 0.5XO_2 + 0.25GLY + 0.25ALD_2 + 0.03KET + 0.25MGLY + 0.5HNO_3 + 0.5NO_2$
110	$CSL + NO_3 \rightarrow HNO_3 + PHO$
111	$ETE + NO_3 \rightarrow 0.8OLNN + 0.2OLND$
112	$OLT + NO_3 \rightarrow 0.43OLNN + 0.57OLND$
113	$OLI + NO_3 \rightarrow 0.11OLNN + 0.89OLND$
114	$DIEN + NO_3 \rightarrow 0.9OLNN + 0.1OLND + 0.9MACR$
115	$ISO + NO_3 \rightarrow 0.9OLNN + 0.1OLND + 0.9MACR$
116	$API + NO_3 \rightarrow 0.1OLNN + 0.9OLND$
117	$LIM + NO_3 \rightarrow 0.13OLNN + 0.87OLND$
118	$TPAN + NO_3 \rightarrow 0.6ONIT + 0.6NO_3 + 0.4PAN + 0.4CH_2O + 0.4NO_2 + XO_2$
119	$ETE + O_3 \rightarrow CH_2O + 0.43CO + 0.37ORA1 + 0.26HO_2 + 0.13H2 + 0.12OH$
120	$OLT + O_3 \rightarrow 0.64CH_2O + 0.44ALD_2 + 0.37CO + 0.14ORA1 + 0.1ORA2 + 0.25HO_2 + 0.4OH + 0.03KET + 0.03KETP + 0.006H_2O_2 + 0.03ETH + 0.19CH_3O_2 + 0.1ETHP$
121	$OLI + O_3 \rightarrow 0.02CH_2O + 0.99ALD_2 + 0.16KET + 0.3CO + 0.011H_2O_2 + 0.14ORA2 + 0.22HO_2 + 0.63OH + 0.23CH_3O_2 + 0.12KETP + 0.06ETH + 0.18ETHP + 0.07CH_4$
122	$DIEN + O_3 \rightarrow 0.9CH_2O + 0.39MACR + 0.36CO + 0.15ORA1 + 0.09O(^3P) + 0.3HO_2 + 0.35OLT + 0.28OH + 0.15MCO_3 + 0.03CH_3O_2 + 0.02KETP + 0.13XO_2 + 0.001H_2O_2$

Table A.7 (continued).

NO.	Reaction
123	$ISO + O_3 \rightarrow 0.9CH_2O + 0.39MACR + 0.36CO + 0.15ORA1 + 0.09 O(^3P) + 0.3HO_2 + 0.35OLT + 0.28OH + 0.15MCO_3 + 0.03CH_3O_2 + 0.02KETP + 0.13XO_2 + 0.001H_2O_2$
124	$API + O_3 \rightarrow 0.65ALD_2 + 0.53KET + 0.14CO + 0.2ETHP + 0.42KETP + 0.85OH + 0.1HO_2 + 0.02H_2O_2$
125	$LIM + O_3 \rightarrow 0.04CH_2O + 0.46OLT + 0.14CO + 0.16ETHP + 0.42KETP + 0.85OH + 0.1HO_2 + 0.02H_2O_2 + 0.79MACR + 0.01ORA1 + 0.07ORA2$
126	$MACR + O_3 \rightarrow 0.4CH_2O + 0.6MGLY + 0.13ORA2 + 0.54CO + 0.08H2 + 0.22ORA1 + 0.29HO_2 + 0.07OH + 0.13OP2 + 0.13MCO_3$
127	$DCB + O_3 \rightarrow 0.21OH + 0.29HO_2 + 0.66CO + 0.5GLY + 0.28MCO_3 + 0.16ALD_2 + 0.62MGLY + 0.11PAA + 0.11ORA1 + 0.21ORA2$
128	$TPAN + O_3 \rightarrow 0.7CH_2O + 0.3PAN + 0.7NO_2 + 0.13CO + 0.04H2 + 0.11ORA1 + 0.08HO_2 + 0.036OH + 0.7MCO_3$
129	$PHO + NO_2 \rightarrow 0.1CSL + ONIT$
130	$PHO + HO_2 \rightarrow CSL$
131	$ADDT + NO_2 \rightarrow CSL + HONO$
132	$ADDT + O_2 \rightarrow 0.98TOLP + 0.02CSL + 0.02HO_2$
133	$ADDT + O_3 \rightarrow CSL + OH$
134	$ADDX + NO_2 \rightarrow CSL + HONO$
135	$ADDX + O_2 \rightarrow 0.98XYLP + 0.02CSL + 0.02HO_2$
136	$ADDX + O_3 \rightarrow CSL + OH$
137	$ADDC + NO_2 \rightarrow CSL + HONO$
138	$ADDC + O_2 \rightarrow 0.98CSLP + 0.02CSL + 0.02HO_2$
139	$ADDC + O_3 \rightarrow CSL + OH$
140	$MCO_3 + NO_2 \rightarrow PAN$
141	$PAN \rightarrow MCO_3 + NO_2$
142	$TCO_3 + NO_2 \rightarrow TPAN$
143	$TPAN \rightarrow TCO_3 + NO_2$
144	$ETHP + NO \rightarrow ALD_2 + HO_2 + NO_2$

Table A.7 (continued).

NO.	Reaction
145	$HC3P + NO \rightarrow 0.047CH_2O + 0.233ALD_2 + 0.623KET + 0.063GLY + 0.742HO_2 + 0.015CH_3O_2 + 0.048ETHP + 0.048XO_2 + 0.059ONIT + 0.941NO_2$
146	$HC5P + NO \rightarrow 0.021CH_2O + 0.211ALD_2 + 0.722KET + 0.599HO_2 + 0.031CH_3O_2 + 0.245ETHP + 0.334XO_2 + 0.059ONIT + 0.876NO_2$
147	$HC8P + NO \rightarrow 0.15ALD_2 + 0.642KET + 0.133ETHP + 0.261ONIT + 0.739NO_2 + 0.606HO_2 + 0.416XO_2$
148	$ETEP + NO \rightarrow 1.6CH_2O + HO_2 + NO_2 + 0.2ALD_2$
149	$OLTP + NO \rightarrow 0.94ALD_2 + CH_2O + HO_2 + NO_2 + 0.06KET$
150	$OLIP + NO \rightarrow HO_2 + 1.71ALD_2 + 0.29KET + NO_2$
151	$ISOP + NO \rightarrow 0.446MACR + 0.354OLT + 0.847HO_2 + 0.606CH_2O + 0.153ONIT + 0.847NO_2$
152	$APIP + NO \rightarrow 0.8HO_2 + 0.8ALD_2 + 0.8KET + 0.2ONIT + 0.8NO_2$
153	$LIMP + NO \rightarrow 0.65HO_2 + 0.4MACR + 0.25OLI + 0.25CH_2O + 0.35ONIT + 0.65NO_2$
154	$TOLP + NO \rightarrow 0.95NO_2 + 0.95HO_2 + 0.65MGLY + 1.2GLY + 0.5DCB + 0.05ONIT$
155	$XYLP + NO \rightarrow 0.95NO_2 + 0.95HO_2 + 0.6MGLY + 0.35GLY + 0.95DCB + 0.05ONIT$
156	$CSLP + NO \rightarrow GLY + MGLY + HO_2 + NO_2$
157	$MCO_3 + NO \rightarrow CH_3O_2 + NO_2$
158	$TCO_3 + NO \rightarrow MCO_3 + CH_2O + NO_2$
159	$KETP + NO \rightarrow 0.54MGLY + 0.46ALD_2 + 0.23MCO_3 + 0.77HO_2 + 0.16XO_2 + NO_2$
160	$OLNN + NO \rightarrow HO_2 + ONIT + NO_2$
161	$OLND + NO \rightarrow 0.287CH_2O + 1.24ALD_2 + 0.464KET + 2NO_2$
162	$ETHP + HO_2 \rightarrow OP2$
163	$HC3P + HO_2 \rightarrow OP2$
164	$HC5P + HO_2 \rightarrow OP2$
165	$HC8P + HO_2 \rightarrow OP2$
166	$ETEP + HO_2 \rightarrow OP2$
167	$OLTP + HO_2 \rightarrow OP2$

Table A.7 (continued).

NO.	Reaction
168	$OLIP + HO_2 \rightarrow OP2$
169	$ISOP + HO_2 \rightarrow OP2$
170	$APIP + HO_2 \rightarrow OP2$
171	$LIMP + HO_2 \rightarrow OP2$
172	$TOLP + HO_2 \rightarrow OP2$
173	$XYLP + HO_2 \rightarrow OP2$
174	$CSLP + HO_2 \rightarrow OP2$
175	$MCO_3 + HO_2 \rightarrow PAA$
176	$MCO_3 + HO_2 \rightarrow ORA2 + O_3$
177	$TCO_3 + HO_2 \rightarrow OP2$
178	$TCO_3 + HO_2 \rightarrow ORA2 + O_3$
179	$KETP + HO_2 \rightarrow OP2$
180	$OLNN + HO_2 \rightarrow ONIT$
181	$OLND + HO_2 \rightarrow ONIT$
182	$ETHP + CH_3O_2 \rightarrow 0.75CH_2O + HO_2 + 0.75ALD_2$
183	$HC3P + CH_3O_2 \rightarrow 0.81CH_2O + 0.992HO_2 + 0.58ALD_2 + 0.018KET + 0.007CH_3O_2 + 0.005MGLY + 0.085XO_2 + 0.119GLY$
184	$HC5P + CH_3O_2 \rightarrow 0.829CH_2O + 0.946HO_2 + 0.523ALD_2 + 0.24KET + 0.014ETHP + 0.049CH_3O_2 + 0.245XO_2$
185	$HC8P + CH_3O_2 \rightarrow 0.753CH_2O + 0.993HO_2 + 0.411ALD_2 + 0.419KET + 0.322XO_2 + 0.013ETHP$
186	$ETEP + CH_3O_2 \rightarrow 1.55CH_2O + HO_2 + 0.35ALD_2$
187	$OLTP + CH_3O_2 \rightarrow 1.25CH_2O + HO_2 + 0.669ALD_2 + 0.081KET$
188	$OLIP + CH_3O_2 \rightarrow 0.755CH_2O + HO_2 + 0.932ALD_2 + 0.313KET$
189	$ISOP + CH_3O_2 \rightarrow 0.55MACR + 0.37OLT + HO_2 + 0.08OLI + 1.09CH_2O$
190	$APIP + CH_3O_2 \rightarrow CH_2O + 2HO_2 + ALD_2 + KET$
191	$LIMP + CH_3O_2 \rightarrow 1.4CH_2O + 0.6MACR + 0.4OLI + 2HO_2$
192	$TOLP + CH_3O_2 \rightarrow CH_2O + HO_2 + 0.35MGLY + 0.65GLY + DCB$

Table A.7 (continued).

NO.	Reaction
193	$XYLP + CH_3O_2 \rightarrow CH_2O + HO_2 + 0.63MGLY + 0.37GLY + DCB$
194	$CSLP + CH_3O_2 \rightarrow CH_2O + 2HO_2 + MGLY + GLY$
195	$MCO_3 + CH_3O_2 \rightarrow CH_2O + HO_2 + CH_3O_2$
196	$MCO_3 + CH_3O_2 \rightarrow CH_2O + ORA2$
197	$TCO_3 + CH_3O_2 \rightarrow 2CH_2O + HO_2 + MCO_3$
198	$TCO_3 + CH_3O_2 \rightarrow CH_2O + ORA2$
199	$KETP + CH_3O_2 \rightarrow 0.75CH_2O + 0.88HO_2 + 0.4MGLY + 0.3ALD_2 + 0.3HKET + 0.12MCO_3 + 0.08XO_2$
200	$OLNN + CH_3O_2 \rightarrow 0.75CH_2O + HO_2 + ONIT$
201	$OLND + CH_3O_2 \rightarrow 0.96CH_2O + 0.5HO_2 + 0.64ALD_2 + 0.149KET + 0.5NO_2 + 0.5ONIT$
202	$ETHP + MCO_3 \rightarrow ALD_2 + 0.5HO_2 + 0.5CH_3O_2 + 0.5ORA2$
203	$HC3P + MCO_3 \rightarrow 0.724ALD_2 + 0.488HO_2 + 0.127KET + 0.508CH_3O_2 + 0.006ETHP + 0.071XO_2 + 0.091CH_2O + 0.1GLY + 0.499ORA2 + 0.004MGLY$
204	$HC5P + MCO_3 \rightarrow 0.677ALD_2 + 0.438HO_2 + 0.33KET + 0.554CH_3O_2 + 0.495ORA2 + 0.018ETHP + 0.237XO_2 + 0.076CH_2O$
205	$HC8P + MCO_3 \rightarrow 0.497ALD_2 + 0.489HO_2 + 0.581KET + 0.507CH_3O_2 + 0.495ORA2 + 0.015ETHP + 0.318XO_2$
206	$ETEP + MCO_3 \rightarrow 0.6ALD_2 + 0.5HO_2 + 0.5CH_3O_2 + 0.8CH_2O + 0.5ORA2$
207	$OLTP + MCO_3 \rightarrow 0.859ALD_2 + 0.501HO_2 + 0.501CH_2O + 0.501CH_3O_2 + 0.499ORA2 + 0.141KET$
208	$OLIP + MCO_3 \rightarrow 0.941ALD_2 + 0.51HO_2 + 0.569KET + 0.51CH_3O_2 + 0.49ORA2$
209	$ISOP + MCO_3 \rightarrow 0.771MACR + 0.506HO_2 + 0.229OLT + 0.494ORA2 + 0.34CH_2O + 0.506CH_3O_2$
210	$APIP + MCO_3 \rightarrow ALD_2 + HO_2 + KET + CH_3O_2$
211	$LIMP + MCO_3 \rightarrow 0.6MACR + 0.4OLI + 0.4CH_2O + HO_2 + CH_3O_2$
212	$TOLP + MCO_3 \rightarrow CH_3O_2 + HO_2 + 0.35MGLY + 0.65GLY + DCB$
213	$XYLP + MCO_3 \rightarrow CH_3O_2 + HO_2 + 0.63MGLY + 0.37GLY + DCB$
214	$CSLP + MCO_3 \rightarrow CH_3O_2 + HO_2 + MGLY + GLY$
215	$MCO_3 + MCO_3 \rightarrow 2CH_3O_2$

Table A.7 (continued).

NO.	Reaction
216	$TCO_3 + MCO_3 \rightarrow CH_3O_2 + MCO_3 + CH_2O$
217	$KETP + MCO_3 \rightarrow 0.5CH_3O_2 + 0.38HO_2 + 0.54MGLY + 0.35ALD_2 + 0.11KET + 0.12MCO_3 + 0.08XO_2 + 0.5ORA2$
218	$OLNN + MCO_3 \rightarrow ONIT + 0.5ORA2 + 0.5CH_3O_2 + 0.5HO_2$
219	$OLND + MCO_3 \rightarrow 0.207CH_2O + 0.516CH_3O_2 + 0.65ALD_2 + 0.167KET + 0.516NO_2 + 0.484ONIT + 0.484ORA2$
220	$OLNN + OLNN \rightarrow 2ONIT + HO_2$
221	$OLNN + OLND \rightarrow 0.202CH_2O + 0.64ALD_2 + 0.149KET + 0.5HO_2 + 1.5ONIT + 0.5NO_2$
222	$OLND + OLND \rightarrow 0.504CH_2O + 1.21ALD_2 + 0.285KET + ONIT + NO_2$
223	$CH_3O_2 + NO_3 \rightarrow CH_2O + HO_2 + NO_2$
224	$ETHP + NO_3 \rightarrow ALD_2 + HO_2 + NO_2$
225	$HC3P + NO_3 \rightarrow 0.048CH_2O + 0.243ALD_2 + 0.67KET + 0.063GLY + 0.792HO_2 + 0.155CH_3O_2 + 0.053ETHP + 0.051XO_2 + NO_2$
226	$HC5P + NO_3 \rightarrow 0.021CH_2O + 0.239ALD_2 + 0.828KET + 0.699HO_2 + 0.04CH_3O_2 + 0.262ETHP + 0.391XO_2 + NO_2$
227	$HC8P + NO_3 \rightarrow 0.187ALD_2 + 0.88KET + 0.845HO_2 + 0.155ETHP + 0.587XO_2 + NO_2$
228	$ETEP + NO_3 \rightarrow 1.6CH_2O + 0.2ALD_2 + HO_2 + NO_2$
229	$OLTP + NO_3 \rightarrow CH_2O + 0.94ALD_2 + 0.06KET + HO_2 + NO_2$
230	$OLIP + NO_3 \rightarrow 1.71ALD_2 + 0.29KET + HO_2 + NO_2$
231	$ISOP + NO_3 \rightarrow 0.6MACR + 0.4OLT + 0.686CH_2O + HO_2 + NO_2$
232	$APIP + NO_3 \rightarrow ALD_2 + KET + HO_2 + NO_2$
233	$LIMP + NO_3 \rightarrow 0.6MACR + 0.4OLI + 0.4CH_2O + HO_2 + NO_2$
234	$TOLP + NO_3 \rightarrow 0.7MGLY + 1.3GLY + 0.5DCB + HO_2 + NO_2$
235	$XYLP + NO_3 \rightarrow 1.26MGLY + 0.74GLY + DCB + HO_2 + NO_2$
236	$CSLP + NO_3 \rightarrow MGLY + GLY + HO_2 + NO_2$
237	$MCO_3 + NO_3 \rightarrow CH_3O_2 + NO_2$
238	$TCO_3 + NO_3 \rightarrow CH_2O + MCO_3 + NO_2$
239	$KETP + NO_3 \rightarrow 0.54MGLY + 0.46ALD_2 + 0.77HO_2 + 0.23MCO_3 + 0.16XO_2 + NO_2$

Table A.7 (continued).

NO.	Reaction
240	OLNN + NO_3 → ONIT + HO_2 + NO_2
241	OLND + NO_3 → $0.28CH_2O$ + $1.24ALD_2$ + 0.469KET + $2NO_2$
242	XO_2 + HO_2 → OP2
243	XO_2 + CH_3O_2 → CH_2O + HO_2
244	XO_2 + MCO_3 → CH_3O_2
245	XO_2 + XO_2 → PROD
246	XO_2 + NO → NO_2
247	XO_2 + NO_3 → NO_2
248	ALD_2 + hν → CH_3O_2 + HO_2 + CO
249	OP2 + hν → OH + HO_2 + ALD_2
250	PAA + hν → CH_3O_2 + OH
251	KET + hν → MCO_3 + ETHP
252	GLY + hν → $0.3CH_2O$ + 2.4CO + $0.3HO_2$ + $0.95H_2$
253	MGLY + hν → MCO_3 + HO_2 + CO
254	DCB + hν → TCO_3 + HO_2
255	ONIT + hν → $0.2ALD_2$ + 0.8KET + HO_2 + NO_2
256	MACR + hν → CO + CH_2O + HO_2 + MCO_3
257	HKET + hν → CH_2O + HO_2 + MCO_3
258	MNIT + hν → CH_3O + NO

Table A.8. List of Species in NMHC chemistry of the RACM mechanism.

Abbreviation	Species
ADDC	Aromatic-OH Adduct from CSL
ADDT	Aromatic-OH Adduct from TOL
ADDX	Aromatic-OH Adduct from XYL
ALD_2	≥ C2 Aldehydes
API	α-Pinene and Other Cyclic Terpenes with One Double Bond
APIP	API RO_2
CSL	Cresol and other Hydroxy Substituted Aromatics
CSLP	CSL RO_2
DCB	Unsaturated Dicarbonyl
DIEN	Butadiene and Other Anthropogenic Dienes
ETE	Ethene
ETEP	ETE RO_2
ETH	Ethane
ETHP	ETH RO_2
GLY	Glyoxal
HC3	Alkanes, Alcohols, Esters, and Alkynes with OH Rate Constant (298K, 1 atm) Less Than 3.4×10^{-12} cm^3 s^{-1}
HC3P	HC3 RO_2
HC5	Alkanes, Alcohols, Esters, and Alkynes with OH Rate Constant (298K, 1 atm) between 3.4×10^{-12} cm^3 s^{-1} and 6.8×10^{-12} cm^3 s^{-1}
HC5P	HC5 RO_2
HC8	Alkanes, Alcohols, Esters, and Alkynes with OH Rate Constant (298K, 1 atm) Greater 6.8×10^{-12} cm^3 s^{-1}
HC8P	HC8 RO_2
HKET	Hydroxy Ketone
ISO	Isoprene
ISOP	ISO RO_2
KET	Ketones

Table A.8 (continued).

Abbreviation	Species
KETP	KET RO_2
LIM	d-Limonene and Other Cyclic Diene-Terpenes
LIMP	LIM RO_2
MACR	Methacrolein and Other Unsaturated Monoaldehydes
MCO3	Acetyl Peroxy and Higher Saturated Acyl Peroxy Radicals
MGLY	Methyl Glyoxal and Other α-carbonyls Aldehydes
OLI	Internal Alkenes
OLIP	OLI RO_2
OLND	NO_3-Alkene Adduct Reacting via Decomposition
OLNN	NO_3-Alkene Adduct Reacting to Form Carbonitrates + HO_2
OLT	Terminal Alkenes
OLTP	OLT RO_2
ONIT	Organic Nitrate
OP2	Higher Organice Peroxides
ORA1	Formic Acid
ORA2	Acetic Acid and Higher Acids
PAA	Peroxyacetic Acid and Higher Analogs
PAN	Peroxyacetyl Nitrate and Higher Saturated PANs
PHO	Phenoxy Radicals and Similar Radicals
TCO3	Unsaturated Acyl Peroxy Radicals
TOL	Toluene and Less Reactive Aromatics
TOLP	TOL RO_2
TPAN	Unsaturated PANs
UDD	Unsaturated Dihydrox Dicarbonyl
XO2	Accounts for Additional NO to NO_2 Conversions

Table A.8 (continued).

Abbreviation	Species
XYL	Xylene and More Reactive Aromatics
XYLP	XYL RO_2

Table A.9. NMHC chemistry of the SAPRC mechanism.

NO.	Reaction
78	$ALK1 + OH \rightarrow RO_2R + ALD_2$
79	$ALK2 + OH \rightarrow 0.246OH + 0.121HO_2 + 0.612RO_2R + 0.021RO_2N + 0.16CO + 0.039CH_2O + 0.155RCHO + 0.417ACET + 0.248GLY + 0.121HCOOH$
80	$ALK3 + OH \rightarrow 0.695RO_2R + 0.07RO_2N + 0.559R_2O_2 + 0.236TBUO + 0.026CH_2O + 0.445ALD_2 + 0.122RCHO + 0.024ACET + 0.332MEK$
81	$ALK4 + OH \rightarrow 0.835RO_2R + 0.143RO_2N + 0.936R_2O_2 + 0.011CH_3O_2 + 0.011MCO_3 + 0.002CO + 0.024CH_2O + 0.455ALD_2 + 0.244RCHO + 0.452ACET + 0.11MEK + 0.125PROD2$
82	$ALK5OH \rightarrow 0.653RO_2R + 0.347RO_2N + 0.948R_2O_2 + 0.026CH_2O + 0.099ALD_2 + 0.204RCHO + 0.072ACET + 0.089MEK + 0.417PROD2$
83	$ETE + OH \rightarrow RO_2R + 1.61CH_2O + 0.195ALD_2$
84	$ETE + O_3 \rightarrow 0.12OH + 0.12HO_2 + 0.5CO + CH_2O + 0.37HCOOH$
85	$ETE + NO_3 \rightarrow RO_2R + RCHO$
86	$OLE1 + OH \rightarrow 0.91RO_2R + 0.09RO_2N + 0.205R_2O_2 + 0.732CH_2O + 0.294ALD_2 + 0.497RCHO + 0.005ACET + 0.119PROD2$
87	$OLE1 + O_3 \rightarrow 0.155OH + 0.056HO_2 + 0.022RO_2R + 0.001RO_2N + 0.076CH_3O_2 + 0.345CO + 0.5CH_2O + 0.154ALD_2 + 0.363RCHO + 0.001ACET + 0.215PROD2$
88	$OLE1 + NO_3 \rightarrow 0.824RO_2R + 0.176RO_2N + 0.488R_2O_2 + 0.009ALD_2 + 0.037RCHO + 0.024ACET + 0.511RNO3$
89	$OLE2 + OH \rightarrow 0.918RO_2R + 0.082RO_2N + 0.001R_2O_2 + 0.244CH_2O + 0.732ALD_2 + 0.511RCHO + 0.127ACET + 0.072MEK + 0.061BALD + 0.025MACR + 0.025ISOPROD$
90	$OLE2 + O_3 \rightarrow 0.378OH + 0.003HO_2 + 0.033RO_2R + 0.002RO_2N + 0.137R_2O_2 + 0.197CH_3O_2 + 0.006RCOO_2 + 0.269CH_2O + 0.456ALD_2 + 0.305RCHO + 0.045ACET + 0.026MEK + 0.006PROD2 + 0.042BALD + 0.026MACR$
91	$OLE2 + NO_3 \rightarrow 0.391NO_2 + 0.442RO_2R + 0.136RO_2N + 0.711R_2O_2 + 0.03CH_3O_2 + 0.079CH_2O + 0.507ALD_2 + 0.151RCHO + 0.102ACET + 0.001MEK + 0.015BALD + 0.048MVK + 0.321RNO3$
92	$ARO1 + OH \rightarrow 0.224HO_2 + 0.765RO_2R + 0.011RO_2N + 0.055PROD2 + 0.118GLY + 0.119MGLY + 0.017PHEN + 0.207CRES + 0.059BALD + 0.491DCB1 + 0.108DCB2 + 0.051DCB3$
93	$ARO2 + OH \rightarrow 0.187HO_2 + 0.804RO_2R + 0.009RO_2N + 0.097GLY + 0.287MGLY + 0.087BACL + 0.187CRES + 0.05BALD + 0.561DCB1 + 0.099DCB2 + 0.093DCB3$
94	$ISO + OH \rightarrow 0.907RO_2R + 0.093RO_2N + 0.079R_2O_2 + 0.624CH_2O + 0.23MACR + 0.32MVK + 0.357ISOPROD$

Table A.9 (continued).

NO.	Reaction
95	$ISO + O_3 \rightarrow 0.266OH + 0.066RO_2R + 0.008RO_2N + 0.126R_2O_2 + 0.192MARCO_3 + 0.275CO + 0.592CH_2O + 0.1PROD2 + 0.39MACR + 0.16MVK + 0.204HCOOH + 0.15RCOOH$
96	$ISO + NO_3 \rightarrow 0.187NO_2 + 0.749RO_2R + 0.064RO_2N + 0.187R_2O_2 + 0.936ISOPROD$
97	$TRP1 + OH \rightarrow 0.75RO_2R + 0.25RO_2N + 0.5R_2O_2 + 0.276CH_2O + 0.474RCHO + 0.276PROD2$
98	$TRP1 + O_3 \rightarrow 0.567OH + 0.033HO_2 + 0.031RO_2R + 0.18RO_2N + 0.729R_2O_2 + 0.123MCO_3 + 0.201RCOO_2 + 0.235CH_2O + 0.205RCHO + 0.13ACET + 0.276PROD2 + 0.001GLY + 0.031BACL$
99	$TRP1 + NO_3 \rightarrow 0.474NO_2 + 0.276RO_2R + 0.25RO_2N + 0.75R_2O_2 + 0.474RCHO + 0.276RNO3$
100	$RO_2R + NO \rightarrow NO_2 + HO_2$
101	$RO_2R + HO_2 \rightarrow ROOH$
102	$RO_2R + NO_3 \rightarrow NO_2 + HO_2$
103	$RO_2R + CH_3O_2 \rightarrow HO_2 + 0.75CH_2O + 0.25CH_3OH$
104	$RO_2R + RO_2R \rightarrow HO_2$
105	$R_2O_2 + NO \rightarrow NO_2$
106	$R_2O_2 + HO_2 \rightarrow HO_2$
107	$R_2O_2 + NO_3 \rightarrow NO_2$
108	$R_2O_2 + CH_3O_2 \rightarrow CH_3O_2$
109	$R_2O_2 + RO_2R \rightarrow RO_2R$
110	$R_2O_2 + R_2O_2 \rightarrow XXX$
111	$RO_2N + NO \rightarrow RNO3$
112	$RO_2N + HO_2 \rightarrow ROOH$
113	$RO_2N + NO_3 \rightarrow NO_2 + HO_2 + MEK$
114	$RO_2N + CH_3O_2 \rightarrow HO_2 + 0.25CH_3OH + 0.5MEK + 0.5PROD2 + 0.75CH_2O$
115	$RO_2N + RO_2R \rightarrow HO_2 + 0.5MEK + 0.5PROD2$
116	$RO_2N + R_2O_2 \rightarrow RO_2N$
117	$RO_2N + RO_2N \rightarrow MEK + HO_2 + PROD2$

Table A.9 (continued).

NO.	Reaction
118	$CH_3O_2 + NO_3 \rightarrow CH_2O + HO_2 + NO_2$
119	$MCO_3 + NO_2 + M \rightarrow PAN$
120	$PAN \rightarrow MCO_3 + NO_2$
121	$MCO_3 + NO \rightarrow CH_3O_2 + NO_2$
122	$MCO_3 + HO_2 \rightarrow 0.75CCOOOH + 0.25CCOOH + 0.25O3$
123	$MCO_3 + NO_3 \rightarrow CH_3O_2 + NO_2$
124	$MCO_3 + CH_3O_2 \rightarrow CCOOH + CH_2O$
125	$MCO_3 + RO_2R \rightarrow CCOOH$
126	$MCO_3 + R_2O_2 \rightarrow MCO_3$
127	$MCO_3 + RO_2N \rightarrow CCOOH + PROD2$
128	$MCO_3 + MCO_3 \rightarrow 2CH_3O_2$
129	$RCOO_2 + NO_2 \rightarrow PAN2$
130	$PAN2 \rightarrow RCOO_2 + NO_2$
131	$RCOO_2 + NO \rightarrow NO + ALD_2$
132	$RCOO_2 + HO_2 \rightarrow 0.75RCOOOH + 0.25RCOOH + 0.25O3$
133	$RCOO_2 + NO_3 \rightarrow NO_2 + ALD_2 + RO_2R$
134	$RCOO_2 + CH_3O_2 \rightarrow RCOOH + CH_2O$
135	$RCOO_2 + RO_2R \rightarrow RCOOH$
136	$RCOO_2 + R_2O_2 \rightarrow RCOO_2$
137	$RCOO_2 + RO_2N \rightarrow RCOOH + PROD2$
138	$RCOO_2 + MCO_3 \rightarrow CH_3O_2 + ALD_2 + RO_2R$
139	$RCOO_2 + RCOO_2 \rightarrow 2ALD_2 + 2RO_2R$
140	$BZCOO_2 + NO_2 \rightarrow PBZN$
141	$PBZN \rightarrow BZCOO_2 + NO_2$
142	$BZCOO_2 + NO \rightarrow NO_2 + BZO + R_2O_2$

Table A.9 (continued).

NO.	Reaction
143	$BZCOO_2 + HO_2 \rightarrow 0.75RCOOOH + 0.25RCOOH + 0.25O3$
144	$BZCOO_2 + NO_3 \rightarrow NO_2 + BZO + R_2O_2$
145	$BZCOO_2 + CH_3O_2 \rightarrow RCOOH + CH_2O$
146	$BZCOO_2 + RO_2R \rightarrow RCOOH$
147	$BZCOO_2 + R_2O_2 \rightarrow BZCOO_2$
148	$BZCOO_2 + RO_2N \rightarrow RCOOH + PROD2$
149	$BZCOO_2 + MCO_3 \rightarrow CH_3O_2 + BZO + R_2O_2$
150	$BZCOO_2 + RCOO_2 \rightarrow ALD_2 + RO_2R + BZO + R_2O_2$
151	$BZCOO_2 + BZCOO_2 \rightarrow 2BZO + 2R_2O_2$
152	$MARCO_3 + NO_2 \rightarrow MAPAN$
153	$MAPAN \rightarrow MARCO_3 + NO_2$
154	$MARCO_3 + NO \rightarrow NO_2 + CH_2O + MCO_3$
155	$MARCO_3 + HO_2 \rightarrow 0.75RCOOOH + 0.25RCOOH + 0.25O_3$
156	$MARCO_3 + NO_3 \rightarrow NO_2 + CH_2O + MCO_3$
157	$MARCO_3 + CH_3O_2 \rightarrow RCOOH + CH_2O$
158	$MARCO_3 + RO_2R \rightarrow RCOOH$
159	$MARCO_3 + R_2O_2 \rightarrow MARCO_3$
160	$MARCO_3 + RO_2N \rightarrow 2RCOOH$
161	$MARCO_3 + MCO_3 \rightarrow CH_3O_2 + CH_2O + MCO_3$
162	$MARCO_3 + RCOO_2 \rightarrow CH_2O + MCO_3 + ALD_2 + RO_2R$
163	$MARCO_3 + BZCOO_2 \rightarrow CH_2O + MCO_3 + BZO + R_2O_2$
164	$MARCO_3 + MARCO_3 \rightarrow 2CH_2O + 2MCO_3$
165	$TBUO + NO_2 \rightarrow RNO3$
166	$TBUO \rightarrow ACET + CH_3O_2$
167	$BZO + NO_2 \rightarrow NPHE$

Table A.9 (continued).

NO.	Reaction
168	$BZO + HO_2 \rightarrow PHEN$
169	$BZO \rightarrow PHEN$
170	$BZNO_2O + NO_2 \rightarrow XXX$
171	$BZNO_2O + HO_2 \rightarrow NPHE$
172	$BZNO_2O \rightarrow NPHE$
173	$ALD_2 + OH \rightarrow MCO_3$
174	$ALD_2 + NO_3 \rightarrow MCO_3 + HNO_3$
175	$RCHO + OH \rightarrow 0.034RO_2R + 0.001RO_2N + 0.965RCOO_2 + 0.034CO + 0.034ALD_2$
176	$RCHO + NO_3 \rightarrow HNO_3 + RCOO_2$
177	$ACET + OH \rightarrow CH_2O + MCO_3 + R_2O_2$
178	$MEK + OH \rightarrow 0.37RO_2R + 0.042RO_2N + 0.616R_2O_2 + 0.492MCO_3 + 0.096RCOO_2 + 0.115CH_2O + 0.482ALD_2 + 0.37RCHO$
179	$ROOH + OH \rightarrow RCHO + 0.34RO_2R + 0.66OH$
180	$GLY + OH \rightarrow 0.63HO_2 + 1.26CO + 0.37RCOO_2$
181	$GLY + NO_3 \rightarrow HNO_3 + 0.63HO_2 + 1.26CO + 0.37RCOO_2$
182	$MGLY + OH \rightarrow MCO_3 + H_2O + CO$
183	$MGLY + NO_3 \rightarrow HNO_3 + MCO_3 + CO$
184	$PHEN + NO \rightarrow 0.24BZO + 0.76RO_2R + 0.23GLY$
185	$PHEN + NO_3 \rightarrow HNO_3 + BZO$
186	$CRES + OH \rightarrow 0.24BZO + 0.76RO_2R + 0.23MGLY$
187	$CRES + NO_3 \rightarrow HNO_3 + BZO$
188	$BALD + OH \rightarrow BZCOO_2$
189	$BALD + NO_3 \rightarrow HNO_3 + BZCOO_2$
190	$MACR + OH \rightarrow 0.5RO_2R + 0.416CO + 0.084CH_2O + 0.416MEK + 0.084MGLY + 0.5MARCO_3$
191	$MACR + O_3 \rightarrow 0.008HO_2 + 0.1RO_2R + 0.208OH + 0.1RCOO_2 + 0.45CO + 0.2CH_2O + 0.9MELY + 0.333HCOOH$
192	$MACR + NO_3 \rightarrow 0.5HNO_3 + 0.5RO_2R + 0.5CO + 0.5MARCO_3$

Table A.9 (continued).

NO.	Reaction
193	$MVK + OH \rightarrow 0.3RO_2R + 0.025RO_2N + 0.675R_2O_2 + 0.675MCO_3 + 0.3CH_2O + 0.675RCHO + 0.3MGLY$
194	$MVK + O_3 \rightarrow 0.064HO_2 + 0.05RO_2R + 0.164OH + 0.05RCOO_2 + 0.475CO + 0.1CH_2O + 0.95MGLY + 0.351HCOOH$
195	$ISOPROD + OH \rightarrow 0.67RO_2R + 0.041RO_2N + 0.289MARCO_3 + 0.336CO + 0.055CH_2O + 0.129ALD_2 + 0.013RCHO + 0.15MEK + 0.332PROD2 + 0.15GLY + 0.174MGLY$
196	$ISOPROD + O_3 \rightarrow 0.4HO_2 + 0.048RO_2R + 0.048RCOO_2 + 0.285OH + 0.498CO + 0.125CH_2O + 0.047ALD_2 + 0.21MEK + 0.023GLY + 0.742MGLY + 0.1HCOOH + 0.372RCOOH$
197	$ISOPROD + NO_3 \rightarrow 0.799RO_2R + 0.051RO_2N + 0.15MARCO_3 + 0.572CO + 0.15HNO_3 + 0.227CH_2O + 0.218RCHO + 0.008MGLY + 0.572RNO_3$
198	$PROD2 + OH \rightarrow 0.379HO_2 + 0.473RO_2R + 0.07RO_2N + 0.029MCO_3 + 0.049RCOO_2 + 0.213CH_2O + 0.084ALD_2 + 0.558RCHO + 0.115MEK + 0.329PROD2$
199	$RNO3 + OH \rightarrow 0.338NO_2 + 0.113HO_2 + 0.376RO_2R + 0.173RO_2N + 0.596R_2O_2 + 0.01CH_2O + 0.439ALD_2 + 0.213RCHO + 0.006ACET + 0.177MEK + 0.048PROD2 + 0.31RNO3$
200	$DCB1 + OH \rightarrow RCHO + RO_2R + CO$
201	$DCB1 + O_3 \rightarrow 1.5HO_2 + 0.5OH + 1.5CO + GLY$
202	$DCB2 + OH \rightarrow R_2O_2 + RCHO + MCO_3$
203	$DCB3 + OH \rightarrow R_2O_2 + RCHO + MCO_3$
204	$MNIT + h\nu \rightarrow CH_3O + NO$
205	$ALD_2 + h\nu \rightarrow CH_3O_2 + HO_2 + CO$
206	$RCHO + h\nu \rightarrow ALD_2 + RO_2R + CO + HO_2$
207	$ACET + h\nu \rightarrow MCO_3 + CH_3O_2$
208	$MEK + h\nu \rightarrow MCO_3 + ALD_2 + RO_2R$
209	$ROOH + h\nu \rightarrow OH + HO_2 + RCHO$
210	$GLY + h\nu \rightarrow 2CO + 2HO_2$
211	$GLY + h\nu \rightarrow CH_2O + CO$
212	$MGLY + h\nu \rightarrow MCO_3 + HO_2 + CO$
213	$BACL + h\nu \rightarrow 2MCO_3$

Table A.9 (continued).

NO.	Reaction
214	BALD + hν → XXX
215	MACR + hν → $0.34HO_2$ + $0.33RO_2R$ + 0.33OH + $0.67MCO_3$ + 0.67CO + $0.67CH_2O$ + $0.33MARCO_3$
216	MVK + hν → $0.3CH_3O_2$ + 0.7CO + 0.7PROD2 + $0.3MARCO_3$
217	PROD2 + hν → $0.96RO_2R$ + $0.04RO_2N$ + $0.515R_2O_2$ + $0.667MCO_3$ + $0.333RCOO_2$ + $0.506CH_2O$ + $0.246ALD_2$ + 0.71RCHO
218	ISOPROD + hν → $1.233HO_2$ + $0.467MCO_3$ + $0.3RCOO_2$ + 1.233CO + $0.3CH_2O$ + $0.467ALD_2$ + 0.233MEK
219	RNO3 + hν → NO_2 + $0.341HO_2$ + $0.564RO_2R$ + $0.095RO_2N$ + $0.152R_2O_2$ + $0.134CH_2O$ + $0.431ALD_2$ + 0.147RCHO + 0.02ACET + 0.243MEK + 0.435PROD2
220	DCB2 + hν → RO_2R + $0.5MCO_3$ + $0.5HO_2$ + CO + R_2O_2 + 0.5GLY + 0.5MGLY
221	DCB3 + hν → RO_2R + $0.5MCO_3$ + $0.5HO_2$ + CO + R_2O_2 + 0.5GLY + 0.5MGLY

Table A.10. List of Species in NMHC chemistry of the SAPRC mechanism.

Abbreviation	Species
ACET	Acetone
ALD2	Acetaldehyde and Glycolaldehyde
ALK1	Alkanes and Other Non-aromatic Compounds That React Only with OH and Have k_{OH} between 2 × 10^2 and 5 × 10^2 ppm^{-1} min^{-1} (Primarily Ethane)
ALK2	Alkanes and Other Non-aromatic Compounds That React Only with OH and Have k_{OH} between 5 × 10^2 and 2.5 × 10^3 ppm^{-1} min^{-1} (Primarily Propane and Acetylene)
ALK3	Alkanes and Other Non-aromatic Compounds That React Only with OH and Have k_{OH} between 2.5 × 10^3 and 5 × 10^3 ppm^{-1} min^{-1}
ALK4	Alkanes and Other Non-aromatic Compounds That React Only with OH and Have k_{OH} between 5 × 10^3 and 1 × 10^4 ppm^{-1} min^{-1}
ALK5	Alkanes and Other Non-aromatic Compounds That React Only with OH and Have k_{OH} Greater Than 1 × 10^4 ppm^{-1} min^{-1}
ARO1	Aromatics with $k_{OH} < 2 \times 10^4$ ppm^{-1} min^{-1} (Primarily Toluene and Other Monoalkyl Benzenes)
ARO2	Aromatics with $k_{OH} > 2 \times 10^4$ ppm^{-1} min^{-1} (Primarily Xylene and Polyalkyl Benzenes)
BACL	Biacetyl
BALD	Aromatic Aldehydes
$BZCOO_2$	Peroxyacyl Radial Formed from Aromatic Aldehydes
$BZNO_2O$	Nitro-substituted Phenoxy Radical
BZO	Phenoxy Radicals
CCOOH	Acetic Acid
CRES	Cresols
DCB1	Reactive Aromatic Fragmentation Products That Do Not Undergo Significant Photodecomposition to Radicals
DCB2	Reactive Aromatic Fragmentation Products Which Photolyze with α-Dicarbonyl-like Action Spectrum
DCB3	Reactive Aromatic Fragmentation Products Which Photolyze with Acrolein Action Spectrum
ETE	Ethene
GLY	Glyoxal $(CHO)_2$
HCOOH	Formic Acid

Table A.10 (continued).

Abbreviation	Species
ISO	Isoprene
ISOPROD	Lumped Isoprene Product Species
MACR	Methacrolein and Acrolein
MAPAN	PAN Analogues Formed from MACR
$MARCO_3$	Peroxyacyl Radicals Formed from MACR and Other Acroleins
MCO_3	Acetyl Peroxy Radicals
MEK	Ketones and Other Non-Aldehyde Oxygenated Products Which Reacts with OH Radicals Slower Than 5×10^{-12} cm^3 $molec^{-2}$ sec^{-1}
MGLY	Methyl Glyoxal
MVK	Methyl Vinyl Ketone
NPHE	Nitrophenols
OLE1	Alkenes (Other Than Ethene) with $k_{OH} < 7 \times 10^4$ ppm^{-1} min^{-1} (Primarily Terminal Alkenes)
OLE2	Alkenes with $k_{OH} > 7 \times 10^4$ ppm^{-1} min^{-1} (Primarily Internal or Disubstituted Alkenes)
PAN	Peroxyacetyl Nitrate
PAN2	PPN and Other Higher Alkyl PAN Analogues
PBZN	PAN Analogues Formed from Aromatic Aldehydes
PHEN	Phenol
PROD2	Ketones and Other Non-Aldehyde Oxygenated Products Which Reacts with OH Radicals Faster Than 5×10^{-12} cm^3 $molec^{-2}$ sec^{-1}
R_2O_2	Peroxy Radical Operator Representing NO to NO_2 Conversion without HO_2 Formation
RCHO	Lumped ≥ C3 Aldehydes
$RCOO_2$	Peroxy Propionyl and Higher Peroxy Acyl Radicals
RCOOH	Higher Organic Acid
RNO_3	Lumped Organic Nitrates
RO_2N	Peroxy Radical Operator Representing NO Consumption with Organic Nitrate Formation
RO_2R	Peroxy Radical Operator Representing NO to NO_2 Conversion with HO_2 Formation

Table A.10 (continued).

Abbreviation	Species
ROOH	Lumped Higher Organic Hydroperoxides
TBUO	t-Butoxy Radicals
TRP1	Biogenic Alkenes Other Than Isoprene (Primarily Terpenes)

REFERENCES

Andersson-Sköld, Y. and D. Simpson (1999). Comparison.of the chemical schemes of the EMEP MSC-W and. IVL photochemical trajectory models. *Atmospheric Environment*, **33**, 1111-1129.

Atkinson, R. (1994). Gas-phase tropospheric chemistry of organic compounds. *Journal of Physical and Chemical Reference Data*, Monograph **2**, 1-216.

Atkinson, R. (1997). Gas-phase tropospheric chemistry of volatile organic compounds: 1. Alkanes and alkenes. *Journal of Physical and Chemical Reference Data*, **26**, 215-290.

Atkinson, R. (2000). Atmospheric chemistry of VOCs and NO_x. *Atmospheric Environment*, **34**, 2063-2101.

Bloss, W. J., J. D. Lee, G. P. Johnson, R. Sommariva, D. E. Heard, A. Saiz-Lopez, J. M. C. Plane, G. McFiggans, H. Coe, M. Flynn, P. Williams, A. R. Rickard, and Z. L. Fleming (2005). Impact of halogen monoxide chemistry upon boundary layer OH and HO_2 concentrations at a coastal site. *Geophysical Research Letters*, **32**, L06814, doi: 10.1029/2004GL022084.

Brewer, D. A., M. A. Ogliaruso, T. R. Augustsson, and T. R. Levine (1984). The oxidation of isoprene in the troposphere: Mechanism and model calculations. *Atmospheric Environment*, **18**, 2723-2744.

Brune, W. H., P. S. Stevens, and J. H. Mather (1995). Measuring OH and HO_2 in the troposphere by laser-induced fluorescence at low pressure. *Journal of Atmospheric Chemistry*, **52**, 3328-3336.

Brune, W. H., I. C. Faloona, D. Tan, A. J. Weinheimer, T. Campos, B. A. Ridley, S. A. Vay, J. E. Collins, G. W. Sachse, L. Jaegle, and D. J. Jacob (1998). Airborne in situ OH and HO_2 observations in the cloud-free troposphere and lower stratosphere during SUCCESS. *Geophysical Research Letters*, **25**, 1701-1704.

Carter, W. P. L. (1990). A detailed mechanism for the gas-phase atmospheric reactions of organic compounds. *Atmospheric Environment*, **24A**, 481-518.

Carter, W. P. L. (1994). Calculation of reactivity scales using an updated Carbon Bond IV mechanism. Report to Coordinating Research Council, Auto/Oil Air Quality Improvement Research Program, Atlanta, Georgia.

Carter, W. P. L. (2000). Documentation of the SAPRC-99 chemical mechanism for VOC reactivity assessment. Final report to California Air Resources Board Contract No. 92-329 and 95-308.

Carter, W. P. L., J. A. Pierce, D. Luo, and I. L. Malkina (1995). Environmental chamber studies of maximum incremental reactivities of volatile organic compounds. *Atmospheric Environment*, **29**, 2499-2511.

Carter, W. P. L., D. Luo, and I. L. Malkina (1997). Environmental chamber studies for development of an updated photochemical mechanism for VOC reactivity assessment. Final report to California Air Resources Board Contract 92-345, Coordinating Research Council, Inc., Project M-9, and National Renewable Energy Laboratory Contract ZF-2-12252-07.

Chameides, W. L. and J. C. G. Walker (1973). A photochemical theory of tropospheric ozone. *Journal of Geophysical Research*, **78**, 8751-8760.

Chen, G. (1995). A study of tropospheric photochemistry in the subtropical/tropical North and South Atlantic. *Dissertation*, Ph.D. Thesis, Georgia Institute of Technology, Atlanta GA.

Chen, G., D. Davis, J. Crawford, B. Heikes, D. O'Sullivan, M. Lee, F. Eisele, L. Mauldin, D. Tanner, J. Collins, J. Barrick, B. Anderson, D. Blake, J. Bradshaw, S. Sandholm, M. Carroll, G. Albercook, and A. Clarke (2001). An assessment of HO_x chemistry in the tropical Pacific boundary layer: Comparison of model simulations with observations recorded during PEM Tropics A. *Journal of Atmospheric Chemistry*, **38**, 317-341.

Crawford, J. H. (1997). An analysis of the photochemical environment over the western, North Pacific based on aircraft observations. *Dissertation*, Ph.D. Thesis, Georgia Institute of Technology, Atlanta GA.

Crawford, J. H., D. Davis, G. Chen, J. Bradshaw, S. Sandholm, Y. Kondo, S. Liu, E. Browell, G. Gregory, B. Anderson, G. Sachse, J. Collins, J. Barrick, D. Blake, R. Talbot, and H. Singh (1997). An Assessment of ozone photochemistry in the extratropical western north Pacific: Impact of continental outflow during the late winter/early spring. *Journal of Geophysical Research*, **102**, 28,469-28,487.

Crawford, J., D. Davis, J. Olson, G. Chen, S. Liu, G. Gregory, J. Barrick, G. Sachse, S. Sandholm, B. Heikes, H. Singh, and D. Blake (1999a). Assessment of upper tropospheric HO_x sources over the tropical Pacific based on NASA GTE/PEM data: Net effect on HO_x and other photochemical parameters. *Journal of Geophysical Research,* **104**, 16,255-16,273.

Crawford, J., D. Davis, G. Chen, R. Shetter, M. Müller, J. Barrick, and J. Olson (1999b). An assessment of cloud effects on photolysis rate coefficients: Comparison of experimental and theoretical values. *Journal of Geophysical Research*, **104**, 5725-5734.

Crutzen, P. J. (1973). A discussion of the chemistry of some minor constituents in the stratosphere and troposphere. *Pure and Applied Geophysics*, **106-108**, 1385-1399.

Crutzen, P. J. (1974). Photochemical reaction initiated by and influencing ozone in unpolluted tropospheric air. *Tellus*, **26**, 45- 5.

Davis, D. D., G. Chen, W. Chameides, J. Bradshaw, S. Sandholm, M. Rodgers, J. Schendal, S. Madronich, G. Sachse, G. Gregory, B. Anderson, J. Barrick, M. Shipham, J. Collins, L. Wade, and D. Blake (1993). Photostationary state analysis of the NO_2-NO system based on airborne observations from the subtropical/tropical North and South Atlantic. *Journal of Geophysical Research*, **98**, 23,501-23,523.

Davis, D. D., J. Crawford, G. Chen, W. Chameides, S. Liu, J. Bradshaw, S. Sandholm, G. Sachse, G. Gregory, B. Anderson, J. Barrick, A. Bachmeier, J. Collins, E. Browell, D. Blake, S. Rowland, Y. Kondo, H. Singh, R. Talbot, B. Heikes, J. Merrill, J. Rodriguez, and R. E. Newell (1996). Assessment of the ozone photochemistry tendency in the western North Pacific as inferred from PEM-West A observations during the fall of 1991. *Journal of Geophysical Research*, **101**, 2111-2134.

Davis, D., G. Grodzinsky, G. Chen, J. Crawford, F. Eisele, L. Mauldin, D. Tanner, C. Cantrell, W. Brune, D. Tan, I. Faloona, B. Ridley, D. Montzka, J. Walega, F. Grahek, S. Sandholm, G. Sachse, S. Vay, B. Anderson, M. Avery, B. Heikes, J. Snow, D. O'Sullivan, R. Shetter, B. Lefer, D. Blake, N. Blake, M. Carroll, and Y. Wang (2001). Marine latitude/altitude OH distributions: Comparison of Pacific Ocean observations with models. *Journal of Geophysical Research*, **106**, 32,691-32,707.

Davis, D. D., G. Chen, J. H. Crawford, S. Liu, D. Tan, S. T. Sandholm, P. Jing, D. M. Cunnold, B. DiNunno, E. V. Browell, W. B. Grant, M. A. Fenn, B. E. Anderson, J. D. Barrick, G. W. Sachse, S. A. Vay, C. H. Hudgins, M. A. Avery, B. Lefer, R. E. Shetter, B. G. Heikes, D. R. Blake, N. Blake, Y. Kondo, and S. Oltmans (2003). An assessment of western North Pacific ozone photochemistry based on springtime observations from NASA's PEM-West B (1994) and TRACE-P (2001) field studies. *Journal of Geophysical Research*, **108**, 8,829, doi: 10.1029/2002JD003232.

Davis, M. E. (1984). Numerical Methods and Modeling for Chemical Engineers, John Wiley & Sons, New York, pp. 152-154.

DeMore, W. B., S. P. Sander, D. M. Golden, R. F. Hampson, M. J. Kurylo, C. J. Howard, A. R. Ravishankara, C. E. Kolb, and M. J. Molina (1997). Chemical kinetics and photochemical data for use in stratospheric modeling, Evaluation Number 12. *JPL* *pubication 97-4*, NASA, Jet Propulsion Laboratory, California Institute of Technology, Pasadena, California.

Derwent, R. G. (1990). Evaluation of a number of chemical mechanisms for their application in models describing the formation of photochemical ozone in Europe. *Atmospheric Environment*, **24A**, 2615-2624.

Derwent, R. G. (1993). Evaluation of the chemical mechanism employed in the EMEP photochemical oxidant model. *Atmospheric Environment*, **27A**, 277-280.

Dodge, M.C. (2000). Chemical oxidant mechanisms for air quality modeling: Critical review. *Atmospheric Environment*, **34**, 2103-2130.

Eisele, F. L. and D. J. Tanner (1991). Ion-Assisted Tropospheric OH Measurements. *Journal of Geophysical Research*, **96**, 9295-9308.

Eisele, F. L., G. H. Mount, F. C. Fehsenfeld, J. Harder, E. Marovich, J. Roberts, D. J. Tanner, and M. Trainer (1994). An intercomparison of tropospheric OH and ancillary trace gas measurements at Fritz Peak Observatory, Colorado. *Journal of Geophysical Research*, **99**, 18,605-18,626.

Eisele, F. L., R. L. Mauldin III, D. J. Tanner, J. R. Fox, T. Mouch, and T. Scully (1997). An inlet sampling duct for airborne OH and sulfuric acid measurements. *Journal of Geophysical Research*, **102**, 27,993-28,002.

Gery, M. W., G. Z. Whitten, and J. P. Killus (1988). Development and testing of the CBM-IV for urban and regional modeling. Report to the U.S. Environmental Protection Agency, EPA/600/3-88-012.

Gery, M. W., G. Z. Whitten, J. P. Killus, and M. C. Dodge (1989). A photochemical kinetics mechanism for urban and regional scale computer modeling. *Journal of Geophysical Research*, **94**, 12,925-12,956.

Hass, H., P. J. H. Builtjes, , D. Simpson, ,and R. Stern (1997). Comparison of model results obtained with several European regional air quality models. *Atmospheric Environment*, **31**, 3259-3279.

Hough, A. M. (1991). Development of a two-dimensional global tropospheric model: Model chemistry. *Journal of Geophysical Research*, **96**, 7325-7362.

Houweling, S., F. J. Dentener, and J. Lelieveld (1998). The impact of nonmethane hydrocarbon compounds on tropospheric photochemistry. *Journal of Geophysical Research*, **103**, 10,673-10,696.

Jeffries, H. E. and S. Tonnesen (1994). A comparison of two photochemical reaction mechanisms using mass balence and process analysis. *Atmospheric Environment*, **28**, 2991-3003.

Jimenez, P., J. M., Baldasano, and D. Dabdub (2003). Comparison of photochemical mechanisms for air quality modeling. *Atmospheric Environment*, **37**, 4179-4194.

Kasting, J. F. and H. B. Singh (1986). Nonmethane hydrocarbons in the troposphere: Impact on the odd hydrogen and odd nitrogen chemistry. *Journal of Geophysical Research*, **91**, 13,239-13,256.

Kuhn M., P. J. H. Builtjes, D. Poppe, D. Simpson, W. R. Stockwell, Y. Andersson-Sköld, A. Baart, M. Das, F. Fiedler, Ø. Hov, F. Kirchner, , P. A. Makar, J. B. Milford, M. G. M. Roemer, R. Ruhnke, A. Strand, B. Vogel, and H. Vogel (1998). Intercomparison of the gas-phase chemistry in several chemistry and transport models. *Atmospheric Environment*, **32**, 693-709.

Logan, J. A., M. J. Prather, S. C. Wofsy, and M. B. McElroy (1981). Tropospheric chemistry: A global perspective. *Journal of Geophysical Research,* **86**, 7210-7254.

Levy, H. (1971). Normal atmosphere: Large radical and formaldehyde concentrations predicted. *Science*, **173**, 141-143.

Levy, H. (1972). Photochemistry of the lower troposphere. *Planetary and Space Science*, **20**, 919-935.

Liang, J. and M. Z. Jacobson (2000). Comparison of a 4000-reaction chemical mechanism with the Carbon Bond IV and an adjusted Carbon Bond IV-EX mechanism using SMVGEAR II. *Atmospheric Environment*, **34**, 3015-3026.

Lin, X., M. Trainer, and S. C. Liu (1988). On the nonlinearity of the tropospheric ozone production. *Journal of Geophysical Research*, **93**, 7291-7297.

Liu, S. C., M. Trainer, F. C. Fehsenfeld, D. D. Parrish, E. J. Williams, D. W. Fahey, G. Hübler, and P. C. Murphy (1987). Ozone production in the rural troposphere and the implications for regional and global ozone distributions. *Journal of Geophysical Researc*h, **92**, 4191-4207.

Luecken, D. J., G. S., Tonnesen, and J. E., Sickles (1999). Differences in NO_y speciation predicted by three photochemical mechanisms. *Atmospheric Environment*, **33**, 1073-1084.

Lurmann, F. W., A. C. Lloyd, and R. Atkinson (1986). A chemical mechanism for use in long-range transport/acid deposition computer modeling. *Journal of Geophysical Research*, **91**, 10,905-10,936.

Madronich, S. and S. Flocke (1998). The role of solar radiation in atmospheric chemistry, in Handbook of Environmental Chemistry, edited by P. Boule, Springer-Verlag, Heidelberg, pp. 1-26.

Martinez, R. I., J. T. Herron, and R. E. Huie (1981). The mechanism of ozone-alkene reactions in the gas phase: A mass spectrometric study of the reactions of eight linear and branched-chain Alkenes. *Journal of American Chemical Society*, **103**, 3807-3820.

Middleton, P., W. R. Stockwell, and W. P. L. Carter (1990). Aggregation and analysis of volatile organic compound emissions for regional modeling. *Atmospheric Environment*, **24A**, 1107-1133.

Miyoshi, A., S. Hatakeyama, and N. Washida (1994). OH radical-initiated photooxidation of isoprene: An estimate of global CO production. *Journal of Geophysical Research*, **99**, 18,779-18,787.

Mount, G. H., F. L. Eisele, D. J. Tanner, J. W. Brault, P. V. Johnston, J. W. Harder, E. J. Williams, A. Fried, and R. Shetter (1997). An intercomparison of spectroscopic laser long-path and ion-assisted in situ measurements of hydroxyl concentrations during the tropospheric OH photochemistry experiment, fall 1993. *Journal of Geophysical Research*, **102**, 6437-6455.

Niki, H., P. D. Maker, C. M. Savage, L. P. Breitenbach, and M. D. Hurley (1987). FTIR spectroscopic study of the mechanism for the gas-phase reaction between ozone and tetramethylethylene. *Journal of Physical Chemistry*, **91**, 941-946.

Nouaime, G., S. B. Bertman, C. Seaver, D. Elyea, H. Huang, P. B. Shepson, T. K. Starn, D. D. Riemer, R. G. Zika, and K. J. Olszyna (1998). Sequential oxidation products from tropospheric isoprene chemistry: MACR and MPAN at a NO_x-rich forest environment in the southeastern U.S. *Journal of Geophysical Research*, 103, 22,463-22,471.

Olson, J., M. Prather, T. Berntsen, G. Carmichael, R. Chatfield, P. Connell, R. Derwent, L. Horowitz, S. Jin, M. Kanakidou, P. Kasibhatla, R. Kotomarthi, M. Kuhn, K. Law, J. Penner, L. Perliski, S. Sillman, F. Stordal, A. Thompson, and O. Wild. (1997). Results from the intergovernmental panel on climate change photochemical model intercomparison (PhotoComp). *Journal of Geophysical Research*, **102**, 5979-5991.

Olson, J. R., J. H. Crawford, D. D. Davis, G. Chen, M. A. Avery, J. D. W. Barrick, G. W. Sachse, S. A. Vay, S. T. Sandholm, D. Tan, W. H. Brune, I. C. Faloona, B. G. Heikes, R. E. Shetter, B. L. Lefer, H. B. Singh, R. W. Talbot, and D. R. Blake (2001). Seasonal differences in the photochemistry of the South Pacific: A comparison of observations and model results from PEM-Tropics A and B. *Journal of Geophysical Research*, **106**, 32,749-32,766.

Paulson, S. E. and J. J. Orlando (1996). The reactions of ozone with. alkenes: An important source of HO_x in the boundary layer. *Geophysics Research Letters*, **23**, 3727-3730.

Poisson, N., M. Kanakidou, and P. J. Crutzen (2000). Impact of non-methane hydrocarbons on tropospheric chemistry and the oxidizing power of the global troposphere: 3-dimensional modelling results. *Journal of Atmospheric Chemistry*, **36**, 157-230.

Sander, S. P., R. R. Friedl, D. M. Golden, M. J. Kurylo, R. E. Huie, V. L. Orkin, G. K. Moortgat, A. R. Ravishankara, C. E. Kolb, M. J. Molina, and B. J. Finlayson-Pitts (2002). Chemical kinetics and photochemical data for use in atmospheric studies, Evaluation number 14. *JPL publication 02-25*, NASA, Jet Propulsion Laboratory, California Institute of Technology, Pasadena, California.

Shallcross, D. E. and P. S. Monks (2000). New directions: A role for isoprene in biosphere-climate-chemistry feedbacks. *Atmospheric Environment*, **34**, 1659-1660.

Starn, T. K., P. B. Shepson, S. B. Bertman, J. S. White, B. G. Splawn,, D. D. Riemer, R. G. Zika, and K. J. Olszyna (1998). Observations of isoprene chemistry and its role in ozone production at a semi-rural site during the 1995 Southern Oxidants Study. *Journal of Geophysical Research*, **103**, 22,425-22,435.

Stockwell, W. R. (1986). A homogenous gas phase mechanism for use in a regional acid deposition model. *Atmospheric Environment*, **20**, 1615-1632.

Stockwell, W. R., P. Middleton, J. S. Chang, and X. Tang (1990). The second generation regional acid deposition model chemical mechanism for regional air quality modeling. *Journal of Geophysical Research*, **95**, 16,343-16,367.

Stockwell, W. R., F. Kirchner, M. Kuhn, and S. Seefeld (1997). A new mechanism for regional atmospheric chemistry modeling. *Journal of Geophysical Research*, **102**, 25,847-25,879.

Strand, A. and Ø. Hov (1994). A two-dimensional global study of tropospheric ozone production. *Journal of Geophysical Research*, **99**, 22,877-22,895.

Trainer, M., E. Y. Hsie, S. A. McKeen, R. Tallamraju, D. D. Parrish, F. C. Fehsenfeld, and S. C. Liu (1987). Impact of natural hydrocarbons on hydroxyl and peroxy radicals at a remote site. *Journal of Geophysical Research*, **92**, 11,879-11,894.

Vogt, R., R. Sander, R. von Glasow, and P. Crutzen (1999). Iodine chemistry and its role in halogen activation and ozone loss in the marine boundary layer: A model Study. *Journal of Atmospheric Chemistry*, **32**, 375 – 395.

von Glasow, R., R. Sander, A. Bott, and P. J. Crutzen (2002). Modeling halogen chemistry in the marine boundary layer. 1. Cloud-free MBL. *Journal of Geophysical Research*, **107**, 4341, doi: 10.1029/2001JD000942.

Wang, Y., D. J. Jacob, and J. A. Logan (1998). Global simulation of tropospheric O_3-NO_x-hydrocarbon chemistry, 3. Origin of tropospheric ozone and effects of non-methane hydrocarbons. *Journal of Geophysical Research*, **103**, 10,757-10,767.

Whitten, G. Z., H. Hogo, and J. P. Killus (1980). The Carbon-Bond mechanism: A condensed kinetic mechanism for photochemical smog. *Environmental Science and Technology*, **14**, 690-700.

VITA

Xingyi Gong was born on February 11th, 1973 to his parents Jinglin Yuan and Zhonglin Gong in Beijing. After graduation from high school, he attended Amoy (Xiamen) University in 1991 where he graduated with a B.S. degree in marine chemistry in 1995. He then entered Peking (Beijing) University and earned his M.S. degree in environmental chemistry in 1998. In September 1998, he came to the United States to pursue a Ph.D. degree in atmospheric chemistry at the Georgia Institute of Technology under the supervision of Dr. Douglas D. Davis for seven years. This thesis marks the completion of that goal.